Interferometry as a tool to calibrate evolutionary tracks

Dissertation
zur Erlangung des akademischen Grades
Dr. rer. nat.

vorgelegt dem Rat der Physikalisch-Astronomischen Fakultät
der Friedrich-Schiller-Universität Jena

eingereicht von Dott. Magistrale Felice Cusano
geboren am 17.07.1979 in Neapel (Italien)

Gutachter

1. Prof. Dr. Artie P. Hatzes

2. Prof. Dr. Sebastian Wolf

3. Prof. Dr. Güenter Wiedemann

Tag der letzten Rigorosumsprüfung: 14.06.2012

Tag der öffentlichen Verteidigung: 14.06.2012

Zusammenfassung

Der wichtigste Parameter eines Sterns ist seine Masse, denn die Masse bestimmt die gesamte Entwicklung des Sterns von seinem Anfang bis zu seinem Ende. Das Problem ist, dass in viele Fällen die Masse des Sterne nur aus theoretischen Rechnung abgeleitet werden kann und nicht durch direkte Messung gemessen werden kann. Es ist daher für die gesamte Astronomie von großer Wichtigkeit, die Masse von einigen Sternen zu messen um damit die theoretischen Rechnungen zu prüfen und zu kalibrieren. In der hier vorgestellten Arbeit werden die Massen von zwei sehr unterschiedlichen Arten von Sternen bestimmt: Riesensterne und junge Vorhauptreihensternen. Die Messungen der Masse erlaubt es, für die Entwicklungs-wegrechnungen für diese Arten von Sternen zu testen. Dies es wichtig, da im Gegensatz zu Hauptreihensternen erst wenige Messungen der Masse von Vorhauptreihensternen und von Sternen die die Hauptreihe bereits verlassen haben gibt. Grund für das weitgehende Fehlen solcher Tests ist die bisher sehr begrenzte Auflösung der Teleskope. In der vorliegenden Arbeit wird exemplarisch gezeigt, dass die jetzt in Betrieb genommenen Interferometer in diesem Bereich einen Entscheidenden Beitrag liefern können. Der erste Teil der vorliegenden Arbeit widmet sich den jungen Sternen, der zweite den Riesensternen.

Die beste Mglichkeit zur Bestimmung der wahren Masse junger Sterne ist die Beobach-tung von Doppelsternen. Allerdings gab es bis jetzt das Problem, dass die meisten Ster-nentstehungsregionen so weit entfernt sind, dass die mit Seeing-limitierten Teleskopen optisch auflösbaren Doppelsterne Umlaufperioden von Jahrhunderten haben. Es gibt bei jungen Ster-nen zwar einige bedeckende Doppelsterne aber diese sind für solche Tests wenig geeignet da sie wahrscheinlich im Laufe ihrer Entwicklung einen Massenaustausch gemacht haben. Das Projekt war daher bisher praktisch undurchführbar. Erst die Inbetriebnahme von optischen Interferometern machte es möglich, dieses Projekt durchzuführen. Optische Interferometer haben eine Auflösung im Bereich von wenigen tausendstel Bogensekunden und erlauben Dop-pelsterne mit Umlaufperioden bis herunter zu 50 Tagen auflösen. In Vorbedingung für das Projekt wurden zunächst einem eine geeignete Stichprobe von Doppelsternen mit Umlauf-perioden zwischen 50 Tagen bis einigen Jahren zusammenzustellen. Zu Beginn der Arbeit waren nur sehr wenige Doppelstern mit geeigneten Perioden bekannt. Der erste Schritt war daher, solchen Objekte zu identifizieren. Dazu wurde zunächst eine sehr umfangreiche, spektroskopische Kampagne durchgeführt in der 600 Spektren junger Sterne aufgenommen wurden. Das Ergebnis ist eine Liste von insgesamt 13 Doppelsternen im relevanten Perio-denbereich.

Bereits die spektroskopisch bestimmten Bahnen erlauben die Massenverhältnisse der Sterne zu bestimmen. Damit konnte ich bereist einen ersten Test der Entwicklungsmodelle durchführen. Es zeigte sich, dass die Modelle von Baraffe et al. (1998) am besten zu den Beobachtungen passten.

Im nächsten Schritt war die Bestimmung der wahren Masse von Doppelsternen durch Kombination von hochpräzisen Radialgeschwindigkeitsmessungen mit Daten vom VLTI-Interferometer auf dem Cerro Paranal. Für die Radialgeschwindigkeitsmessungen wurde HAPRS, das zur

Zeit beste Instrument seiner Art auf der Welt, verwendet. HARPS ist am ESO 3.6-m-Teleskop in La Silla montiert. Leider zeigte sich, dass das VLTI zwar die gesetzten Anforderungen in Punkto Auflösung erreicht, nicht aber in Punkto Empfindlichkeit. Auch bei der Zusammenschaltung von drei 8-m-Teleskpen können zur Zeit nur die hellsten Quellen dieser Liste beobachtet werden.

Die Instrumentellen Fortschriite sind aber so enorm, dass es in wenigen Jahre möglich sein wird die gesamte Liste schon mit den 1.8-m großen Hilfsteleskopen (ATs) beobachtet werden kann.

Da die Bestimmung der Massen von jungen Sternen durch Kombination von VLTI-Messungen und Radialgeschwindigkeitsmessungen eine ganz neue Methode ist, ist es zunächst vor allem wichtig zu zeigen, dass die Methode auch wirklich funktioniert. Als Beispiel habe ich daher das hellste Objekt der Liste beobachtet: HD113449. Auch hier ergab sich, dass die Modelle von Baraffe et al. (1998) am besten sind. Zusammenfassend kann gesagt werden, dass die bisherigen Resultate den Schluss nahe legen, dass die Modelle von Baraffe et al. (1998) am realistischen sind.

Der zweite Teil der Arbeit beschäftigt sich mit der Messung der Masse von Riesensternen. Auch hier wurde wissenschaftliches Neuland betreten. Aus der Theorie der Sterne ergibt sich dass die Frequenz des Maximum von Sternschwingungen im Wesentlichen nur durch das Verhältnis von Masse zum Radius ^{2} gegeben ist. Durch Bestimmung der Frequenz des Maximums der Sternschwingungen durch Radialgeschwindigkeitmessungen und der Messung des Radius des Sterns mit Hilfe von einem Interferometer läst sich also die Masse des Sterns bestimmen und somit die Entwicklungswege von Riesensternen testen. Da diese viel heller als die jungen Sterne sind, konnten 30 Riesensterne mit dem, VLTI und dem CHARA Interferometer erfolgreich untersucht werden. Es zeigt sich, dass die von Salasnich et al. (2000) veröffentlichten Rechung am Besten die Beobachtungen wiedergeben.

Zusammenfassend kann gesagt werden, dass die beiden neue entwickelten Methoden zur Bestimmung von Sternmassen sehr erfolgreich sind und mit Hilfe von weiteren Messungen die Entwicklungswege von Sternen genau untersucht werden können.

Abstract

Up to now, the only way to determine the masses of single stars at different ages was to use the so-called evolutionary tracks. These are the outcome of complicated theoretical models that draw on the HR diagram the time changing of temperature and luminosity of stars at fixed masses. Depending on the authors, the model input physics is different and, as a consequence, the evolutionary tracks for stars of the same masses are different. It is therefore of crucial importance to test which models better predict the observations.

In this PhD-thesis I present new methods to determine physical parameters of young and evolved stars, combining spectroscopy with high angular resolution observations performed with optical interferometers. In particular, two different types of stars will be treated: pre-main sequence (PMS) stars and giant stars. The first part of the thesis will discuss PMS stars, while the subject of the second part will be giant stars.

Combining the relative positions of two stars in a binary system measured through optical interferometry, with spectroscopy it is possible to measure the dynamical masses of the binary components. In the case of PMS stars, as a first step toward the calibration of the tracks, I performed a spectroscopic survey using FEROS [1] to search for young binaries. The result was the collection of a sample of 13 young spectroscopic binary systems suitable for interferometric observations. For these binaries, I determined the orbital parameters and in two cases the mass ratios. The interferometric observations unfortunately showed that while the VLTI[2] reaches the design specification in terms of resolution, it falls short of the expectations in terms of sensitivity. Nevertheless, in the cause of exo-planet hunting I discovered an interesting bright young binary system, namely HD113449, with an orbital period of 216 days. I obtained interferometric observations of this object in service mode with the near-infrared focal instrument AMBER[3] at the VLTI. Combing these data with the spectroscopic observations performed with HARPS[4] at ESO and CRIRES[5] at ESO, I determined the masses of the two components of HD113449. Comparing these mass values and the mass ratios of the two spectroscopic binaries with three different sets of evolutionary tracks, I found that the Baraffe et al. (1998) tracks fit better the observations.

In the case of the test of evolutionary tracks for post main sequence stars, I measured the diameters of 30 giant stars, of which 7 planet hosting, using AMBER at VLTI and the CHARA[6] array. A first test was done comparing the diameters estimated from three different sets of evolutionary tracks with the interferometrically measured ones. This test showed that on average all the models predict the measured within 1σ, but the Salasnich et al. (2000) models are the ones better fitting the observations. In the case of HD170693, a giant star hosting a planet with an orbital period of 478 days, I also obtained time series observations

---

[1] The Fiber-fed Extended Range Optical Spectrograph
[2] Very Large Telescope Interferometer (ESO, Chile)
[3] Astronomical Multi-BEam combineR
[4] High Accuracy Radial velocity Planet Searcher
[5] CRyogenic high-resolution InfraRed Échelle Spectrograph
[6] Center for High Angular Resolution Astronomy (Georgia State University, USA)

with the high resolution spectrograph in the Thüringer Landessternwarte Tautenburg, deriving the oscillation frequencies thanks to an asterosismological analysis of the measured radial velocities. Combining this information with the interferometrically-measured diameter, I obtained the mass of this giant, which is in good agreement with the one coming from the evolutionary tracks. In the future other spectroscopic time series observations performed on the remaining giant stars of the sample will allow the determination of the masses of 29 of them, putting strong constrains on the models.

The thesis is organised as follows. In Chapter 1 a brief historical introduction about the development of optical interferometry is given. In Chapter 2 the physical principles at the base of the interferometry are given, together with how an optical interferometer works. In the same Chapter, the two interferometers used to acquire the data analysed in this thesis, namely the VLTI and the CHARA array, are described in details. Chapter 3 gives information about the treatment of interferometric data, mainly the AMBER ones, which are the most used in this thesis. In Chapters 4 and 7, the scientific aims of the thesis are illustrated, divided in two Chapters in order to treat separately the test of the evolutionary tracks of PMS and evolved stars. In Chapters 5 and 8 the methods used to reduce and analyse the spectroscopic and interferometric data for young and giant stars are presented, respectively. In Chapter 6 and 9 the results of the thesis are presented together with the discussions. The Conclusions are given in Chapter 10.

Contents

Chapter 1

Introduction

Achieving higher and higher resolution has been important for the advancement of astronomy. Unfortunately this advancement came to halt when telescopes reached the seeing limit in the 19th century. A break trough was achieved with the invention of interferometers, adaptive optics and later with space telescopes. In here I summarised the history of the optical interferometry, introducing also the scientific case of the thesis.

1.1 The need of high angular resolution in astronomy

The Sun is at a distance from the Earth of about 150×10^6 km, and with its 1.4×10^6 km diameter has an average angle in the sky of 32 arcmin. For a long time this was the only star that could be spatially resolved. The reason is that the angular diameter of stars is very small. Betelgeuse for example has an apparent diameter of only 50 mas (1 mas = 10^{-3} arcsec), although it is amongst the stars with the largest apparent diameter. The distance between the earth and the stars is simply so huge that their apparent diameters are of the order of few tens of mas even in the best cases.

Galileo for the first time resolved Jupiter as a disk, studying the revolutions of its moons around it, which at that time was an important argument for the heliocentric model of our solar system. Since the time of Galileo the resolution of telescopes have increased, resulting in a better understanding of the universe.

The angular resolution of a telescope is dictated basically by its aperture, the wavelength of observation and by the atmosphere. The last is a critical aspect in the determining the resolution power of a telescope. In an ideal case where there is no atmosphere the capability of an instrument to resolve two point sources in the sky is given by the equation, $\theta = 1.22$ λ/D, where θ is the angle in the sky expressed in radians (1 radian = 206265 arcsec), D is the diameter of the telescope and λ the wavelength of observation. This means that if one observes an object in the sky at visible wavelength, say 5500 Å, with a telescope of 10 meters aperture, it is possible to achieve in principle a resolution of about 20 mas. This means that it is possible to spatially resolve only few objects in the sky. In the real world, where we have to deal also with the presence of the atmosphere, the situation is even worse. The blurring of the atmosphere reduces the resolution of all telescopes even the largest to a few tenth of arcsec, equivalent to the resolution of 10 to 20 cm telescopes. However, today adaptive optics and speckle interferometry can overcome the limitation caused by the atmosphere, so
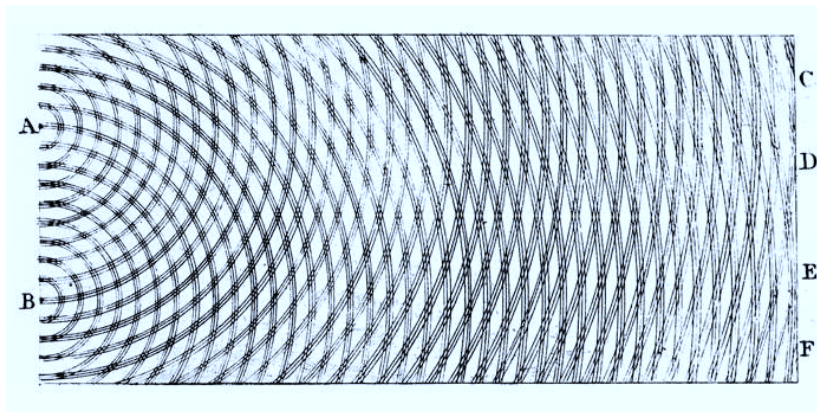
Figure 1.1: *Young representation of the two-slit experiment, based on his observations of interference in water waves.*

that diffraction limited images can nowadays be obtained. Of course the distortions caused by the atmosphere can be completely avoided if the telescope is put into the space. The Hubble Space Telescope (HST) for example, which has an aperture of 2.4 m, can achieve routinely a resolution of 50 mas. The disadvantage of space telescopes is the high realisation costs. The planned giant ground-based telescope, equipped with AO-systems, like the E-ELT (European-Extremely Large Telescope, 42 m diameter) and the American TMT (Thirty Meter Telescope, 30 m), will offer a resolution up to 3-4 mas. Building such AO-systems is however also challenging.

Another approach in order to obtain high angular resolution without gigantic costs and technical issues, is to use interferometry. Ground-based interferometers can achieve a resolution even higher than that of space telescopes and is limited only by the spacing of the individual telescopes.

1.2   History of Long Baseline Interferometry

In an interferometer the light coming from a source in the sky is collected simultaneously by two or more telescopes and then combined to form fringes. The angular resolution that is achieved with an interferometer is given by λ/B where B is the distance between the telescopes, called also *baseline*. By placing several telescopes at large distances from each other, it is possible to achieve spatial resolution comparable to that of a single dish telescope with diameter B. Interferometry is technologically challenging, and also requires a highly sophisticated process of data-reduction. The physical basis of the interferometry is the interference of light waves. Interference of light waves was already observed by Grimaldi in the 17th century. At that time Grimaldi was not able to give a scientific explanation for this phenomenon, and he simply concluded that the light is of "immaterial nature". This idea was subsequently confirmed by the contemporary works of R. Hooke and C. Huygens, who described the light as a wave and introduced the concept of wavelength. The interference was scientifically explained a century later by Young and Fresnel. In 1803, Young described an experiment where sunlight collected from a small pinhole hits a narrow strip of cards. The light beams coming out from the edges of the strip overlapped on a screen producing a series
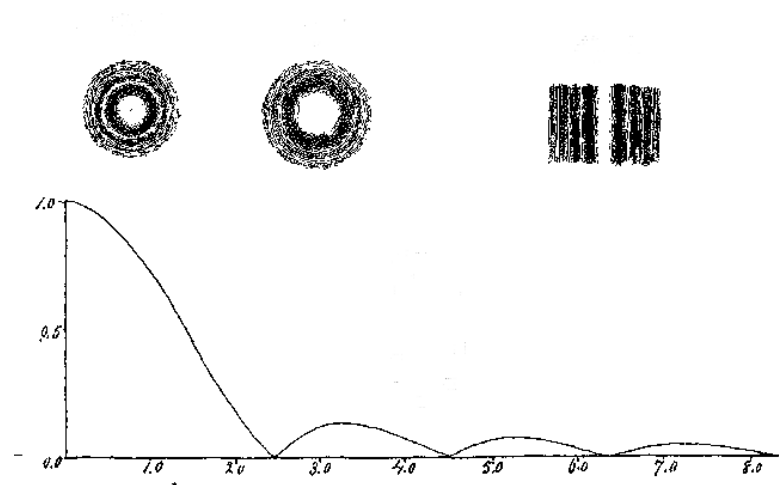
Figure 1.2: *The original figure published by Michelson on the measurements of the diameters of the Jupiter moons. The top panel shows from left to the centre the differences between a star and an object of finite angular size observed with a telescope provided with a circular diaphragm. On the right he shows the fringes produced by a star observed with his interferometer. The curve just below, is a plot of the model visibility of the fringes vs. baseline for an uniformly illuminated circular disk.*

of interference fringes. The central light was white and the outer coloured. By shadowing the light coming from one of the two edges he saw a dimming of the fringe contrast, until the fringes disappeared when one ray was completely obscured. This supported the idea that the interference is a superposition of waves, in analogy to the interference of water waves (see Figure 1.1). He concluded that the light is composed of waves. Young then idealised the experiment, substituting the narrow strip with a pair of pinholes, which is the way in which is known in general today. Young used the interference phenomena, to measure the wavelength of light at different colours. After Young's early experiments the theory of light-waves was further developed by Fresnel, Arago, Fraunhofer and Fizau. Fizeau was the first person to understand that the loss of contrast of the interference fringes can be used to measure the size of the light source. Fizeau in 1867 was a member of the jury for the Bordin price of that year. The aim was to conduct an experiment to determine the direction of vibration of the hypothetical ether produced by polarised light. Although the members of jury, included Fizau, agreed that none of the works presented was worthy of the price, they where impressed by the work of W. Jenker from Berlin, who had proposed to use interference fringes to solve the problem. In his report Fizau summarised the merit of Jenker's work and described another possible application of interferometry that is the measurement of star diameters using two separated slits in front of a telescope aperture. Five years later Stephan wrote to Fizeau about his initial experiments based on his idea at the Observatoire de Marseille. Stephan masked the large Foucault telescope to define two aperture spaced of 50 cm. All the stars that he observed were not resolved, except Sirius which later on turned out not to be resolved, but was too low on the horizon when he observed it. After one year of observations of most of the stars brighter than 4 mag with a separation of 65 cm between the two aperture, he deduced that the all stars must have an angular diameter smaller than 0.158 arcsec (Stephan
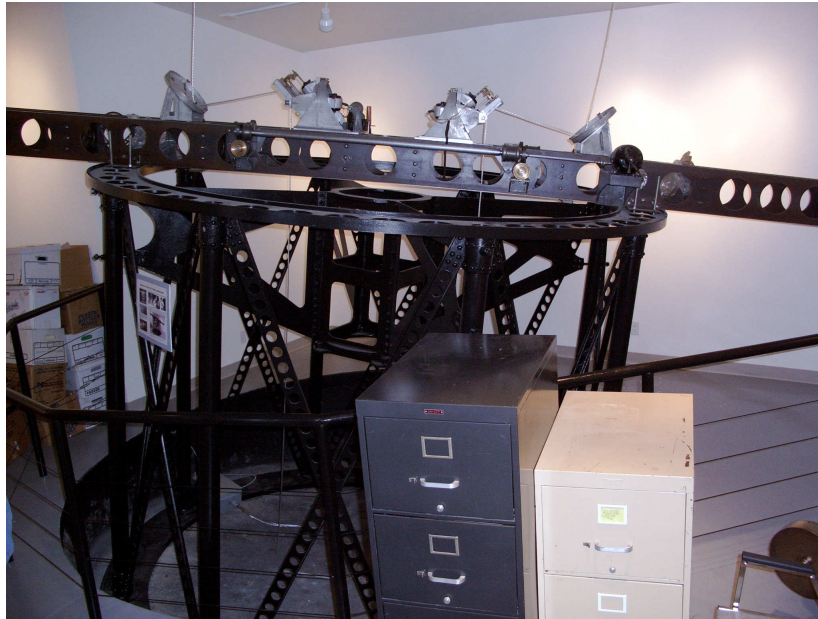
Figure 1.3:   *This photo shows the original 6 m interferometer that Michelson mounted on the top of the 100inch-telescope. The two 15 cm movable mirrors are visible on the two arms. This instrument was used to measure for the first time the diameter of stars, and is now on display at Mount Wilson.*

1874). The idea of masking a telescope aperture to measure the diameter of a star was then also used by A. A. Michelson.

In 1890 Michelson described in a famous article the instrument which he built in order to measure interferometric fringes of objects in the sky (Michelson 1891b). He discussed the results obtained not only for an uniform disk star and binary, but also for a limb-darkened star using a model previously developed for the Sun. In this work is already present the idea of the coherent function, a concept that was later developed in detail by Zernike (1938). In 1891 Michelson used the first version of a modern interferometer, composed of a pair of slits with variable spacing in front of the 12-inch aperture telescope on Mount Hamilton, to measure the diameters of the four Galilean moons of Jupiter, founding good agreement with other methods (Michelson 1891a, see Figure 1.2).

This work was followed by (Schwarzschild 1896) and (Anderson 1920) who used the same technique to measure the separation of a few binary stars. These first experiments showed the possibility to achieve angular resolution close to the diffraction limit λ/B of a telescope, loosing on the other hand the image capability of the instrument. As the next step, Michelson developed the idea of building a new interferometer mounted on the top of the 100-inch in Mount Wilson (see Figure 1.3). The apertures of the new interferometer were made by two movable 15 cm mirrors mounted on a rigid beam 6 meters long. This equipment was mounted in front of the aperture of the telescope. Michelson used this instrument to measure the diameter of α Orionis (Michelson & Pease 1921) and Pease measured the diameters of other 6 stars (Pease 1931). In these early works they noted also that despite the seeing it was possible to achieve very high angular resolutions. Today interferometer, in which the entire instrument is pointed towards a star in the sky (like in the Michelson's setup), are called Michelson's interferometer in memory of these early works.

Figure 1.4: *The I2T built by Labeyrie and collaborator at the Nice Observatoy in 1975. It is possible to see the two small telescopes that were used to collect the first fringes of the interferometer.*

Pease afterwards tried to built an interferometer with a baseline of about 15 m (Pease 1931), but this instrument was not stable enough. Only the diameter of one additional star was determined during its observations. With the technology available at the time it seemed that there were no additional targets to be observed with interferometry. For this reason this observational technique was not used for 30 years. The situation changed with the development of radio interferometry. This led indirectly to a renaissance of the optical interferometry in the 1950s, with the birth of intensity interferometry by Brown & Twiss (1957). In this interferometer the light coming from a source is collected independently by two photo-multipliers attached to two movable telescopes. The output of the photo-multipliers is then sent to a central correlator. This new system had the great advantage to be independent from the atmosphere and to work with long baselines. On the other hand the new technique was working only for bright stars and the phase information of the fringes was completely lost. The Narrabri Stellar Intensity Interferometer (NSII, Australia) worked for more than 20 years and diameters of 60 stars in the southern hemisphere were determined. After all stars bright enough to be studied with this instrument were observed, the interferometer was dismounted.

In 1974 Labeyrie was the first to detect fringes in the combined light from two separate telescopes (Labeyrie 1975). This type of interferometer is called Fizeau interferometer. The great advantage compared to the intensity interferometer is that much fainter stars can be observed. Compared to the Michelson interferometer the advantage is that much larger-baselines can be achieved. Labeyrie's prototype interferometer at the Observatoire de Nice was moved to a plateau in the Maritime Alps. It became known as the Interféromètre á 2 Tèlescope (I2T, Figure 1.4). For 10 years it was the only modern working interferometer. The observing program of the I2T was directed primarily at measuring stellar diameters and orbits of binary stars (e.g. Koechlin et al. 1979; Koechlin & Rabbia 1985; di Benedetto & Rabbia 1987). During this time Di Benedetto and Conti (1983) pioneered direct infrared interferometry, implementing a new optical table for the I2T with a design that was influenced

by the work of McCarthy and Low (1975).

Labeyrie invented in the same period also another technique to reach the diffraction limit of a telescope called speckle interferometry (Labeyrie 1970). This method takes advantage of the randomness of the atmospheric fluctuations in order to obtain high resolution images with a conventional telescope. In order to obtain fringes, the first generation of Fizeau and Michelson interferometers had to use small apertures to ensure the coherence of the light coming from each telescope. Shao and Staelin specifically required small apertures in their design of an astrometric interferometer (Shao & Staelin 1977), and Tango and Twiss stressed that by restricting the aperture size and tilt-correcting the incoming beams, coherence losses could be greatly reduced (Tango & Twiss 1980). Apertures of only several centimetres in diameter were therefore used in 1979 by Shao and Staelin with their Mark I prototype interferometer (Shao & Staelin 1980). Other interferometers have followed this approach like the Sydney University Stellar Interferometer (Davis & Tango 1985) and the Infrared Michelson Array (Dyck et al. 1993). Stellar interferometry was adapted to wide-angle astrometry by Shao and his collaborators, by applying the principles of phase-measurement interferometry to the determination of stellar positions and proper motions. Shao and Staelin demonstrated in 1979 that atmospheric phase variations can be measured and corrected in real time (Shao & Staelin 1980). Then they initiated a program of development leading to the construction of the Mark III interferometer (Shao et al. 1988). Although the Mark III was primarily intended as an astrometric instrument, it also proved to be a powerful tool for the measurement of stellar diameters and orbits of binaries. Its program of astrometry was completed in 1993 by the researchers working for the US Naval Observatory and the Naval Research Laboratory. These two organisations have subsequently cooperated in the construction of the Navy Prototype Optical Interferometer (NPOI). Ground based astrometry potentially could permit the detection of extrasolar planets (Shao & Colavita 1992). In December 1984 Baldwin and collaborators made the first measurement of closure phase at an optical telescope (Baldwin et al. 1986). After this initial success using aperture masks, several new interferometers were designed specifically for optical synthesis imaging. Because it was now possible to combine the light from 3 or more telescopes simultaneously, schemes for combining 4 or 6 beams were implemented. In 1993 Baldwin and his group were the first to measure closure phase using separated telescopes. Over the 1995-96 the first images were produced, initially at the Cambridge Optical Aperture Synthesis Telescope (Baldwin et al. 1994, 1996) and soon after at the Navy Prototype Optical Interferometer (Armstrong 1994).

1.3   Presently used interferometers

Currently there are several astronomical optical interferometers operating at different wavelengths and with different configurations and baselines. It is worth mentioning some of the most used and scientifically prolific. The CHARA array is operating at Mount Wilson Observatory in California, at the same site as the Michelson original experiment. It consists of six 1 meter telescopes arranged along three axes with a maximum separation length of 300m and can operate in 6 different bands from the V to the K band. The Keck interferometer is located on the top of Mauna Kea in Hawaii, and it uses two 10 meter telescopes which are separated by a fixed distance of 85 meters. This interferometer operate at IR wavelengths.

COAST is located in Cambrigeshire at the Mullard Radio Astronomy Observatory. It is a multi-element optical interferometer with baseline of up to 100 meters. It is used mainly as a testbed for subsystems and components intended for VLTI and future optical interferometers, although limited astrophysical programmes are also carried out. The VLTI (Very Large Telescope Interferometer) located at Cerro Paranal, Chile, uses either up to three of the four 8.2 m or four movable 1.8 m telescopes. The former are fixed while the latter can be moved to 30 different positions. Two interferometric instruments are currently in use at the VLTI: MIDI and AMBER. AMBER allows one to combine simultaneously the light coming from three telescopes. A number of very ambitious projects to built new optical interferometers are under study. The MRO (Magdalena Ridge Observatory) Interferometry is one of these. Under construction on the Magdalena Mountains in New Mexico, this interferometer is planned to operate at wavelengths between 0.6 and 2.4 microns with baselines from 7.5 to 340 m using ten telescopes of 1.4 m of aperture. Its primary scientific goal is to produce images of faint and complex astronomical targets at very high resolution.

In this thesis I will present results obtained with the CHARA array and the VLTI. Both interferometers will be described in more details in Chapter 2. The purpose of this thesis is to introduce new methods to calibrate evolutionary tracks for young and evolved stars, using optical interferometry. The aim of the thesis will be explained in detail in Chapters 4 and 7.

Chapter 2

The art of optical Interferometry

In the previous Chapter I described the history of optical interferometry. In this Chapter the basics of interferometry are presented, together with the detailed description of the VLTI and the CHARA array.

2.1 Physical principles

The physical principle at the basis of astronomical optical interferometry is the interference of light rays. Interference occurs when two electromagnetic waves of the same frequency with a phase difference overlap. Such waves are called coherent. As an example let us take an electromagnetic wave illuminating a screen with two pinholes which are separated by a small distance d, as shown in Figure 2.1. Using the Huygens principle, the emerging wavefront can be modelled as two spherical waves originating from the pinholes. At a given point T placed on the screen at a distance L $\gg$ d in respect to the two pinholes, the two waves overlap. The different path-length that they follow until this point T causes a phase difference between the waves which is proportional to the distance between the pinholes d and to the wavelength. If we call Δ the difference path-length, the phase difference is $\phi=2\pi\Delta/\lambda$ and the two wave equations are $E_1=E_0\exp(i\omega t)$ and $E_2=E_0\exp(i\omega t + \phi)$. The result of the overlap of the two waves is a series of bright and dark strips on the screen, the interference fringes. If L $\gg$ d then $\Delta \sim \theta \times$d, where θ is the angle formed by the line connecting the mid point between the two apertures and T, and the normal towards the screen. Maxima of the fringes are observed for values of Δ that are multiple integers of the wavelength:

$$m\lambda \approx d\theta \qquad\qquad m = 0, 1, 2....n \qquad\qquad (2.1)$$

The contrast of the fringes is parametrised by a quantity called visibility. The visibility can be written as:

$$V = |\mathbf{V}|e^{-i\phi} \qquad\qquad (2.2)$$

where $\mathbf{V} = \frac{I_{max}-I_{min}}{I_{max}+I_{min}}$, with I_{max} and I_{min} the maximum and the minimum intensity of the fringes respectively. The phase ϕ is given by the position of the first maxima in respect to a reference zero point of the phase. The visibility thus describes the fringe contrast. It is an important quantity of interferometry as it contains information about the properties of the source. As illustration in the Chapter 2.3 I will derive the visibility for a number of important astrophysical objects.
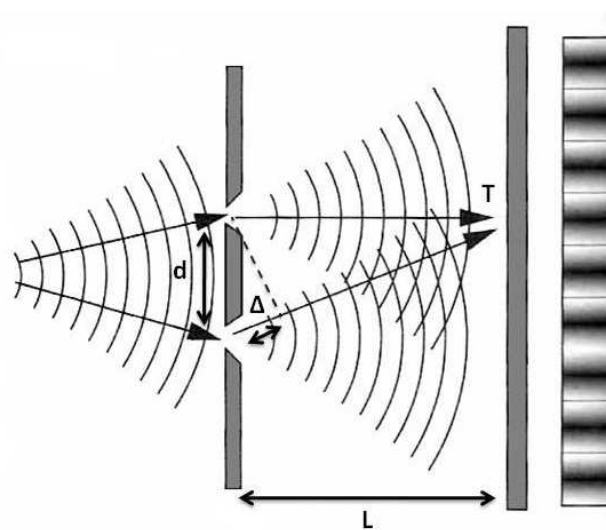
Figure 2.1: *Schematising of the Young's double slit experiment. A wave hits the screen with two small pinholes which act as waves emitter. The two waves have a phase difference which is proportional to Δ. Interference fringes are observed on the screen.*

2.2   The coherence of light

As mentioned above, two light waves can only interfere if they are spatially and temporally coherent. Unfortunately astronomical objects do not consist of a small number of point sources emitting monochromatic, coherent light. Nevertheless, under certain conditions fringes are observed.

The first condition regards the extension of a source. To explain the concept of spatial coherence let us take the same situation as described in Chapter 2.1. Considering now a point source that is slightly offset with respect to the one considered in the discussion, we record on the screen a new set of fringes which is shifted in respect to the one produced by the other source. A shift of half a fringe corresponds to a path difference of $\frac{1}{2}$ λ between the waves received at the two pinholes. The criterion to observe the blurring of the fringes, indeed is that the path difference between light waves coming from different points is of $\frac{1}{2}$ λ. If we consider that an extended source is composed of many point sources, each of these points will produce a set of fringes which is shifted in respect to the other ones by a quantity which depends on the path difference. The effect of the blurring of the fringes becomes relevant if the source is too large or if the separation between the two pinholes is too large. The separation between the two pinholes at which the fringes disappear is called the coherence distance d_c and it depends on the source size, through the equation $d_c = \frac{\lambda}{2\alpha}$, where α is the angular diameter of the source. When the pinholes are separated by a distance larger than d_c, the two waves are not any longer coherent and no interference is observed. This was the original idea of Michelson for measuring angular diameters of stars with his interferometer (see Chapter 1.2).

To observe fringes, a source has to be spatially and temporally coherent. Let us assume that we observe a source composed of several emitters which radiate at slightly different frequencies $\omega \pm \delta\omega$. Waves from the individuals emitters have different phases. Let us
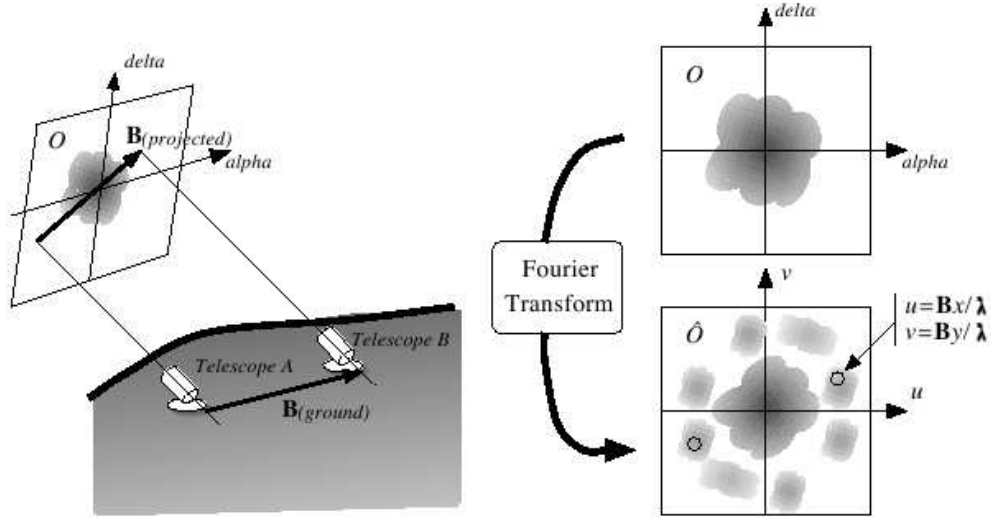
Figure 2.2: *Schematic explanation of the Van Cittert-Zerniche theorem. The Fourier transform of the brightness distribution of the object is equal to the visibility in the uv-plane (right). Also shown in this figure is the projection of the baseline in to the plane of the sky (left). The two open circles at the bottom right are the uv sampling by the baseline.*

furthermore assume that we observe the radiation at the time t=0 and t=τ. Now if $\tau\delta\omega$ is larger than π, the average phase of the radiation will be unrelated to the phase at t=0, and no interference will be observed. The so called coherence time is thus defined as $\tau_c = \frac{\pi}{\delta\omega}$. This concept is very important for interferometry. The reason is that if the path difference between two beams is larger than cτ_c no fringes will be seen, even if they are spatially coherence.

2.3 The Van Cittert-Zernike theorem

The quantitative relationship between the source size and the structure and the degree of coherence is summarised in a theorem derived independently by Zerniche and van Cittert in the 1930s. The theorem is known as the Van Cittert-Zerniche theorem. This theorem states that the normalised Fourier transform of the brightness distribution of an astronomical source is equal to its complex visibility (cfr. Equation 2.2). The theorem is explained schematically in Figure 2.2. We now consider a source with an angular intensity distribution I(α,β). This source is observed with an interferometer, which has two receivers located in the same plane at a distance of $\vec{\mathbf{B}}$=(B$_x$,B$_y$). Then the Van Cittert-Zerniche theorem has the form:

$$V(u,v) = \frac{\iint I(\alpha,\beta)e^{-2\pi i(\alpha u + \beta v)}\, d\alpha d\beta}{\iint I(\alpha,\beta)\, d\alpha d\beta} \tag{2.3}$$

where u and v are the Fourier conjugate variables of the angular position α and β in sky.

Their value is given by:

$$u = \frac{B_{px}}{\lambda} \qquad\qquad v = \frac{B_{py}}{\lambda} \qquad\qquad (2.4)$$

where B_{px} and B_{py} are the coordinates of the projected baselines in the plane in the sky normal to the line of sight. In other words, B_{px} and B_{py} are the components of the baseline as seen from the object. The plane of the Fourier transform is described by the two coordinates u and v, and is defined as the uv-plane.

The difference between a single dish telescope and a stellar interferometer resides in the sampling of the incident wavefront. A telescope of diameter D, can be described as a low pass filter with cut-off frequency D/λ. In this way the incoming wavefront is spatially filtered by the telescope and all spatial frequencies up to the cut-off frequency are transmitted. When observing with an interferometer, the sampling of the incident wavefront is no longer continuous and depends on the position of the telescopes. The Fourier transform of the object brightness is measured at discrete spatial frequencies. The quantity that describes which spatial frequencies are observed is the projected baseline. This depends on the length and orientation of the baselines, the declination of the source, the latitude of the observatory and the hour angle of the observations. The relation between the baseline vector B and the projected baseline B_p is given by:

$$\begin{pmatrix} B_{px} \\ B_{py} \\ B_{pz} \end{pmatrix} = \begin{pmatrix} -\sin(l)\sin(h) & \cos(h) & \cos(l)\sin(h) \\ \sin(l)\cos(h)\sin(\delta)+\cos(l)\cos(\delta) & \sin(h)\sin(\delta) & -\cos(l)\cos(h)\sin(\delta)+\sin(l)cos(\delta) \\ -\sin(l)\cos(h)\cos(\delta)+\cos(l)\sin(\delta) & -\sin(h)\cos(\delta) & \cos(l)\cos(h)\cos(\delta)+\sin(l)\sin(\delta) \end{pmatrix} \begin{pmatrix} B_x \\ B_y \\ B_z \end{pmatrix}$$

$$(2.5)$$

where l is the latitude of the observatory, h is the hour angle and δ is the declination of the star. The uv-plane can be sampled by observing at different hour angles (equations 2.4 and 2.5). By combining observations at different hour angles and by placing the telescopes at different positions, the uv-plane can be filled. If the visibility is measured for a large number of points in the uv-plane, the image of the object can be also reconstructed.

However a full reconstruction of a source requires one to measure both $|\vec{V}|$ and ϕ. While a measure of the modulus is easy, finding the phase is a serious problem. In the Fizeau interferometer, the offset of the central fringe from the optical axis gives in principle the phase, but since the fringes are also shifted laterally randomly by atmospherically induced phase changes at the two apertures, it is not possible to determine the phase. This means that the modulus of the visibility can be easily measured while the phase not. Most of the works done so far with optical interferometers thus have focused on the modulus of the visibility. This has been done by fitting visibility models, like for example circular or elliptic star, binary pairs, to the measured visibility, deriving some free parameters. Since the time of Michelson, measurements of the visibility modulus have been used in order to measure the diameters of stars and the relative positions of stars in binary systems. The phase information however is not completely lost if simultaneous observations are carried out using three or more telescopes. A relative phase of the visibility, indeed, can be obtained using a technique called closure phase (Jennison 1958; Cornwell 1989). In this method the phase fluctuation due to the atmosphere cancel out. In order to understand the method, let us assume that we have three telescopes with which we measure V simultaneously for each baseline. The phase shift induced by the atmosphere on the top of one of the telescope is ϕ_0. If we take in account that
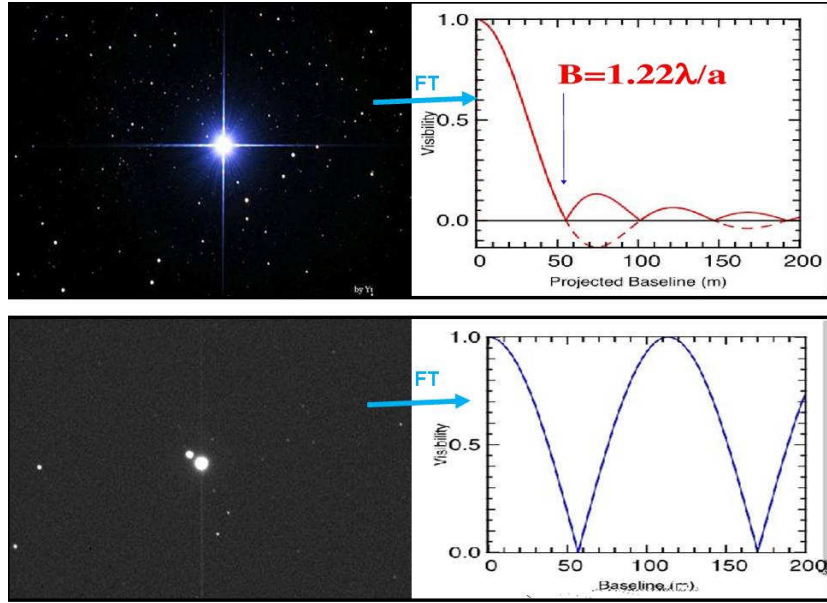
Figure 2.3: *Examples of Van Cittert-Zernicke theorem. On the top schematising of the fourier transform of a star with a uniform disk. The bottom panel is similar to the top panel, but for a binary. For the uniform disk it is also indicated the first zero of the bessel function, that can be used to determine the angular diameter of the star.*

ϕ_0 is independent by time during the observing period, the sum of the phases of the fringes for each baseline is given by:

$$\Phi_{123} = (\phi_{12} - \phi_0) + \phi_{23} + (\phi_{31} - \phi_0) = \phi_{12} + \phi_{23} + \phi_{31} \tag{2.6}$$

The closure phase can be used in several ways. For example, it can be used to confirm the circular-symmetric distribution of the light in a target for which $\Phi_{123}{=}0$. For a binary star it can be used to improve the determination of the angular separation and the flux ratio of the two components, fitting the closure phase simultaneously with the modulus of the visibility to the models.

2.3.1   A few important examples

2.3.1.1   Single star

The angular diameter of single stars can be determined with just a few interferometric measurements, by using the van Cittert-Zernicke theorem. The brightness distribution of a single star, which can be easily approximated by a constant disk function, is in the Fourier space:

$$V(\theta) = \frac{2J_1(\frac{\pi B \theta}{\lambda})}{\frac{\pi B \theta}{\lambda}} \tag{2.7}$$

with J_1 the Bessel function of the first order, θ the angular diameter of the star and B the projected baseline. The diameter of the star can be determined by measuring the visibility at different baselines and using equation 2.7. The only unknown parameter in equation 2.7 is θ. Error of less than 1% for the angular diameter can be achieved with high quality data and a certain number of baselines.

2.3.1.2   Double stars

A binary system consisting of two unresolved stars with intensity I_1 and I_2, separated by an angle ρ, can be described as the sum of two delta functions. The Fourier transform of this intensity distribution is given by:

$$V(\vec{\rho}) = \sqrt{\frac{1 + f^2 + 2f cos(\frac{2\pi\vec{\mathbf{B}}\cdot\vec{\rho}}{\lambda})}{1 + f^2}} \tag{2.8}$$

with f the flux ratio between the two stars $f = I_2/I_1$, $\vec{\rho}$ the separation vector given by $|\rho|$ and the position angle, and $\vec{\mathbf{B}}$ the projected baseline vector. By fitting the observed visibility to the 2.8, it is possible to derive the three free parameters: the flux ratio at a fixed λ, the angular separation, and the position of the two stars. Observations with different baselines in length and orientation, are needed in order to constrain the model. Figure 2.3 shows examples of visibility variation with baseline for a single (upper panel) and a double stars (lower panel).

2.4   Atmospheric perturbations

The spatial fluctuation induced by the atmosphere on a wavefront are characterised by a spatial scale r_0 called the Fried's parameter. The Frieds parameter corresponds to the diameter of the circular aperture over which the root mean square of the wavefront perturbation is one radian. Fried's parameter varies with wavelength with $\lambda^{6/5}$ and at the best astronomical sites takes values of order 15 cm at 5000 Å. Practically all telescopes with diameter smaller than r_0 will give diffraction limited images while bigger telescope will give highly distorted and speckled images. To give an idea of this parameter it is interesting to compare the value of the ratio D/r_0, with D the diameter of the telescope. At centimetre radio wavelengths, r_0 is of order of 30 km thus for the VLBA (Very Long Baseline Array) dishes D/r_0 is $\sim 10^{-3}$. In the case of the 8 m UTs, at 2.2μm, $D/r_0 \sim 11$. The difference of a factor 10^4 between the radio and the optical regime demonstrates the importance of the atmosphere for optical interferometry.

The major effects of the wavefront distortions is a rapid increase in the visibility fluctuations, with the increasing telescopes size. To reduce the effect of spatial wavefront distortions, today optical interferometers use different strategies. Some use adaptive optics systems to correct the spatial perturbation across each telescope, while others use optical fibers to spatially filter the light that is sent to the beam combiners. The optical fibers which are used accept only a specific spatial mode of the incident radiation field. This can be chosen so to be "orthogonal" to components of the field associated to the atmospheric perturbations.

The so called coherence time t_0 of the wavefront measures the time over which the root main square variation of the wavefront phase is one radian. The precise relation between t_0 and r_0 is very complex, but in a first approximation we can relate these two parameters by fluctuation arising from wind motion in front of the telescopes. In this case the coherence time can be written as $t_0 = 0.314\ r_0/v$, where v is the wind velocity. Typical values of t_0 at observatory sites are between 2 and 20 ms at 5000 Å and scale with wavelength. The effect of the temporal fluctuations is to add an additional randomly and fluctuating component to

the geometric delay, which can be compensated using active fringe-tracking. This means that the optical path delay fluctuations can be monitored and corrected by a fringe tracker.

2.5   Astronomical Optical Interferometers

Basically what happens in an astronomical interferometer is that the light coming from the source in the sky is collected by two or more telescopes, and then sent to a instrument that produces interference. Depending on the configuration we distinguish between three different kind of interferometers:

1. The Michelson interferometer; In this type of interferometer, the whole instrument is pointed towards the sky (like in Michelson's setup). Thus, there are no delay-lines. The advantage of this type of interferometer is that it has a large field of view. The disadvantage is that it is not possible to have such an instrument with a very large baseline on the ground. Currently the largest Michelson interferometer is the Large Binocular Telescope Interferometer (LBTI), which uses two telescope of 8.4 m aperture separated by 14.4 m.

2. The Fizeau interferometer; This type of interferometer works with separated telescopes and it has the advantage that the telescopes can be positioned at large distances. The disadvantage of the Fizeau interferometers is that it requires delay lines and has a small field of view. Example of Fizeau interferometers are the VLTI and the CHARA, which will be described in details in Sect. 2.6.

3. The intensity interferometer; This type of interferometer is made by two optical telescopes equipped with photomultiplier tubes separated by a certain baseline. Both telescopes are pointed to the same astronomical source, and the intensity measurements are transmitted to a central correlator facility. The intensity interferometer has the disadvantage that it requires a large amount of light. Thus only very bright sources can be observed. This technique is now only used in radio interferometry.

I will focus on the Fizeau interferometers used in this work. Interference fringes appear if two rays of light have a difference path of some wavelength. In the Fizeau interferometers it is fundamental to compensate the path difference between two rays of light, coming from two different telescopes. Delay-lines are required to make the path difference equal. One of the two rays has to be compensated for the missing path that is equal to $B \sin\theta$, with θ the angle between the telescope and the normal to the plane of target in the sky and B the baseline between the two telescopes. Usually this compensation is made by moving reflecting mirrors on rails, which track the movement of the star in the sky (see Figure 2.5). This part of the interferometer usually is called delay line, due to the fact that the compensation usually is done on the ray which has the shortest path. To better understand the functioning of the modern optical interferometer, I describe in the next paragraphs how the Fizeau interferometers VLTI and CHARA work.

Figure 2.4: *Panomaramic view of the VLTI at Cerro Paranal. Four UTs and three ATs are visible. Some of the station where the ATs can be positioned are also visible.*

2.6   The VLTI

The VLTI (Haguenauer et al. 2008) is the ESO optical interferometer located on top of the Cerro Paranal in Chile (see Figure 2.4). It is working in two different modes: one is using the 8 meter unit telescope (UTs) of the VLT (which is mostly used in stand-alone for non interferometric observations) and the other is using the 1.8 meter auxiliary telescopes (ATs) forming the VLT Interferometer Small Array (VISA). The ATs are not used for stand alone operation, but only for interferometric observations and they can be moved in different positions. The baselines available range from 16 m using the ATs to 130 m with the UTS. In the future baseline up to 200 m will be reached for some configuration of the ATs. The positions of the fixed UTs and of the VLTI station for the ATs, are made in such a way to maximise the number of baseline with different lengths and orientations. The sub systems of the VLTI are the same for the ATs and UTs. These consist of: 1) an optical system of mirrors to transport the beams; 2) a system of delay-lines; 3) a set of stabilization devices. The optical train of the VLTI is illustrated in Figure 2.5. The beam from each telescope is transferred by optical reflections through a first tunnel and then through the delay-line tunnel up to the VLTI laboratory. Star-light from the UTs is brought to the VLTI laboratory via the Coudé mirror train. Each Coudé mirror train is equipped with an adaptive optics system called MACAO (Multi-Application Curvature Adaptive Optics). The AO-system removes the wavefront distortions introduced by the atmosphere of the earth. It uses a deformable mirror located in the Coudé mirror train. In good conditions, MACAO can be used with a
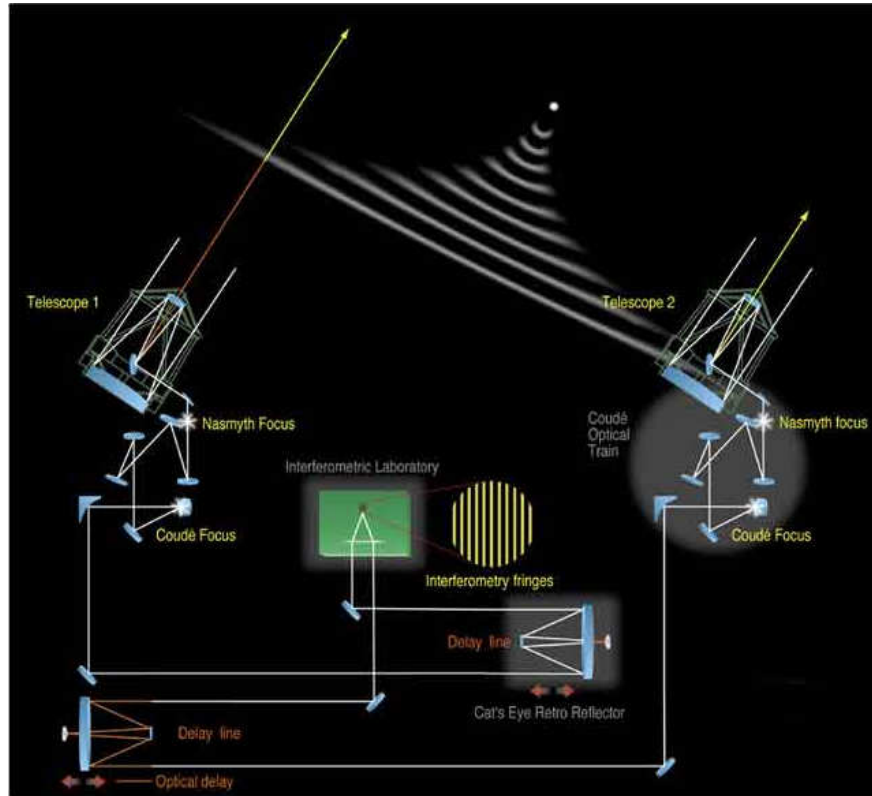
Figure 2.5: *Schematic view and working principle of the VLTI. Light coming from a source is collected by two telescopes (in this case two UTs) and then, after the difference path compensation, is sent to the instrument room, where the light interferes.*

star as faint as V=17.

VLTI has four ATs, but currently only three can be used simultaneously. However, the baselines can be switched quickly between different configurations, the ATs can be only relocated during day-time. Two ATs can be relocated on a daily basis. Any relocation of the ATs is followed by a night of calibration. Like for the UTs, a Coudé mirror train brings the stellar light from the ATs to the delay-line. Each ATs is equipped with tip-tilt wavefront corrector called STRAP (System for Tip-tilt Removal with Avalanche Photodiodes) acting on one of the movable mirrors of the telescope.

The delay lines are used to compensate the optical path difference (OPD) between the two telescopes, from the incoming stellar waveplane to the instrument entrance. Each delay-line consists of a carriage that can move along rails to adjust the optical path length. The carriage contains retro-reflecting optics. One carriage is fixed, the other continuously moves in order to compensate the OPD for the apparent sidereal motion. Optical delays between 11 m and 111 m can be realised. Not all points of the sky above the horizon can be observed at any time with any baselines. Particularly the longest baselines can be only used for objects close to the zenith. All available baselines for the UTs and ATs are presented schematically and summarised in the Figure 2.6.

The atmospheric turbulence makes an additional difference in the OPD of two rays called piston. This additional OPD is adjusted by FINITO (Le Bouquin et al. 2008). FINITO is

Baseline	Distance (m)
E0-G0	16
G0-H0	32
E0-H0	48
UT2-UT3	47
UT1-UT2	57
UT3-UT4	62
D0-H0	64
H0-G1	72
D0-G1	72
UT2-UT4	89
K0-G1	90
A0-G1	90
A0-H0	96
UT1-UT3	102
A0-K0	128
UT1-UT4	130
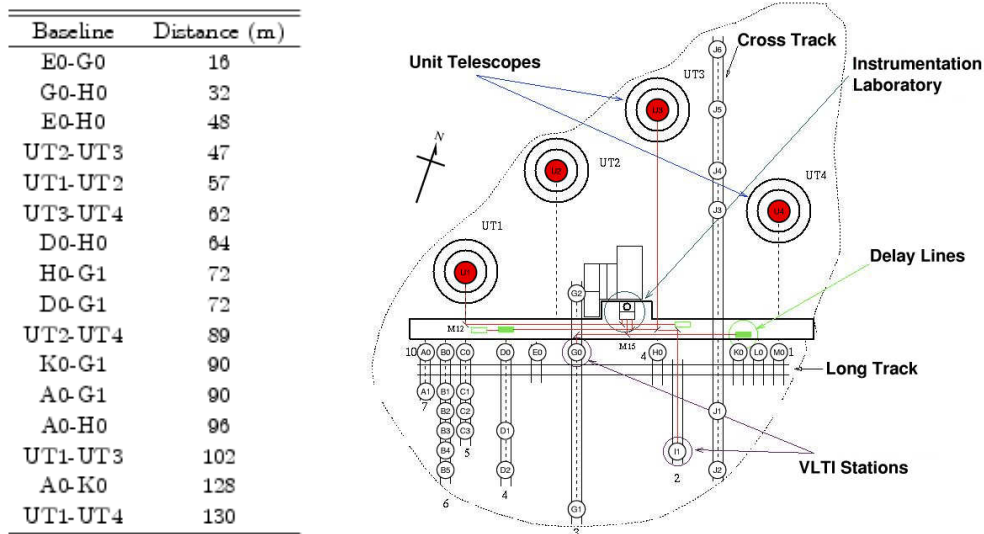
Figure 2.6: *The table on the left gives the baselines which are available for the VLTI. While the UTs are at fixed positions, the ATs can be moved to a number of locations along the rails, giving many different baselines. On the right a schematic view of the positions to which the ATs can be moved and the location of the UTs.*

the VLTI fringe-tracker, its purpose is to compensate the effect of atmospheric turbulence on the two telescopes.

2.6.1 The instruments of the VLTI

In the VLTI laboratory, where the light is delivered, there are the instruments that make possible the interference of the light beams. The first of this in chronological order was VINCI (VLT Interferometer Commissioning Instrument, Kervella et al. 2000). This instrument has been used as a test-bed for almost 2 years starting from December 2001. VINCI was using two telescopes (initially two siderostats and then two UTs). Its main purpose was to test the performance of the VLTI, but also scientific program were carried out, like for example observations of active stars like Eta Carinae (Kervella 2007) and Achernar (Kervella & Domiciano de Souza 2006).

Currently two instruments are operating at the VLTI: MIDI (MID-infrared Interferometric instrument) and AMBER (Astronomical Multi-BEam CombineR).

MIDI is the mid-infrared instrument of the VLTI that combines two beams of light coming either from the ATs or from the UTs. Only measures of visibility are possible, because the phase information is lost in the atmospheric blurring. MIDI uses a half-reflecting plate to combine the two beams. The instrument works in the N band which covers a spectral range between 8 to 13 μm. MIDI allows to obtain spectral dispersed fringes with two different resolution (R=30 or R=230) or fringes with no dispersion on different sources with a narrow field of view.

AMBER (Petrov et al. 2007) is the near infrared VLTI instrument that combines the light coming from three telescopes. For this reason AMBER allows to obtain visibility mea-

Figure 2.7: *One of the 1 m telescope of the CHARA array (left) and part of the delay lines under the CHARA laboratory (right)*

surements as well as closure phase measurements. I will describe in details AMBER in the Chapter 3.1, giving the fact that I used it for most of my work.

In the near future another instrument will be operating at the VLTI, this instrument is PRIMA (Phase-Referenced Imaging and Micro-arcsecond Astrometry). The Prima facility is a system designed to enable simultaneous interferometric observations of two objects, that are separated by 1 arcmin. This instrument will improve the sensitivity by using two objects, a bright guide star near a fainter object. The brighter is used as a reference to stabilise the fringes and for the correction of the atmospheric pistons allowing longer integration time. PRIMA most probably will be offered to the scientific community at the end of the year 2011.

2.7   The CHARA array

The CHARA Array (ten Brummelaar et al. 2005) consists of six 1 m aperture telescopes arranged in a Y-shaped configuration. The configuration has 15 baselines ranging from 34 to 331 m. With this configuration 10 different closure phase measurements are possible. The interferometer consists of the six telescopes which collect the light, vacuum light beam transport tubes, optical path length delay lines, beam management systems and beam combination systems. The Array is located at the Mount Wilson Observatory nearby Los Angeles, California, a site that is well known for excellent astronomical seeing, which makes it ideal for optical interferometry. The light pollution from the city does not effect the instrument, because of its small field of view, and because only bright stars are being observed. The CHARA array is built in a nonrenduntant Y configuration with two telescopes located along each of the three arms of the interferometer. The light from the telescopes is injected into vacuum tubes and then in to the central beam synthesis facility, an L-shaped building, which houses the delay lines for the optical path compensation. The beams combination is achieved with two instruments: "CHARA classic" and FLUOR. The "CHARA classic" is a pupil-plane IR beam combiner. FLUOR (the Fiber-Linked Unit for Optical Recombination) was used

at the IOTA interferometer on Mount Hopkins since 1995 and was then moved to Mount Wilson in 2003. In the Chapter 8.1.2 I will discuss more in detail the array and the "CHARA classic", which I use to measure the diameter of a sample of giant stars.

Chapter 3

Reducing interferometric data

The visibility is essentially the Fourier-transform of the brightness distribution of the source in the sky. If visibility measurements with many different baselines and their phases are obtained, an image of the object can be reconstructed. If only a few measurements of the modulus of the visibility are obtained, it is still possible to constrain the shape of the source. Thus a large number of visibilities measurements are only required in order to reconstruct a source of a complicated brightness distribution. For example if one knows that the source is a sphere, it is possible to determine its diameter from just one calibrated visibility measurement. Using three baselines it is possible to determine the separation and the position angle of a binary.

In this Chapter I summarise the data acquisition and reductions which leads to the determination of the interferometric observables in the case of the VLTI instrument AMBER, which I use in this thesis.

3.1 The VLTI-instrument AMBER

AMBER is one of the two VLTI instrument (see Chapter 2.2). It is a multi-beams combiner that works in the near-IR. In more details AMBER (Figure 3.1) combines the light coming from three different telescopes, using single-mode optical fiber in order to perform spatial filtering of the turbulent wavefront. The instrument can be used both with the 8-m UTs or with the 1.8-m ATs. Light is collected in three spectral bands J (1.25 μm), H (1.65 μm) and K (2.2 μm), and three different spectral resolution R= $\lambda/\Delta\lambda$=35, 1500, and 10000 are possible.

The first practical applications of single-mode fibers to carry and recombine the light was first proposed by Connes et al. (1987) with his FLOAT interferometer. This was a laboratory experiment that demonstrated furthermore with the IOTA interferometer the on sky feasibility of such instrument. Coude Du Foresto et al. (1997) demonstrated that the use of single-mode waveguides could increase the performance of optical interferometry, thanks to their property of spatial filtering, which change phase fluctuations of the atmospheric turbulent wavefront into intensity fluctuations. The effect of single-mode waveguide is to propagate only the part of the incoming electromagnetic wave projected on its first mode. As a result the wavefront at the output of the fiber is a perfect plane and the intensity profile is perfectly stable and deterministic, and can be calibrated in the data reduction process. The
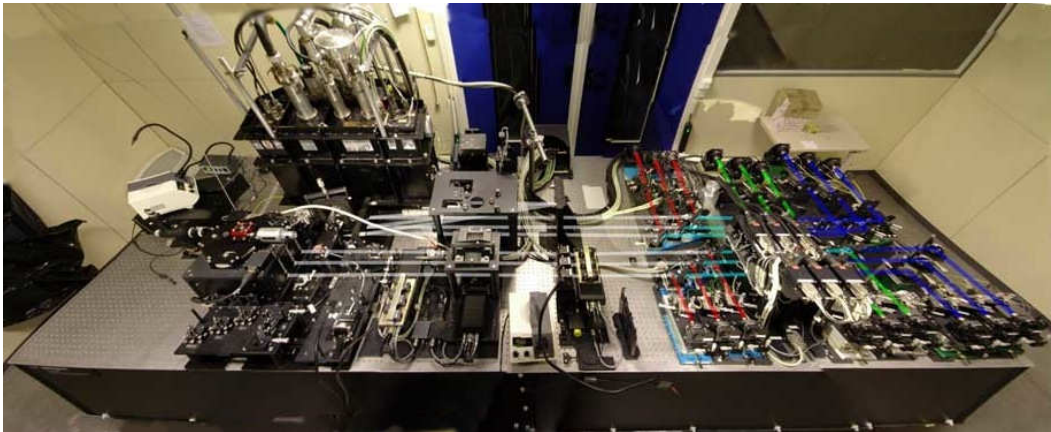
Figure 3.1:   *AMBER in the VLTI laboratory at Paranal. Beams from three telescopes enter the instrument from the left (light grey beams) and then travel to the recombination unit on the right. Before entering the fibers the beams are divided in the J, H and K band (red, green and blue rays, respectively).*

disadvantage in using optical fiber is that only a fraction of the light, namely the coupling coefficient, is entering the fiber. This coupling coefficient depends not only on the brightness source distribution, but also on the turbulence of earth atmosphere, which is characterised by the Strehl ratio.[1] In order to minimise light-loss entering the fibers, the telescopes of the VLTI are equipped with adaptive optics or tip-tilt corrector systems. The coupling coefficient has a strong impact on the estimated visibility, for this the fluctuations are monitored in real time thanks to dedicated photometric output.

3.1.1   Working scheme

Figure 3.2 shows schematically how AMBER works. It can be divided in three major steps. First, the incoming light is separated into the near-infrared J, H and K bands, and these separated light beams are injected into the J, H and K fibers. The beams are spatially filtered by the single-mode fibers that convert phase fluctuation of the wavefront into intensity fluctuation which are monitored. At this stage, a pair of conjugated cylindrical mirrors compress the output beams by a factor of 12. After the compression, these beams are injected in the entrance slit of the spectrograph. For each of the three beams a beam-splitter placed inside the spectrograph divides the light in two beams, one for the interference and the other for the photometric monitoring. The beam-splitter induces three different angles so that each photometric beam is imaged at a different location of the detector. These are called photometric channels and each of these is relative to the beam coming from one of the three telescopes. The remaining part of the light is overlapped, in pairs of two, on the detector image plane to form fringes. These light-beams selected for the interference are arranged so that they form at a fixed non-redundant setup of the pupil. This means that the ray of light are arranged in such a way that the three pairs of beam (A-B, B-C, A-C) each form at a fixed and unique distance, i.e., the distance between beams A and B is different from that between

---

[1]It is the ratio between the observed peak intensity at the detection plane of a telescope from a point source and the theoretical maximum peak intensity of a perfect imaging system.
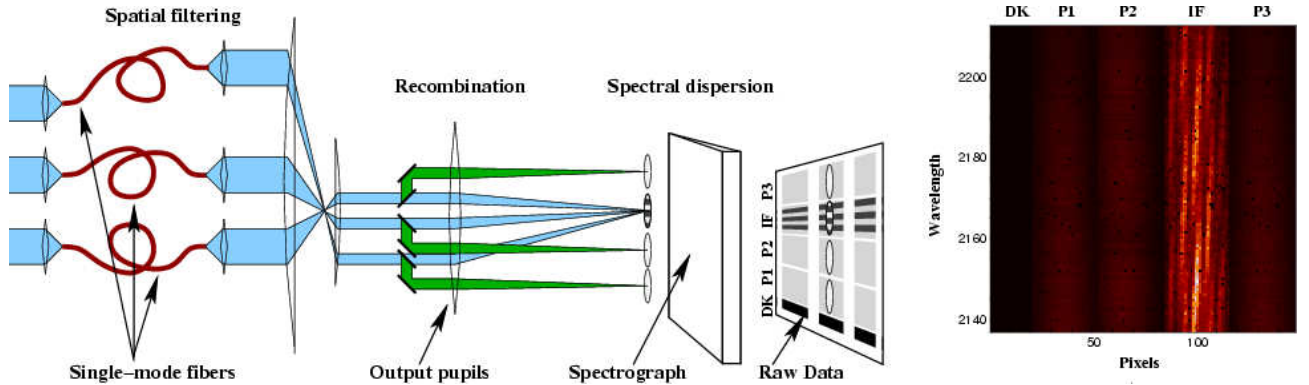
Figure 3.2: *Schematic layout of AMBER. The beams from the three telescopes are spatially filtered by the fiber (left). The outputs are then separated by a set of mirrors and prisms (centre), in two part one for the interference and one for the photometry (green rays in the picture). The photometric and interferometric beams are then spectrally dispersed and then recorded on the detector (right).*

B and C, and again different from that between A and C. These distances are fixed by the re-arrangement and for this independent from the pointing direction in the sky. In this way the fringe spacings corresponding to the three baselines, are always the same, avoiding the problem of overlapping fringes on the imaging device.

The interferogram and the photometric beams are then dispersed in wavelength with a spectrograph. Three configurations of the spectrograph are available: low resolution (LR) with R=35, medium resolution (MR) with R=1500 and high resolution (HR) with R=10000. The detector is an array of 512x512 pixels. The vertical direction is aligned with the wavelength direction. The first 20 pixel are always masked and thus do not receive any light. This part of the detector is used in order to measure the bias. As mentioned above, the three beams are separated into three photometric and one interferometric channel, which contains the interference signal. The 4 beams are dispersed and spread over four vertical areas on the detector. In summary the raw AMBER data consists of: 1) a dark column (noted DK) which contains masked pixels; 2) three columns, two following DK (P1 and P2) and one at the extreme right of the detector (P3), formed usually by 32 pixels, that are the photometric outputs. They record the photometric signal coming from each of the three telescopes; 3) a column (IF), the fourth, with the interferometric output. It shows the interference fringes arising from the recombination of the beams. The panel on the right of Figure 3.2 shows a raw-frame taken with AMBER. The interferometric information is in the channel marked with IF. The individual image that is recorded during the detector integration time (DIT) is called a frame. Usually one thousand frames are taken during one observation of a star. The resulting data are stored in a data-cube which is called "exposure".

3.2   Data reduction: theory and basic principles

Because the interferometric channel IF (Figure 3.2) carries the interferometric signal of all three baselines, we require a method that allows one to disentangle the signal so that the visibility measurements of the three baselines are obtained. For this we have to know the intensity of the light coming from the three telescopes which are in channel P1, P2 and

P3. We also require the so called P2V matrix which is derived in this section. AMBER as mentioned before works with the light coming from three telescopes. When only the ith beam is illuminated, the signal recorded in the interferometric channel is the photometric flux F^i spread out over an Airy pattern a_k^i which is the diffraction pattern of the ith output pupil weighted by the single-mode of the fiber, where k is the pixel number on the detector. Then, F^i results in the total source photon flux N attenuated by the total transmission of the ith optical train t^i, i.e. the product of the optical throughput (including atmosphere and optical train of the VLTI and the instrument) and the coupling coefficient of the single mode fiber:

$$F^i = N t^i \tag{3.1}$$

When two beams, i and j are brought to interference simultaneously, the interferometric component is superimposed on the photometric continuum. The coherent flux F_c^{ij} is the product of the photometric fluxes, weighted by the visibility:

$$F_c^{ij} = 2N\sqrt{t^i t^j} V^{ij} e^{i(\Phi^{ij} + \Phi_P^{ij})} \tag{3.2}$$

where $V^{ij} e^{i(\Phi^{ij})}$ is the complex modal visibility, Φ_P^{ij} is a phase that takes in account potential differential atmospheric piston. Strictly speaking the modal visibility is not the source visibility. The relation between the modal visibility and the source visibility can be found in Mege et al. (2003) and Tatulli et al. (2004), here I treat the complex modal visibility as the observable.

The interferometric signal recorded on the detector is given by the sum of the continuum and interferometric part, that is:

$$i_k = \sum_{i=1}^{3} a_k^i F^i + \sum_{i<j=1}^{3} \sqrt{a_k^i a_k^j} C_B^{ij} Re[F_c^{ij} e^{i(2\pi\alpha_k f^{ij} + \phi_s^{ij} + \Phi_B^{ij})}] \tag{3.3}$$

where ϕ_s^{ij} is the instrumental phase taking in account any possible misalignment and differential phase between the beams a_k^i and a_k^j. C_B^{ij} and Φ_B^{ij} are the loss of contrast and the phase shift due to polarisation difference between the two beams, respectively. Equation 3.3 thus describes the fringe pattern in the interferometric channel (IF). The first term of the equation 3.3 is called the continuum part (DC) and the second term the interferometric part (AC).

In order to model the interferogram, it is possible to re-write equation 3.3 in this way:

$$i_k = \sum_{i=1}^{3} a_k^i F^i + \sum_{i<j=1}^{3} [c_k^{ij} R^{ij} + d_k^{ij} I^{ij}] \tag{3.4}$$

where c_k^{ij} and d_k^{ij} are called the carrying waves, in analogy with the telecommunications data processing, of the signal, since they carry (in terms of amplitude modulation) R^{ij} and I^{ij} that are directly connected to the complex coherent flux. They can be written as:

$$c_k^{ij} = C_B^{ij} \frac{\sqrt{a_k^i a_k^j}}{\sqrt{\sum_k a_k^i a_k^j}} \cos\left(2\pi\alpha_k f^{ij} + \phi_S^{ij} + \Phi_B^{ij}\right) \tag{3.5}$$

$$d_k^{ij} = C_B^{ij} \frac{\sqrt{a_k^i a_k^j}}{\sqrt{\sum_k a_k^i a_k^j}} \sin\left(2\pi\alpha_k f^{ij} + \phi_S^{ij} + \Phi_B^{ij}\right) \tag{3.6}$$

and

$$R^{ij} = \sqrt{\sum_k a_k^i a_k^j \mathrm{Re}[F_c^{ij}]} \qquad\qquad I^{ij} = \sqrt{\sum_k a_k^i a_k^j \mathrm{Im}[F_c^{ij}]}. \tag{3.7}$$

The photometric flux determined using the photometric channel is P^i. If we know the ratio v_k^i between this flux and the DC component of the interferogram, through a calibration process, we can estimate the later using this formula:

$$F^i a_k^i = P^i v_k^i \tag{3.8}$$

We can now calculate the DC corrected interferogram through the formula:

$$m_k = i_k - \sum_{i=1}^3 P^i v_k^i \tag{3.9}$$

that can be written as:

$$m_k = c_k^{ij} R^{ij} - d_k^{ij} I^{ij} \tag{3.10}$$

This equation describes the linear connection between the pixels of the detector and the complex visibility. Written in matrix form this becomes:

$$\begin{pmatrix} m1 \\ | \\ m_{N_{pix}} \end{pmatrix} = \begin{pmatrix} .. & c_1^{ij} & .. & .. & d_1^{ij} & .. \\ | & : & | & | & : & | \\ .. & c_{N_{pix}} & .. & .. & d_{N_{pix}}^{ij} & .. \end{pmatrix} \begin{pmatrix} : \\ R^{ij} \\ : \\ I^{ij} \\ : \end{pmatrix} = \mathrm{V2PM} \begin{pmatrix} : \\ R^{ij} \\ : \\ I^{ij} \\ : \end{pmatrix} \tag{3.11}$$

In this equation it appears the V2PM matrix (visibility to pixel matrix), which contains information about the carrying waves, the Airy patterns of the fibers, the coding frequencies and the instrumental differential phases. Together with v_k^i, they entirely describe the instrument and once calibrated the pixels of the detector and the coherent flux are linearly correlated.

3.3   Calibration process

The calibration of the V2PM is carried out with an internal source located in the Calibration and Alignment Unit of AMBER (see Figure 3.1 in the bottom centre). The calibration consists of an acquisition sequence of calibration files. This sequence is summarised in Table 3.1 and explained hereafter. The first step consists in deriving the fraction of the flux measured between the interferometric and the photometric channels. This is done by opening just one shutter (i.e. light from one telescope, steps 1, 2 and 3 in the Table 3.1) and measuring with high accuracy the flux on the two channels, finding in this way the ratio v_k^i. The second step

Step	Sh 1	Sh 2	Sh 3	Phase γ_0
1	O	C	C	no
2	C	O	C	no
3	C	C	O	no
4	O	O	C	no
5	O	O	C	yes
6	C	O	O	no
7	C	O	O	yes
8	O	C	O	no
9	O	C	O	yes

Table 3.1: *Summary of the performed sequence for the AMBER calibration process. The first column is the number of the step of the calibration process. The second, the third and the fourth columns indicate if the shutter is opened (O) or closed (C). The last column indicates if the phase shift γ_0 is added.*

consists in the determination of the carrying waves c_k^{ij} and d_k^{ij}. This is done opening two shutters simultaneously (steps 4, 6, and 8) and for each pair of beams the interferogram is recorded on the detector. Such interferogram, corrected for its DC component, allows one to determine c_k^{ij}. Given the fact that we need two carrying waves for each baseline, we need to have two independent measurements of the interferogram. For this, the previous procedure is repeated introducing a known phase shift γ_0, close to 90 degree, using piezoelectric mirrors in the entrance of the beams 2 or 3 (steps 5, 7 and 9). To estimate the coherent fluxes R^{ij} and I^{ij}, which are at the basis of the whole AMBER observables, one has to invert and solve the equation 3.11. This is possible by performing a χ^2 linear fit with the coherent fluxes as unknown parameters. The solution is given by the equation:

$$[R^{ij}, I^{ij}] = P2VM[m_k] \tag{3.12}$$

with P2VM the generalised inverse of the V2PM matrix. P2VM means Pixel to Visibility Matrix since it allows a determination of the complex visibility from the interferogram recorded on the detector. Once R^{ij} and I^{ij} are determined, the squared visibility is derived by calculating the ratio between the squared coherent flux and the photometric fluxes. Using equations 3.1 and 3.2 the squared visibility is given by:

$$\frac{|F_c^{ij}|^2}{4F^i F^j} = \frac{R^{ij^2} + I^{ij^2}}{4P^i P^j \sum_k v_k^i v_k^j} = \frac{|V^{ij}|^2}{V_c^{ij^2}} \tag{3.13}$$

with $V_c^{ij^2}$ the visibility of the internal source that for the output pupil 1-3 is resolved. From this equation we can seen that the squared visibility of the observed target in the sky is weighed by V_c (the visibility of the internal source) that has to be cancelled out. This is possible doing the necessary atmospheric calibration observing a calibrator star of known visibility, close to the scientific target. Because the single frames are usually noisy, many frames are averaged in a data cube. Using the squared visibility with respect to the normal value is of great advantage because it allows one to better handle the problem of the random

differential piston. Considering also the detector and photon noise and averaging on a set of frames the squared visibility is given by:

$$\frac{|\overline{V^{ij}}|^2}{V_c^{ij^2}} = \frac{\langle R^{ij^2} + I^{ij^2} \rangle - Bias\{R^{ij^2} + I^{ij^2}\}}{4P^i P^j \sum_k v_k^i v_k^j} \tag{3.14}$$

where the $\langle\ \rangle$ indicates an average on the frames. This is the basic formula that is used in the data reduction to estimate the squared visibility of the fringes. The Bias present in this formula is the mathematical evaluation of the projection of the measurements error $\sigma(m_k)$ in to the real and imaginary axes of the coherent fluxes. Namely this Bias is the product of the squared $\sigma(m_k)$ for the coefficients of the carrying waves matrix. The error on the squared visibility can be derived from the 3.14:

$$\sigma^2(|\overline{V^{ij}}|^2) = \frac{1}{M} \left[\frac{\langle |C^{ij}|^4 \rangle_M - \langle |C^{ij}|^2 \rangle_M^2}{\langle |C^{ij}|^2 \rangle_M^2} + \frac{\langle P^{i^2} P^{j^2} \rangle_M - \langle P^i P^j \rangle_M^2}{\langle P^i P j \rangle_M^2} \right] |\overline{V^{ij}}|^{2^2} \tag{3.15}$$

with $C^{ij} = R^{ij^2} + I^{ij^2} - Bias\{R^{ij^2} + I^{ij^2}\}$ the coherent flux, and M is the number of frames averaged. This equation and eq. 3.14 are used for the determination of the squared visibility and its error in the data reduction. Due to the fact that AMBER works with three different baselines, measurements of closure phases are possible. The phase information of the fringes in this way is not completely lost and image reconstructions in some cases are also possible and could be performed (Le Bouquin et al. 2009; Kraus et al. 2009). By definition the closure phase is the phase of the so-called bis-spectrum B^{123} that is the ensemble average of the coherent flux triple product:

$$\overline{B}^{123} = \langle C^{12} C^{23} C^{13} \rangle \tag{3.16}$$

The closure phase then is:

$$\overline{\Phi_B}^{123} = atan \left[\frac{\mathrm{Im}(\overline{B}^{123})}{\mathrm{Re}(\overline{B}^{123})} \right] \tag{3.17}$$

The closure phase measured by AMBER might not coincide with the one of the object due to some bias in the internal calibration. For this reason the closure phase has to be calibrated observing a point source or a source of known diameter. Observations of a calibrator star just before or after the scientific target are of a fundamental important to estimate the two interferometric observables: the visibility and the closure phase.

3.4 Data reduction in practice

The individual frames are stored in a data-cube named exposure. An AMBER exposure is composed usually of 1000 frames each of only few ms DIT. The single frame contained in this data cube are composed by the interferogram plus the three photometric channels (see on the right of Figure 3.2), as explained above. Each exposure is stored in a fits (Flexible Image Transport System, Hanisch et al. 2001) file, which also contains information about the scientific target, the calibrator stars, the internal calibration etc. To extract the visibility and the closure phase from these frames a software package has been developed by the
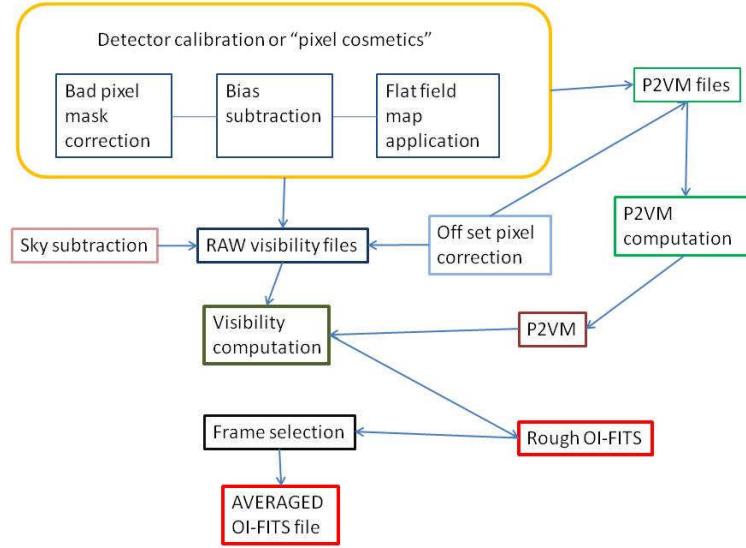
Figure 3.3: *Block diagram of the AMBER data reduction process.*

AMBER consortium. This software package consists of a library of C functions, called *amdlib*. This library can be used by various front-end applications. One of these makes use of the program language Yorick and is called *AmmYorick*. In this work I mainly used this software *AmmYorick* for all the data reduction steps. The block diagram in Figure 3.3 summarises the AMBER data reduction steps, that I will explain hereafter. The first part of the data reduction is centred around the calibration of the infrared CCD camera. Basically three files are need to do this: the bad pixel mask, the flat field and the bias. The bad pixel mask contains the positions of all the defective pixels on the detector and is updated every 6 months. All pixels that are flagged valid are converted to photoevent counts. The detector bias pattern is constant in time, but depends on the DIT and the size and the location of the sub-windows on the detector used. Thus, after each change of the detector setup, a new pixel bias map is measured prior to the observations. This bias map is made by averaging a large number of frames acquired with the detector facing a cold shutter. The bias is then simply subtracted from all the frames. After this correction, the detector may still be affected by a variable bias, which is corrected using the masked column of pixel (the DK column). Pixel-values are then converted to photoevent counts by multiplying by the pixel's gain which is constant on the detector. The frame are then corrected by a flat field map acquired during laboratory test. After this, the V2PM is determined, which is fundamental for the data-reduction. The *AmmYorick* function for this task is *amdlibComputeP2vm*. This function processes the 9 files acquired in the calibrations sequence described in the previous paragraph, computing the v_k^i coefficients and the carrying waves c_k^{ij} and d_k^{ij} of the V2PM matrix (equation 3.11). The result is stored in a fits file, which for historical reasons is called P2VM. The P2VM matrix has to be computed every time the instrument configuration is changed. This means that the set of files necessary to compute the P2VM, is acquired every time there is a readjustment in the setting of the instrument. The computation of visibility
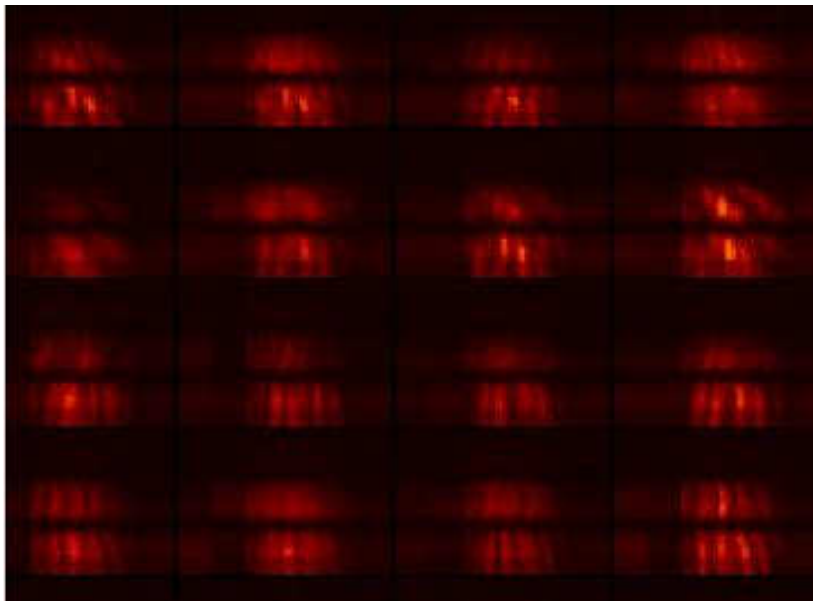
Figure 3.4: *Example of the visibility variations when the fringe tracker FINITO is not used. Shown here is a set of 16 frames of the same exposure of the young binary star HD113449 analysed in this thesis. The star has a magnitude in the K band of 5.5.*

is done using the function *amdlibComputeOiData*. This function, using a valid P2VM file, calculates the visibility for each frame of a data-cube. The sequence of reduction steps made by the function *amdlibComputeOiData* can be summarised as follows:

1. invert the V2PM matrix;

2. extract raw visibilities;

3. correct for biases, compute de-biased V^2 visibilities;

4. compute closure phase;

5. compute spectra;

6. write the OI-fits file

The OI-fits (Optical-Interferometer fits, Pauls et al. 2005) is a standard file format for the storage of optical interferometric data. In the OI-fits file, together with the measured object visibility and the closure phase, all the information about the observational setup, like baseline length and orientation, resolution of the spectrograph, etc are stored. A frame selection usually is done on the final OI-fits file to obtain averaged V^2 visibilities. One of the selection criteria is based on the signal to noise ratio of the frames, where only the frames with the highest S/N are considered for the average. Other selection criteria are based on the fringe contrast and on the estimated piston. The selection of the best frames in calculating the average V^2 is always required. This because the fringe contrast changes frames by frames, when FINITO is not used (see for example the Figure 3.4). The average of the best frame procedure is usually done both on the scientific target and on the calibrator stars. In order

to derive the calibrated squared visibility the transfer function of the instrument is required. This is derived by comparing the observed visibility of the calibrator star with the expected one. Usually unresolved stars, that means for the VLTI stars with an angular diameter smaller than 1 mas, or stars of known angular diameter, are used as calibrators. Once the visibility has been measured for a certain baseline and wavelength the squared transfer function (tf^2) is given by:

$$tf^2 = \frac{\text{V}^2_{cobs}}{\text{V}^2_{th}} \tag{3.18}$$

with V^2_{cobs} the squared visibility of the calibrator star measured by AMBER and V^2_{th} the theoretical calculated visibility using the square of the equation 2.7 with the known diameter. When the calibrator star is not resolved, V_{th}=1 and the tf^2 is simply V^2_{cobs}. The tf^2 of the instrument is then derived and calibrated visibility can be computed for the science target with:

$$V^2_{scal} = \frac{\text{V}^2_{\text{sobs}}}{tf^2} \tag{3.19}$$

with V^2_{scal} and V^2_{sobs} the squared calibrated visibility and the squared observed visibility of the scientific target, respectively. These two steps are performed in *AmmYorick* by the function *amdlibDivideOiData*.

Chapter 4

Testing evolutionary tracks of PMS stars. I: Introduction

In here I will introduce the scientific case of the thesis, demonstrating the power of optical interferometry applied to stellar physics. The aim of the thesis is to develop new methods in order to test and calibrate evolutionary tracks on the basis of interferometry.

4.1   Application of optical interferometry to stellar physics of young stars

In this thesis I use the power of the optical interferometry to resolve astronomical objects at high angular resolution to derive basic physical parameters of young and evolved stars in order to test the theory.

In the case of young stars I derive the masses of the components of a binary combining spectroscopic observation with optical interferometry. Deriving dynamical masses of Pre-Main Sequence (PMS) stars is of fundamental importance. This is because up to now the only way to estimate masses of young stars is to compare their position in the Hertzsprung-Russell (HR) diagram with respect to the evolutionary tracks for PMS stars. Evolutionary tracks are theoretical curves in the HR diagram showing the evolutionary paths of young stars of fixed mass, from the first phases of their life to the main sequence. The problem however is that tracks published by different authors show large differences, demonstrating that it is important to test them. In some cases the value found for the mass of a young star, can in fact differ by about 50-60% from one set to another (see Figure 4.1 for example). The reason for this is that different authors use different input physics, like the treatment of convection, magnetic field, opacity etc. The lack of knowledge which models to choose, is thus a severe problem for the whole field of star-formation. It is thus important to obtain a number of dynamical masses to test the models and to select the one that fits the observations best.

There are different approaches that allow us to measure the masses of young stars. The best way for determining the masses is to use binary stars. It is possible to identify different kinds of binaries depending on how we detect them. The visual binaries are systems where both components are resolved by direct imaging. In many other cases the angular separation of the two stars is too small to allow them to be separated visually. The binary nature
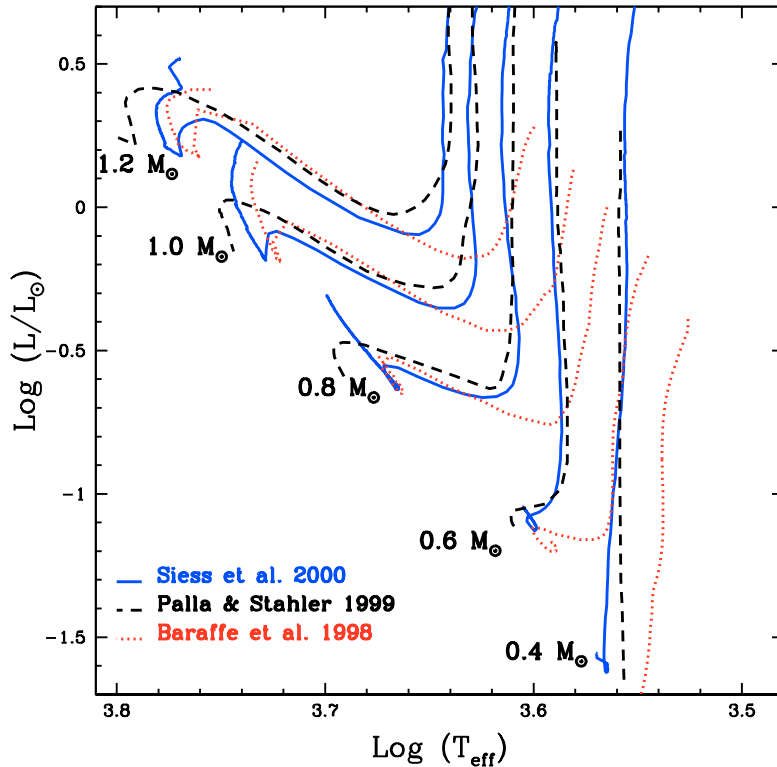
Figure 4.1: *Three of the most used sets of evolutionary tracks (Siess et al. 2000; Palla & Stahler 1999; Baraffe et al. 1998) for PMS stars. The differences between the different models are particularly large for low mass stars (i.e. $\leq 0.6\ M_\odot$)*

then is detected by other methods. Short period binaries can be detected spectroscopically. If both components have about the same brightness and if the separation in velocity space is large, the spectral lines of both components are well separated. Such systems are called SB2-systems. If one component is much fainter then the other, only one set of spectral lines is seen. Such systems can nevertheless be detected by means of RV-measurements (SB1-systems), since the RV of the primary component varies periodically. Dynamical masses of stars in binary systems can be determined using various methods that are summarised as follows:

1. The masses of the stars of an eclipsing SB2-system are derived by combining the RV-curve and the light-curve of the transit. Using this method it is possible to determine the masses and the size of both stars with typically accuracy of 2%.

2. The masses of the stars of a non-eclipsing SB2 system can be derived by combining the RV-measurements with astrometric measurements. Only relative astrometry is needed, i.e. angular separation and position angle of the two components. The determination of the masses using this method is distance independent.

3. The masses of the stars in a SB1-system can be derived if it is converted into an SB2-system. This is often possible by means of high resolution IR spectroscopy. Once the

SB1-system is converted in a SB2-system it is possible to proceed as in item 2. This is the method that I use in this thesis to determine the masses of a young SB1-system.

4. The masses of the stars in a SB1 system can be derived by combining RV analysis with relative astrometry. I this case the masses can be determined if the distance is known. The mass ratio of the system, in fact, has to be derived from the luminosity ratio assuming a mass-luminosity relation.

5. The total mass of the system of a visual binary is determined by means of absolute astrometry .

At first glance eclipsing SB2 systems seem to be the best candidates for testing evolutionary tracks, because the masses are determined with high precision together with stellar radii. Unfortunately the components of these systems are usually so close to each other, that mass exchange between the two components is possible. The stars through this mechanism become active and the original mass of the "birth" is not preserved, making the stars inappropriate to test the evolutionary tracks. The luminosity of both components can also be altered by the activity connected with the interaction. Eclipsing PMS binaries are also very rare. Up to now only four of these systems are known (Casey et al. 1998; Covino et al. 2004; Stassun et al. 2004, 2008).

In the remaining cases the binary stars which can be analysed dynamically are too close to be resolved by the normal telescope to perform relative astrometry. The distance to the nearest star-forming region is so large that binaries that could be resolved with AO-systems on 8 m-class telescope have orbital periods of many decades, or even centuries. Thus, only optical interferometry has the power to resolve binaries in nearby star forming regions with orbital periods down to a year. With the current resolution of the VLTI, it is for example possible, to resolve binaries with separation of less than 0.6 AU (corresponding to an orbital period of ~ 120 days for systems with $M_1 = M_2 = 1$ M$_\odot$) for distances ≤ 150 pc. The masses of two stars in a binary system are thus obtained by combining relative astrometry determined using an interferometer and RV-measurements. Boden et al. (2005) applied this technique to the young SB2-system HD98800 B using the Keck Interferometer. In this work the authors derived the masses of both components with an accuracy of $\sim 8\%$. The masses derived do not fit to the tracks published by Siess et al. (2000) and Baraffe et al. (1998) for solar metallicity ([Fe/H]=0). However an agreement can be achieved if the tracks computed with [Fe/H]=-0.3 by Siess et al. (2000) and [Fe/H]=-0.5 by Baraffe et al. (1998) are used. Recently Laskar et al. (2009) found that the metallicity of HD98800 B could be as low as [Fe/H]=-0.20, but these authors state that additional constraints on the system and on the modelling are needed. An alternative explanation would be that the radiative core in PMS forms at an earlier stage of the evolution than in the models. Clearly more observations are needed.

In order to derive dynamical masses for a large number of young stars a sample of targets useful for interferometric observations was collected by Guenther et al. (2007), in which I participated. In this article 13 young spectroscopic binaries were listed, which have a separation between 4 and 50 mas. These stars have magnitude in the range between the 7th and 10th in the K band, which corresponded to the expected performance of the VLTI at

the time the survey was started. However after the commissioning of the VLTI instrument AMBER the limiting magnitude had to be revised to 7 mag in the K band. Future upgrades of the VLTI will greatly improve the sensitivity, making the observations of all the targets in our sample possible. This will allow us to determine the masses for more than 20 young stars.

The aim of this thesis is to show that it is possible to determine the masses of a young binary by combining VLTI data and RV-measurements. Considering the current performance of AMBER, I choose to observe the relatively bright young binary HD113449. This object was found in a survey done with HARPS (High Accuracy Radial velocity Planet Searcher) on a sample of young stars to search for extrasolar-planets (Guenther, Cusano & Esposito, in preparation). Given the brightness K=5.5 mag, it is possible to observe this binary with AMBER. By combining AMBER data and RV-measurements, I estimate the masses of the components of the young binary HD113449. A first test of the PMS evolutionary tracks is thus performed and presented in this thesis. The details of how the masses of the HD113449 components are determined are given in Chapter 5 and 6.

4.2 PMS evolutionary tracks

As mentioned above different groups calculate evolutionary tracks using different input physics and thus the tracks are different. The most important differences are in the opacity sources, in the treatment of convection and interior, and in the atmospheric boundary conditions. Figure 4.1 shows for a comparison the evolutionary tracks published by Siess et al. (2000), Palla & Stahler (1999) and Baraffe et al. (1998), for stellar masses between 0.4 and 1.2 $M_\odot$. These tracks are the most commonly used in the study of young stellar objects. Systematic differences are seen, particularly for young ages and small masses. The differences between the tracks are larger in terms of temperature than in luminosity. This is mostly due to the different treatment of convection in both the atmosphere and the stellar interior. Given the complexity of a realistic description, the convection is usually modelled using the Mixing Length Theory (MLT, Böhm-Vitense 1958). The basic idea of the MLT is that "bubbles" move from a region of a higher heat content to a region of lower heat content. This means that the bubbles transport convective heat through the fluid. The bubbles rise in the star for a distance l, called the *mixing length*, before they lose their identity and merge with the surrounding fluid. Usually l is measured in terms of the pressure scale height H_p, which is equal to the distance over which the pressure decrease by a factor e. Models of larger mixing lengths (more efficient convection), typically, predict hotter tracks and yield lower masses for a given position of a star in the HR diagram. The exact choice of the mixing length is a large uncertainty in the current models.

The uncertainties in the models also arise from the lack of knowledge of the opacity of some elements and molecules, like the TiO and the H_2O molecules. The line list of the transitions and the oscillator strengths of these two molecules, which are important absorbers in the optical and in the near-IR respectively, is still incomplete. This affects the modelling of the atmosphere of the PMS stars, resulting in incorrect values of the luminosities and temperatures of the stars.

Another important source for the differences of the tracks published by different authors

is the setting of the initial conditions. In all PMS models the initial configuration is a fully convective object starting its contraction along the Hayashi line (Hayashi 1961) from an arbitrarily large radius. The evolution starts with the central ignition of the deuterium at $\sim 5 \cdot 10^5$ K. Studies of the protostellar collapse and accretion phases show that such initial condition are highly simplified and low-mass objects can form with significantly smaller radii. To solve these substantial uncertainties one should use complete models that take also the protostellar collapse into account.

I will now briefly describe the three most commonly used sets of evolutionary tracks for PMS stars. These are also discussed and tested in this thesis.

4.2.1   Palla and Stahler

The Palla and Stahler models cover a mass range between 0.1 and 6 $M_\odot$, with a stellar abundance of Y = 0.28 and Z = 0.02. For the convection they use the MLT with a mixing length parameter $l = 1.5$ H_p. The opacity used is a Rosseland mean opacity, where the opacity depends both, on the composition of the gas, and its thermodynamical state. For the equation of state (EOS) Palla and Stahler use the information given in Pols et al. (1995), where the EOS is based on the principle of Helmholtz free energy minimisation and heavy elements up to the Fe are considered. The grey approximation is used which means that the opacity does not depend on the frequency of the radiation considered. The calculations explicitly include a "birth-line" an initial mass-radius relationship that marks in the HR diagram the region where the transition between the protostellar and the PMS phase happens.

4.2.2   Baraffe et al.

The Baraffe et al. (1998) models of young stars cover the mass range from 0.035 to 1.2 $M_\odot$, and are computed for two helium abundances Y = 0.275 and Y=0.282, with Z = 0.02. The authors use opacities tables from Alexander & Ferguson (1994) and Iglesias & Rogers (1996). As for Palla & Stahler, the convection is modelled by using the MLT, calculating three different set of tracks for: l =1.0, 1.5 and 1.9 H_p. The EOS used is from Saumon et al. (1995). The only elements considered in the calculation are hydrogen and helium. These models make use of the non-grey atmospheres published by Hauschildt et al. (1999), which include molecular opacity sources, like TiO and H_2O and dust grains.

4.2.3   Siess et al.

The evolutionary tracks published by Siess et al. (2000) cover a mass range between 0.1 and 7.0 $M_\odot$. The abundances used in this work are Y = 0.288 and Z = 0.0189. The MLT is fixed to $l = 1.6$. Like Baraffe et al., Siess et al. also use Alexander & Ferguson (1994) and Iglesias & Rogers (1996) opacities and a modified EOS from Pols et al. (1995). These models attempt to include observed properties of the stellar atmosphere as outer boundary conditions, using data from Plez (1992) and Kurucz (1991).

Chapter 5

Testing evolutionary tracks of PMS stars. II: Methods and data reduction

The best way to test the evolutionary tracks is to determine the masses of a number of young binary stars. The first step of this project is to find a number of suitable candidates. Suitable binaries must have orbital periods from few hundred days to few years. In here I present the result of a survey carried out in order to identify a suitable sample of binaries. The spectroscopic observations are presented in the first part, together with the method used to derive temperature and luminosity for two SB2s. In the second part, the interferometric observations of HD113449 and the method used to derive the orbital parameters are presented.

5.1   The young binaries survey

The age and the masses of young stars are usually derived from evolutionary tracks. For all studies of star formation it is thus essential to test and calibrate the tracks. In order to do this, the masses, luminosities and temperatures of a few young stars have to be derived. This can be done by studying binary stars. Determining the masses of young visual binaries however is unsuitable, because most of these stars have distances of the order of 100 pc, which means that binary with separations of a few arcsec have orbital periods of centuries. Eclipsing binaries are not suitable to test the tracks, because it is possible that mass-exchange has happened. Additionally eclipsing binary are very rare. The best objects for testing the tracks are binaries with orbital periods between 0.2 and 3 years. The stars in these systems are well separated so that mass-exchange is unlikely and their orbital periods are short enough to determine the masses in a reasonable amount of time.

The project is feasible within a few years, if VLTI observation and RV measurements are combined. Spectroscopy alone can not be used to estimate the masses of the single components in a binary. For SB1-systems only the mass function $f(M) = \frac{(M_2 \sin i)^3}{(M_1 + M_2)^2}$ can be derived from the RV-measurements, with M_1 and M_2 the mass of the primary and of the secondary, respectively and i the inclination of the orbit to the line of sight. SB2 systems, instead, allows one to determine the mass ratio of the two components and the single masses

times sin$i$. Since interferometric measurements allows one to determine the inclination the true masses of the stars are derived. The first step however is to identify binaries with orbital period of a few years which can be resolved with the VLTI. The survey was carried out by Guenther et al. (2007) and myself. Before the start of this survey in 1998, only three PMS-spectroscopic binaries with orbital periods longer than 50 days located in nearby star-forming region were known (Mathieu 1994). For this reason a search for long-period binaries, suitable for VLTI observations was needed. For the survey known PMS stars brighter than 10 mag in the K band were selected. Visual pairs with a separation of $\leq$ 10 arcsec and stars with v sin $i \geq$ 50 km/s were excluded, because they would make RV-measurements very difficult. Observations were carried out for more than 7 years on a sample of 122 late-type PMS stars in the southern hemisphere. These stars all belong to the Chamaeleon (Cha), Corona Australis (CrA), ρ Ophiuchi (Oph), Lupus (Lup) and Scorpius Centaurus (SC) star-forming regions. The distances of these associations are between 120 and 170 pc, with ages that go from 1 to 30 Myr.

5.1.1 Observations and data reduction

All 122 stars were observed with the ESO Echelle spectrograph FEROS (Fiber-fed Extended Range Optical Spectrograph). FEROS was operated up to October 2002 at the ESO 1.5m-telescope and was then moved to the MPG/ESO-2.2 m telescope. The spectra cover the wavelength region between 3600 and 9200 Å, with a resolving power of $\lambda/\Delta\lambda = 48000$. On the 1.5 m telescope the entrance aperture of the fiber had a projected diameter of 2.7" on the sky, while at MPG/ESO 2.2 m telescope 2.0". As long as FEROS was mounted at the ESO 1.5 m telescope exposure times were set so that a S/N better than 30 was achieved. The exposure times were between 5 and 45 minutes. Since the performance of FEROS dramatically improved when the instrument was moved to the 2.2 m, the S/N went up to typically 50, although we shortened the exposure times. The standard FEROS data reduction pipeline was used for bias subtraction, flat-fielding, scattered light removal, Echelle order extraction and wavelength calibration of the spectra.

When measuring the radial velocity of stars, the question arises as to whether it is better to use several templates of different spectral types or only one template. I tried out both methods using the stars HR3862 (spectral type G0), HR6748 (G5), HR 5777 (K1), HR5568 (K4) and HR 6056 (M0.5) as template. The advantage in using templates of different spectral types is that the spectrum of the template always matches the spectrum of the target well. The disadvantage is that different templates have different RV. One has to determine the RV of each template to a high accuracy. By using just one template I avoid this problem. In this way I just have to determine the RV of one template. This speeds up the detection of binary candidates, because a star that has a RV that is very different from the stars of that region is either not a member or an SB1-system. This approach is used for the HARPS survey for extra-solar planets of F, G and K stars, where an accuracy of 1 m/s is achieved (Lovis et al. 2005). As template I choose the K1 star HR 5777, because is bright (m$_v$ = 4.6) and its absolute RV is well determined (+49.1 ± 0.06 km/s, Murdoch et al. 1993). To measure RV, I split the spectrum into six wavelength regions which are practically free of stellar emission lines and virtually free of telluric lines. The wavelength region are: 4000 to 4850 Å, 4900 to

5850 Å, 5900 to 6500 Å, 6600 to 6860 Å, 7400 to 7500 Å and 7700 to 8100 Å. For each of the wavelength band, I obtained the RVs separately and then averaged these 6 values. The errors in the RV measurements of the PMS stars are determined from the variance of the RV values of the individual spectral regions. For many stars, I could use only the first three regions, because the S/N ratio of the other regions is too low. In such cases I used always the same regions for the same star.

In order to determine the accuracy of the method, we obtained 31 spectra of HR 5777 spread out over the whole observing campaign. These spectra were analysed in the same way as the spectra of our targets. That is, I used one spectrum of HR 5777 as the template and cross-correlated the spectrum with all other spectra taken of HR 5777. The absolute RV of the template was determined by cross-correlating it with the Fourier transform spectrum of the sun, which was re-binned to the same resolution as the FEROS spectra. From this analysis the RVs of HR 5777 are in in perfect agreement with the published RV (49.12±0.06 km s^{-1}, Murdoch et al. 1993). The intrinsic uncertainty of our measurement derived from this analysis results in ± 0.15 km/s. The uncertainty of the RV measurements of the PMS stars, as determined from the variance of the RV measurements of the individual spectral regions, are usually larger than those of HR 5777 due to the fact that PMS stars are very active.

The results of this survey are presented in Chapter 6.1.

5.2   Physical parameters of the SB2s

A first test of the evolutionary tracks can be done comparing the mass-ratios determined from the spectroscopy of SB2-systems, with the mass-ratios derived by the evolutionary tracks. To place the SB2 components on the HR diagram and estimate the mass ratio from the tracks, one needs to determine both their temperature and luminosity. In this section I will describe how the physical parameters of two young SB2-systems, found in the FEROS survey (Guenther et al. 2007) are derived.

The first step is to derive the temperatures of the two components. I determined the temperatures of the primary and of the secondary of the 2-SB2 systems by fitting template spectra from a library. The best fitting template is identified using the minimum chi-square algorithm. The temperatures are then derived by converting the spectral types determined into temperatures by using the conversion table given in Pickles (1998). Spectra of young single star from the FEROS survey were chosen (Guenther et al. 2007) as templates. This means that the template spectra have the same resolution as the spectra of the binaries. I chose from the 80 single stars only weak-lined T-Tauri stars, which have no veiling[1] and have equivalent width of the Hα smaller than 10 Å. The stars having these properties are 28 out of the total. The spectral types of the template spectra range from G3 to M3. The 28 spectra mixed together gave a total of 784 combined spectra. Figure 5.1 shows as an example the best fitting template spectrum and the observed spectrum of RXJ 1559.2-3814. The match between the two spectra is very good.

I then determined the contribution to the total flux at the continuum of each components

---

[1]The veiling is the filling of some photospheric lines by the emission of non-photospheric sources.
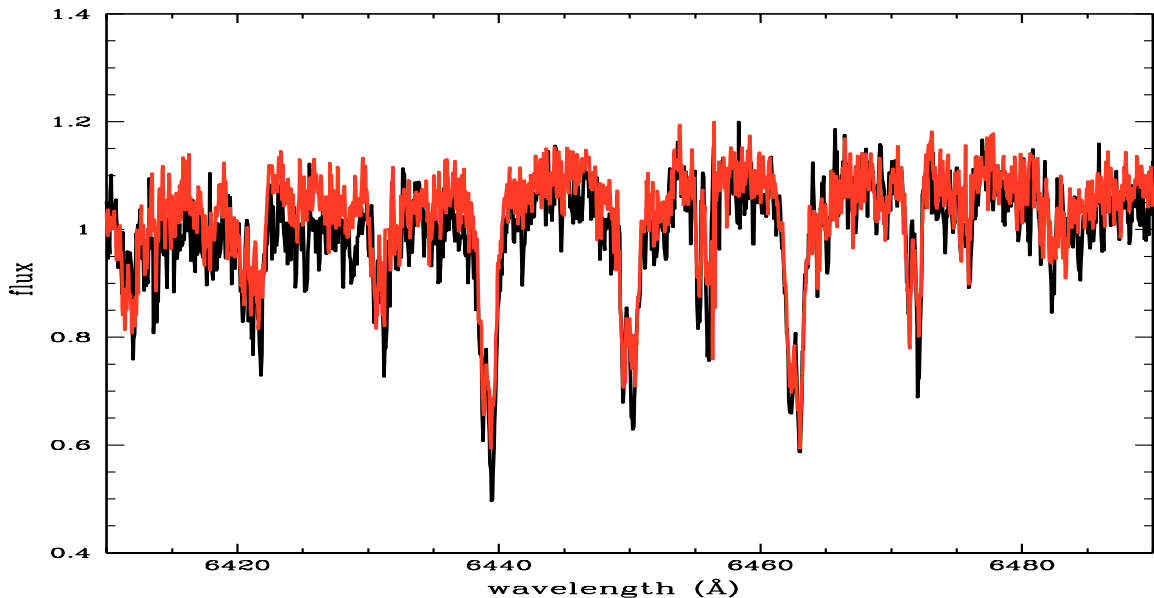
Figure 5.1: *Spectrum of RXJ 1559.2-3814 (in black), together with the best fitting template spectrum (in red), given by the combination of a K7 and M0 star.*

of the binary system. The ratio of the fluxes is derived from the ratio of the equivalent widths (EWs) of the lines visible for both components. For each of the lines measured, the strength of the lines for stars of different temperature was taken into account. One possible source of errors of this method is the determination of the temperatures of the two stars. This is because the EW of the lines depends on temperature. In order to estimate the error I used the best fitting template, the second and the third. For the analysis I used the wavelength region from 5900 to 6500 Å. I derive the bolometric luminosity of the single components by using the measured flux ratio, the V-magnitude of the object and the bolometric corrections from Pickles (1998). Finally it is possible to place the stars into the HR diagram and compare the mass-ratio of the stars with the mass-ratio derived from the tracks. The results of this test are presented in Chapter 6.3, as a first test of the tracks.

5.3   The young binary HD113449

In a survey to search for exo-planet around young stars, I found a very interesting spectroscopic binary bright enough to be observed with AMBER. This object is HD113449. HD113449 is located at a distance of 21.7 ± 0.4 pc (van Leeuwen 2007) and belongs to the moving group AB Doradus (Zuckerman et al. 2004). The presence of lithium indicates that it is a young object. The abundance of lithium implies an age for HD113449 of the order of the Pleiades (152 ± 16Myr, Barnes 2007).

Observations of HD113449 were carried out with HARPS for more then 2 years covering three full orbital periods. The orbital period is 216 days. The HARPS spectra cover the wavelength region from 3780 to 6910 Å at R=115.000. The HARPS pipeline is used in order to measure the RV of this star, from which I solved the SB1-orbit (Figure 5.2). The

Parameter	Value
P	215.96 ± 0.11 d
T_0[HJD]	2450174.9 ± 0.1
γ	-1.98 ± 0.02 km s^{-1}
K_1	13.03 ± 0.02 km s^{-1}
e	0.270 ± 0.005
ω	$117.2 \pm 0.5^{\mathrm{o}}$
$a_1\sin i$	0.249 ± 0.001 AU
f(m)	0.0442 ± 0.0003 M$_\odot$

Table 5.1: *Orbital elements of HD113449*

spectroscopic orbital parameter are given in Table 5.1. The errors of the orbital parameters are very small due to the high precision of HARPS for measuring RV combined with the high amplitude of the RVs variations. From the analysis of the HARPS spectra, I determined the spectral type K0 for the star, in good agreement with the literature (López-Santiago et al. 2006; Gray et al. 2003; Gaidos et al. 2000). The determination of the spectral type is done comparing one of the spectra of HD113449 with a library of 1.500 standard spectra. This procedure is similar to the ROTFIT code described by Frasca et al. (2003). The primary is relatively slowly rotating (P$_{rot}$=6.47 days, Barnes 2007) and has a solar-like metallicity with [Fe/H]=-0.06 (Gaidos & Gonzalez 2002).

The secondary of the SB system is not visible in the HARPS spectra. The amplitude of the RV-variations (see Figure 5.2) indicates that the secondary is most likely a late K or early M stars. Because the brightness-difference between K and M-star is much smaller in the infrared (IR) than in the optical, I used the high-resolution IR spectrograph CRIRES, to detect the lines of the secondary. This instrument has a resolution of R=80.000. One CRIRES spectrum of HD113449 was taken in service mode the night between the 1st and 2nd of January 2008, in the wavelength region between 22360-22930 Å. The spectrum was reduced, using standard procedure. The spectrum clearly shows the spectral lines of the A and B components (Figure 5.3). With just one CRIRES spectrum I was able to convert the SB1-system into an SB2-system. I derived the relative velocity of the two components, using the phase of the orbit of the primary when the CRIRES spectrum was obtained (phase=0.953). At this phase the RV velocities of the A and B component are v$_1$=14.1 $\pm$ 0.2 Km/s and v$_2$=-21.1 ± 0.8 Km/s, respectively. These values give a mass-ratio of q=0.58 $\pm$ 0.03. The CRIRES spectra allowed us to estimate the spectral type of the secondary, by fitting the observed spectra to a library of stars of known spectral type observed with CRIRES. The best match is obtained for an M0V. The error is one subclass.

5.3.1 AMBER observations of HD113449

In order to complete the determination of the masses of the two components of HD113449, interferometric observations are needed. HD113449 is bright enough to be observed with AMBER. The brightness of HD113449 is H=5.674 $\pm$ 0.038 mag and K=5.509 $\pm$ 0.023 mag (Skrutskie et al. 2006). Observations of HD113349 were taken in service mode the night
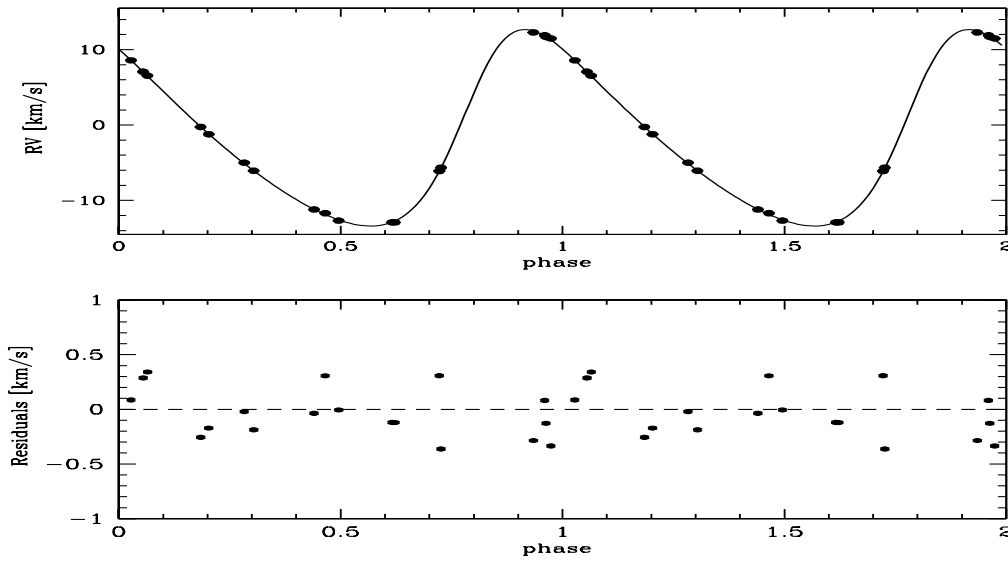
Figure 5.2: *Phase-folded RVs measurements of HD113449 taken with HARPS. The continuum line is the orbit found with a period of 216 days. The residuals, shown in the bottom of the picture, indicate the high quality of the orbital solution found.*
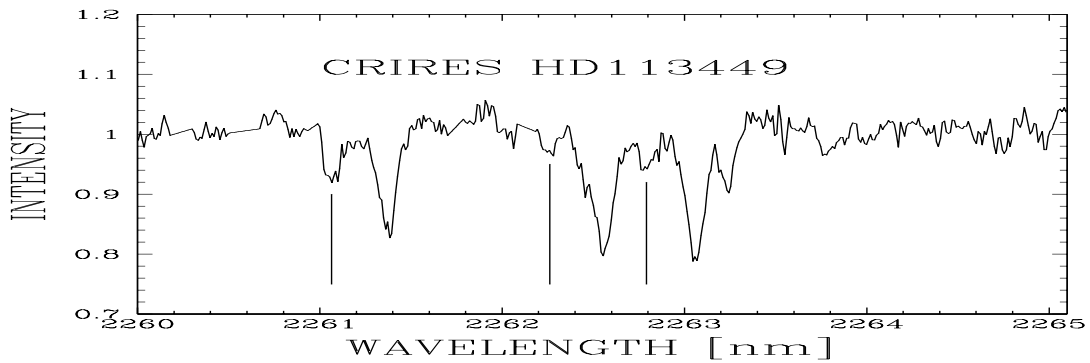
Figure 5.3: *Small part of the CRIRES spectrum of HD113449. The lines of the B component are clearly visible (marked by vertical lines).*

between the 20th and 21st of March 2008. This night corresponds to the phase 0.70 of the orbit. The UTs were used, because the star is too faint for the ATs. The fringe tracker FINITO was not used because the star is too faint for this instrument. AMBER was used in the low resolution (LR) mode. This mode gives spectral dispersed fringes in the J, H and K band (1.460-2.540μm), with a resolution R=35. The telescope used were the UT2, UT3 and the UT4. This telescopes configuration was chosen in order to give an optimal coverage of the uv-plane. Table 5.2 summarises the baselines used. Figure 5.4 shows the configuration used, and the uv coverage of the observations. To resolve a binary, it is of fundamental importance to choose a triangular disposition of the telescopes. This is because the visibility has a sinusoid shape in the uv-plane, oriented in the direction of the angular separation. HD113449 was observed for 45 minutes with AMBER, resulting in 6 exposures of

Telescopes	Baseline (m)	Position Angle (degree)
UT2-UT3	46.635	40.082
UT3-UT4	62.463	110.803
UT2-UT4	89.443	81.321

Table 5.2: *Baselines used for the AMBER observations of HD113449. The position angles are measured respect to the North direction clock-wise.*

1000 frames each. A calibrator star was observed shortly before HD113449. This calibrator is HD111998 and is located at a distance of 3.5 degrees from the science target. HD111998 is a single F5V star with magnitude H=5.082 and K=4.993. The angular diameter of HD111998 is ~ 0.37 mas. This was derived by using the relation for main-sequence stars between the spectral type and the radius given in Schmidt-Kaler (1982), and considering the distance of 32.5 pc (van Leeuwen 2007). With an angular diameter of 0.37 mas the calibrator star is certainly not resolved by the VLTI. HD111998 was observed following the same acquisition procedure of the science target.

5.3.2   Data reduction

The set of data consists of 6 exposures each containing 1000 frames, both for the scientific target and for the calibrator. These data were reduced using a dedicated software package called *ammyorick* (see Chapter 3.4). The first step of the data reduction was the computation of the P2VM, which allows the conversion of the CCD pixel counts into the coherent flux. This was done by processing the internal calibration files with the command *amdlibComputeP2vm*. Once the P2VM was done I calculated the visibilities for each of the 1000 frames in the 6 exposures for the calibrator and for the science target. This was done using the command *amdlibComputeOiData*. Because of the atmosphere of the earth, the fringes are affected by random atmospheric motions. For this reason I selected the best frames in each exposure and then I calculated the averaged visibilities for each wavelength in the H and K band. The star was too faint in the J band so that it was not possible to obtain visibilities in this wavelength regime. For this reason the J band was not used in the data reduction (see for example Figure 5.5, the horizontal black strip on the top is the J band). It turned out that the quality of the data improves if only the best 20% of the frames is kept in each exposure. As selection criterion I used the S/N-ratios of the single frames. This selection and average was performed using the procedure *amdlibPerformFrameSelection*. The result is a set of 6 files for both the science and calibrator star, with the averaged visibilities in the H and K bands. For each of these file the values of the squared visibilities in the H band are 11, each relative to a wavelength in the range from 1.56 to 1.87 μm, with a bin size of 0.03 μm. In the K band the squared visibilities measured are 14, relative to the wavelengths between 1.97 and 2.40 μm with a bin size of 0.03 μm. Finally I converted the raw squared visibilities of HD113449 in calibrated visibilities. For this step I used the line command *amdlibDivideOiData*, which derives the transfer function of instrument, dividing the observed visibility of the calibrator for expected theoretical visibility. This procedure is explained in details in Chapter 3.4. Since the calibrator is unresolved the tf is simply the visibility of the calibrator squared. The cal-
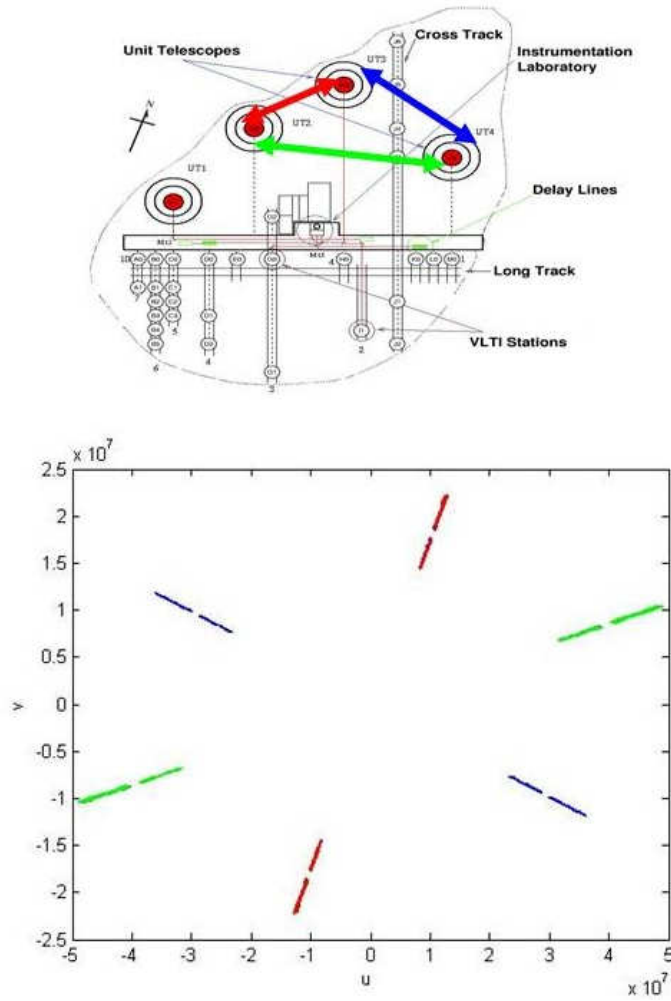
Figure 5.4: *The top panel shows the configuration used for the AMBER observations. The lower panel shows the uv coverage in units of B/λ of the observations.*

ibrated squared visibilities of HD113449 were then determined using *amdlibDivideOiData* which simply divides the raw visibilities of the science target by the tf. The final results were 6 files containing the calibrated visibilities of HD113449 in the H and K bands.

5.3.3   Binary visibility model

In Chapter 2.3.1.2 I introduced the expected visibility for a pair of stars in a binary system. In that case I used the formula for two unresolved point sources. For HD113449 this approximation is still valid, since the angular diameters of the two stars are <0.3 mas. The stars themselves are thus not resolved with the VLTI at these baselines. In order to determine the missing orbital parameters, I developed a dedicated software-package which calculates the squared visibilities of a binary system. This software-package simulates the expected visibilities of a binary, for which all the orbital parameters are known, when observed at a certain date from a given observatory, using a specific set of baselines. To explain how the software works let us take the equation of the visibility of a binary consisting of two unresolved stars

Figure 5.5: *One of the AMBER frames showing the fringes of HD113449. Starting from the left after the DK, the first two and the fourth columns are the photometric outputs from the three single telescopes. The third column contains t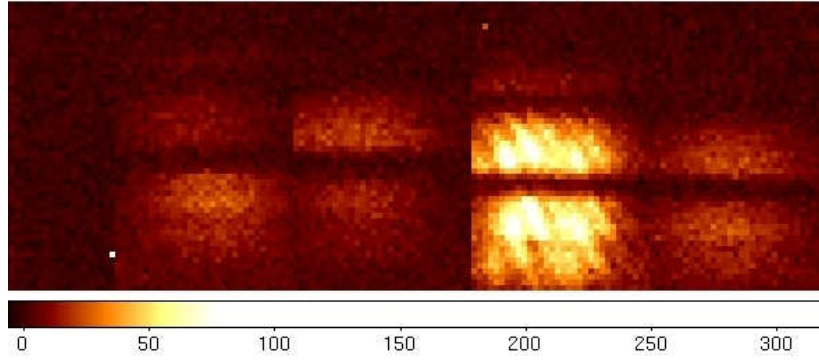he fringes obtained by combining the light coming from the three telescopes, in couples of two. The light is spectral dispersed along the vertical axes, starting from shorter wavelength ($\sim$1.46 μm) on top of the frame. From the top to the bottom are visible the J, H and K bands (separated by two small horizontal dark strips). There is basically no light from the star in the J band.*

(cfr. equation 2.8):

$$V^2 = \frac{1 + f^2 + 2f\cos(2\pi\frac{B_{px}Ra + B_{py}Dec}{\lambda})}{(1+f)^2} \tag{5.1}$$

where B_{px} and B_{py} are the components of projected baselines in the plane of sky, related to the physical baseline by equation 2.5. RA and Dec are the x and y components of the angular separation (see the term ρ in the equation 2.8) in the same plane as that of the projected baseline. These terms, Ra and Dec, are practically the separation between the two stars in right ascension and declination, respectively. The relation between these two components and the orbital parameters of a binary is expressed by the equations:

$$Ra = A(\cos E - e) + B(1 - e^2)^{1/2}\sin E \tag{5.2}$$

$$Dec = C(\cos E - e) + D(1 - e^2)^{1/2}\sin E \tag{5.3}$$

where E is the eccentric anomaly, e is the eccentricity of the orbit and A, B, C and D are the Thiele-Innes constants. The explanation of these parameters is given as follows.

The eccentric anomaly is an angular parameter that defines the position of an object in a Keplerian orbit. Given the time t_{obs} at which the observation is carried out, the period P of the orbit, and the epoch of the passage to the periastron τ, E is derived by solving the transcendental equation:

$$M = 2\pi\frac{(t_{obs} - \tau)}{P}$$
$$M = E - \sin E \tag{5.4}$$

This equation is solved iteratively using 1000 iterations, which is more than sufficient in order to determine E.

The Thiele-Innes constants A, B, C and D, are defined in terms of four of the orbital parameters of a binary system, that is:

$$A = a(\cos\omega\cos\Omega - \sin\omega\sin\Omega\cos i)$$

$$B = a(-\sin\omega\cos\Omega - \cos\omega\sin\Omega\cos i) \qquad (5.5)$$

$$C = a(\cos\omega\sin\Omega + \sin\omega\sin\Omega\cos i)$$

$$D = a(-\sin\omega\cos\Omega + \cos\omega\sin\Omega\cos i)$$

with a the angular semi-major axis of the orbit expresses in radians, ω the longitude of the periastron, Ω the longitude of the ascending node, and i is the inclination of the plane of the orbit to line of sight.

Five of the orbital parameters, P, τ, e, ω and $a_1\sin i$ used to calculate the theoretical squared visibilities were derived spectroscopically from the analysis of the HARPS spectra . The mass ratio q=M_2/M_1, derived by the CRIRES spectrum, combined with $a_1\sin i$ gives the parameter a using the equations:

$$M_1 a_1 = M_2 a_2 \qquad (5.6)$$

$$a = a_1 + a_2 \qquad (5.7)$$

Combining these last two equations with $a_1\sin i$ (see Table 5.1) and q, it gives $a = \frac{0.249}{\sin i}(1+\frac{1}{q})$ AU. Dividing this quantity by the distance of the object in parsec, the angular semi-major axes of the orbit times $\sin i^{-1}$ was obtained. This values was inserted in the equations 5.5.

However, there are still some parameters missing for determining the visibility squared. These parameters are only three: the inclination i, the longitude of the ascending node Ω and the flux ratio f between the two components. To derive these parameters I did as follows: I fixed all the parameters derived spectroscopally and varied the three unknown parameters. More precisely I varied i between 1 and 90 degrees, Ω between 1 and 180 degrees and f in the range between 0.10 and 0.30. The latter parameter is already constrained by the CRIRES spectrum, which shows spectral lines of the A and B components. Thus, f is only varied from 0.1 to 0.3 since values outside this range would be in conflict with the CRIRES spectrum. f was derived separately for the H (f(H)) and K (f(K)) bands assuming that it is constant along each spectral band. For i and Ω I proceeded by steps of one degree while for f(H) and f(K) with steps of 0.01. I obtained in this way a library of theoretical visibilities squared, all calculated for the date and the baseline configuration of the AMBER observation of HD113449. The library was calculated for 11 and 14 different wavelength intervals in the H and K band, respectively. For each of the three baselines, I obtained 324.000 models to be compared with the observations. Given the fact that I had six observations, taken with time difference of a few minutes, I calculated six libraries each corresponding to one observation. This procedure is necessary, because the projected baselines used for the 6 observations are different, due to the motion of the object in the sky. Additionally, I also calculated the closure phases (cfr. eq. 5.17) for all 6 observations. The closure phase allows one to constrain the free parameters even better. To model the closure phase in the case of a binary I used the equation:

$$\Phi_c = \text{atan}\left[\frac{\text{Im}(\text{V}^2)}{\text{Re}(\text{V}^2)}\right] \qquad (5.8)$$

where Im and Re are the imaginary and the real part of the squared visibilities, respectively. By substituting the cosine function in the equation 5.1 with Euler's formula, equations 5.8 is

transformed to:

$$\Phi_c = \arctan\left[\frac{f\sin\left(-2\pi\frac{B_{px}Ra+B_{py}Dec}{\lambda}\right)}{1+f\cos\left(-2\pi\frac{B_{px}Ra+B_{py}Dec}{\lambda}\right)}\right] \tag{5.9}$$

These models were compared to the observations through a Chi-Square minimisation analysis and the results are presented in Chapter 6.4.

Chapter 6

Testing evolutionary tracks of PMS stars. III: Results and discussion

Presented here are the results of the test of the evolutionary tracks. The first section summarizes the properties of the PMS-binaries found. In this section, the mass-ratios of two SB2 binaries are compared with the mass-ratios derived for these star from the evolutionary tracks. This test already allows one to find out, which tracks match the observations best. In section 6.4, the dynamical masses of the stars in the young binary HD113449 are derived and compared with the masses given by the tracks. In Section 6.5 the results of the test are summarized and conclusions are drawn.

6.1 PMS long period spectroscopic binaries

The aim of this survey is to detect young binaries suitable for VLTI observations. Binaries with period longer than 50 days are the best targets for two reason. First of all the components of such long period binary systems can be resolved by the VLTI, given the distance of the region sampled ($\leq$ 150 pc). Second mass exchange between the components is unlikely due to the large separation. Listed in Table 6.1 are all the young binaries with orbital periods between 50 and 3000 days now known. Eight of these where found by the team of Guenther et al. (2007) of which I am member and five where discovered by the authors cited in Table 6.1.

Figure 6.1 shows as an example the spectroscopic orbit of RXJ1220.6-7539, one of the binaries found in this survey. The spectroscopic binaries shown in this table are all brighter than m_k= 10 mag. This limit was chosen because it would have been possible to observe these stars with the VLTI, if the VLTI would have reached the sensitivity that was originally planned. However, after AMBER was commissioned it turned out that the limiting magnitude is only 7 in the K band, which would leave only one of the target listed in Table 6.1. This object is the triple system BS Indi (Guenther et al. 2005). BS Indi is in principle bright enough to be observed with the VLTI. However observation with the VLTI performed in April 2006 and analyzed by me at the end of the same year, shows that even this object is currently too faint for the VLTI. Luckily a young binary (HD113449) was found in the course of another survey. This binary is bright enough to try out the method. Once further upgrades to the VLTI are made, the other stars can also be observed.

Table 6.1: *PMS binaries discovered in this survey. Listed in this table there are also binaries taken from the literature that are suitable for VLTI observations. The second column indicates whether the binary was discovered in our survey (yes) or taken from the literature (no). The third column gives the equivalent width of the Hα line with fi=filled, em=emission and abs=absorption.*

id	This survey	Region	EW Hα [Å]	EW LiI [Å]	Spec type	m_k (mag)	RA (J2000)	DEC (J2000)	Type	Period (days)
HIP 50796[1]	no	TWA	0.20[2]		K5V	7.66 ± 0.03	10 22 18.0	-10 32 15	ST3	570
CS CHA	yes	Cha	-40	0.53 ± 0.01	K4V	8.20 ± 0.03	11 02 26.3	-77 33 36	SB1	≥ 2480
HD 97131[3]	no	TWA			F2V	7.70 ± 0.02	11 10 34.2	-30 27 19	ST3	134
RXJ-7539	yes	Cha	fi	0.21 ± 0.06	K2V	7.93 ± 0.02	12 20 34.4	-75 39 29	SB1	613
MO Lup[4]	yes	Lup	-2.3	0.37 ± 0.02	K7V	8.64 ± 0.02	15 24 03.5	-32 09 51	ST3	> 3000
RXJ1534.1-3916	yes	Lup	abs	0.21 ± 0.02	K1V	8.55 ± 0.02	15 34 07.4	-39 16 18	SB1	> 3000
RXJ1559.2-3814	yes	Lup	-1.4	0.23/0.14		9.34 ± 0.03	15 59 16.1	-38 14 42	SB2	474
GSC 06209-00735	yes	SC	0.3	0.37 ± 0.01	K2V	8.43 ± 0.02	16 08 14.8	-19 08 33	SB1	2045
NTTS 160814-1857[5]	no	SC	0.7		K2V	7.69 ± 0.02	16 11 09.0	-19 04 45	SB1	145
GSC 06213-00306	yes	SC	fi	0.24/0.18		7.43 ± 0.02	16 13 18.5	-22 12 48	SB2	167
Haro 1-14c[6]	no	Oph			K3V	7.78 ± 0.03	16 31 04.4	-24 04 33	SB2	591
NTTS 162819-2423s[5]	no	Oph	em		G8V	7.44 ± 0.02	16 31 20.0	-24 30 04	SB1	89
BS Indi[7]	yes	Tuc	abs	0.18 ± 0.02	K0V	6.57 ± 0.02	21 20 59.8	-52 28 40	ST3	1222

[1] triple system (Torres et al. 2003)

[2] Song et al. (2002)

[3] Torres et al. (2003)

[4] hierarchical triple system consisting of a binary with 12 days, and one with a period > 3000 days Esposito et al. (2007)

[5] Mathieu (1994)

[6] Reipurth et al. (2002) and Simon & Prato (2004)
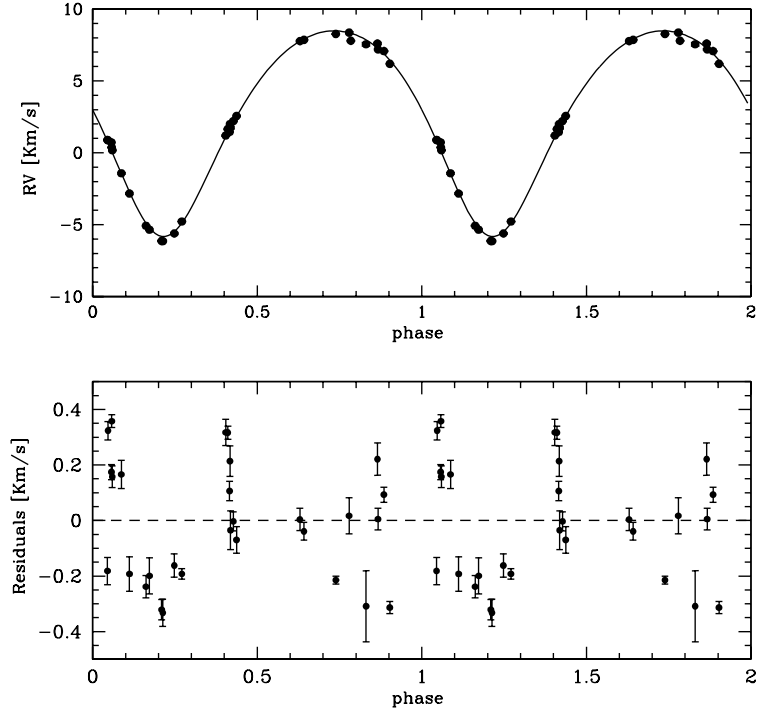
[7] triple system, see Guenther et al. (2005)

Figure 6.1: *Shown in the top pannel are the phase-folded RV measurements of RXJ1220.6-7539. The orbital period is 612.9 ± 0.4 days. The bottom pannel shows the residuals between observations and calculated orbit. The large scatter is due to stellar activity (e. g. spots).*

Nevertheless, as a first test of evolutionary tracks, the mass ratio of the SB2 systems derived from spectroscopy, can be compared to the outcome of the theoretical models. Amongst the newly discovered binaries there are 2 (RXJ1559.2-3814 and GSC 06213-00306) SB2 systems, which I used for this purpose. In the first step I determined the mass ratios of this two from the RV measurements. Temperatures and luminosities were also derived for the individual components of the SB2 systems, using spectral lines analysis and template fitting (see Chapter 5.2). I then estimated the mass ratios from the evolutionary tracks and compared them with the observed ones. In the next I will shortly describe these two young SB2 systems.

6.2 Spectroscopic orbits of the two SB2-systems

From the RV analysis it is possible to derive the spectroscopic orbits for all the systems listed in Table 6.1. In Table 6.2 I report only the orbital parameters of the two newly discovered SB2 systems.

6.2.1 GSC 06213-00306

GSC 06213-00306 is an SB2 consisting of two PMS stars. The equivalent widths of the LiI6708 Å lines are 0.241 ± 0.004 Å and 0.18 ± 0.04 Å for the primary and secondary, respectively. The

Parameter	GSC06213-00306	RXJ1559.2-3814
P (days)	166.9 ± 0.1	474.0 ± 1.0
T_0 (HJD)	2452124.2 ± 1.1	2447834 ± 3.0
γ (km s^{-1})	-6.76 ± 0.06	2.0 ± 0.4
K_1 (km s^{-1})	15.1 ± 0.1	13.4 ± 0.2
K_2 (km s^{-1})	15.7 ± 0.1	14.2 ± 0.2
e	0.226 ± 0.006	0.336 ± 0.005
ω_1 (degrees)	161.8 ± 2.2	336.8 ± 1.9
ω_2 (degrees)	341.8 ± 2.2	156.8 ± 1.9
$a_1 \sin i$ (AU)	0.226 ± 0.002	0.549 ± 0.010
$a_2 \sin i$ (AU)	0.234 ± 0.002	0.581 ± 0.010
$q = \frac{M_2}{M_1}$	0.97 ± 0.01	0.9445 ± 0.027
$M_1 \sin i$ (M$_\odot$)	0.246 ± 0.006	0.444 ± 0.026
$M_2 \sin i$ (M$_\odot$)	0.239 ± 0.006	0.419 ± 0.025

Table 6.2: *Orbital parameters of the newly discovered SB2 systems.*

Hα line is often filled in, and occasionally it appears as an emission line with an equivalent width of -0.1 Å. In total our team took 22 spectra of this binary within about 2500 days. I find an orbital solution with a period of 166.9 ± 0.1 days. Thus, GSC 06213-00306 is a long period, young SB2 binary. The orbital parameters are given in Table 6.2. It is interesting to note that the masses of both components are almost identical.

6.2.2   RXJ 1559.2-3814

For RXJ 1559.2-3814 I obtained a good orbital fit with a period od 474 days. All other parameters are listed in Table 6.2. The equivalent width of the LiI6708 Å is 0.23 Å for the primary and 0.14 Å for the secondary. The average equivalent width of the Hα is -1.4 ± 0.2 Å. The orbital solution is shown in Figure 6.2 with the residuals to the observations. The scatter is due to stellar activity proper of young stars.

6.3   Placing the SB2s in the HR diagram

The luminosities and temperatures derived for the single components of the SB2 systems with the method explained in Chapter 5.2, are given in Table 6.3. The bolometric magnitude of the Sun used is m$_{\odot_{bol}}$=4.75. Once these parameters are determined it is possible to place the stars into the HR diagram, together with three of the most used set of evolutionary tracks (Palla & Stahler 1999; Siess et al. 2000; Baraffe et al. 1998), as shown in Figure 6.3. The mass ratios determined from the tracks are summarized in Table 6.4. These can be compared with the true mass-ratios given in Table 6.2. The parameter $(q_t\text{-}q_s)/\sigma_s$ given in Table 6.4, is a measure of the difference between the true mass-ratio q$_s$ and the mass-ratio derived from the tracks q$_t$ normalized by the error of the measurement σ_s. In the case of RXJ1559.2-3814 the Baraffe et al. (1998) tracks match the observations best. In the case of GSC06213-00306, all three set of tracks give the same result.

The components of both the SB2s are coeval according to the models of the three authors. The age of GSC 06213-00306 derived from the Baraffe isochrone results in 20 Myrs, while the
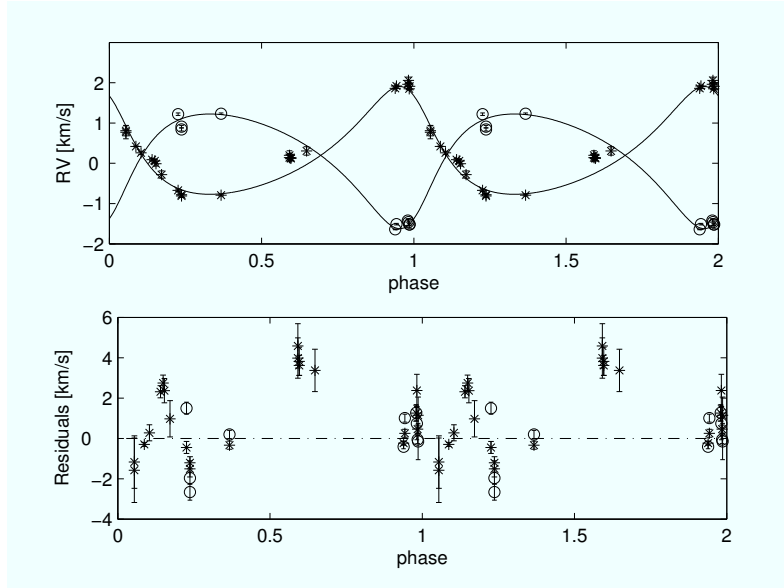
Figure 6.2: *Phase-folded RV measurements of RXJ1559.2-3814. Shown is the orbit of the A and B component for a period of 474 days.*

	id	SpT	$\log T_{eff}$	f (5900-6500Å)	$\log L_{bol}/L_\odot$
RXJ1559.2-3814 A	A	K7	3.602	0.605 ± 0.028	-0.930
	B	M0	3.580	0.395 ± 0.019	-1.040
GSC06213-00306 A	A	K0	3.715	0.520 ± 0.014	0.172
	B	K0-1	3.702	0.480 ± 0.013	0.140

Table 6.3: *This table summarizes the spectral types and the flux ratios of each components of the SB2 systems analyzed in this work. In this first column we give the id of the stars with A for the primary star and B for the secondary. The spectral types derived by fitting the template library are given in the second column. Listed in the last three columns are log T_{eff} using the conversion from spectral type to temperature given in Pickles (1998), the flux-ratios of the two stars in the wavelenght region (5900-6500Å) and the bolometric luminosities.*

Siess and Palla and Stahler tracks give an age of 13-14 Myr and 10-11 Myr, respectively. All these values are in disagreement with the age of 5 Myr (Preibisch & Zinnecker 1999) given as the general accepted value for the Upper Scorpius region. The ages of RXJ 1559.2-3814 derived from evolutionary tracks are 35, 20-25 and 30 Myrs using the Baraffe, Siess and Palla & Stahler models, respectively. The three models are quite in agreement in the errors, giving an average age for this binary of 30 Myrs. RXJ 1559.2-3814 belongs to the Lupus star forming region where star older than 10^7 Myr are found (Wichmann et al. 1997).

6.4 HD113449

In Section 5.3 it was described in detail how the young binary HD113449 was observed with AMBER and how the visibility and the closure phase were derived. Finally I constructed a model of a binary that allows to calculate the visibility and the closure phase for a binary of
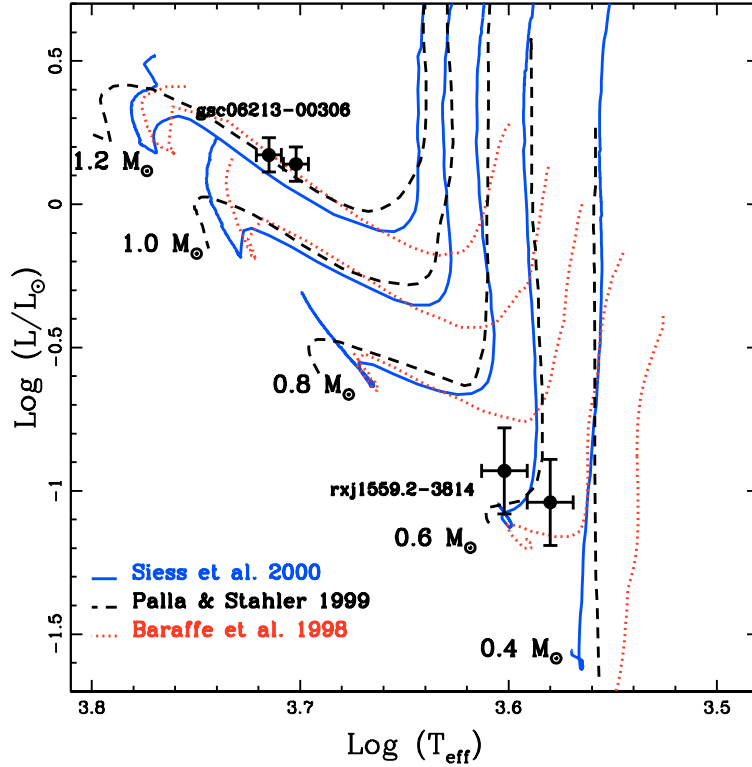
Figure 6.3:   *HR diagram for the SB2 systems. Shown are also the evolutionary tracks taken from Palla & Stahler (1999) (black dashed lines), Siess et al. (2000) (blue solid lines) and Baraffe et al. (1998) (red dotted lines).*

| | RXJ 1559.2-3814 | | GSC 06213-00306 | |
Tracks	q_t	$(q_t\text{-}q_s)/\sigma_s$	q_t	$(q_t\text{-}q_s)/\sigma_s$
Siess	0.77	6.5	~ 1.0	1.5
Palla	0.85	3.6	~ 1.0	1.5
Baraffe	0.93	0.6	~ 1.0	1.5

Table 6.4:   *Mass ratios of RXJ 1559.2-3814 and GSC 06213-00306 derived from the evolutionary tracks (q_t) and comparison with the spectroscopic values (q_s).*

given orbital parameters. By using the parameters of HD113449 determined spectroscopically and using the binary model, the missing parameters are derived by minimizing the difference between the model and the observed visibility and closure phase. This is done by using a χ^2 minimization algorithm. It is important to note that four are free parameters (i, Ω, f(H) and f(K)) which are all derived minimizing simultaneously, 3 visibility curves plus the closure-phase measurement for each wavelength interval. The binary model is able to reproduce all visibilities and closure-phase very well as shown in Figures 6.4 and 6.5. The parameters derived are given in Table 6.5.

The errors are derived from the difference between the parameters found at minimum χ^2 and $\chi^2 + 1$. The figures 6.4 and 6.5 show the best fitting model to the observed squared

Parameters	Value
i	$57 \pm 3^{\mathrm{o}}$
Ω	$138 \pm 4^{\mathrm{o}}$
f(H)	0.15 ± 0.02
f(K)	0.17 ± 0.02

Table 6.5: *Parameters derived from the AMBER observations of HD113449*

visibilities and to the closure phase of HD113449. Figures 6.6 and 6.7 show the χ^2 surfaces for the inclination and Ω. The flux ratio are f(H)=0.15 and f(K)=0.17. The minimum of the Chi-Square, is found for values around $\Omega = 138^{\mathrm{o}}$ and $i = 57^{\mathrm{o}}$. As can be seen in Figures 6.6 and 6.7, the inclination i is much better constrained than Ω. Figure 6.9 shows the relative orbits of the B component around the A component, indicating the position of the two stars when the AMBER observation was carried out.

Once the orbital parameters were derived from the AMBER data, I obtained the masses of the two components. Combining the value found for the inclination with the mass function (see Table 5.1) and the mass ratio, derived from the RV analysis, I obtained the values of the masses for the single components of HD113449. The mass of the primary is $M_1 = 0.960 \pm 0.087$ $M_{\odot}$ and the mass of the secondary is $M_2 = 0.557 \pm 0.050$ $M_{\odot}$. Using the measured flux ratio in the H and K band and the magnitude reported in 2MASS for HD113449, I was able to derive the H-K color of the components. The colors are: $(H\text{-}K)_1$=0.147 $\pm$ 0.019 and $(H\text{-}K)_2$=0.283 $\pm$ 0.020 for the primary and secondary star, respectively. If the color of the secondary is compatible with a spectral type M0-1V, following the table of Pickles (1998), the primary, using the H-K color, results in a color cooler than a K0 star. This probably is due to the presence of a dusty envelope around the primary that emits in the near-IR or simply to fact the correlation between temperature and color for PMS stars is not currently well understood.

To put the two system components of HD113449 into the HR diagram, the temperature and the bolometric luminosity of both are needed. The temperature was determined converting the spectral type (see Chapter 5.3) into temperature by using the table of Pickles (1998). This gives a temperature of $T_1 = 5188 \pm 153$K and $T_2 = 3802 \pm 121$K, for the primary and the secondary, respectively, where the error was derived using an error of one subclass. I derived, finally, the luminosity of the two stars using the flux-ratios derived interferometrically, the total luminosity given in the 2MASS-catalogue, the Hipparcos distance (van Leeuwen 2007) and the bolometric correction given in Pickles (1998).

From this procedure results that the primary has a bolometric luminosity of $L_1 = 0.396 \pm 0.08$ $L_{\odot}$ and the secondary of $L_2 = 0.031 \pm 0.007$ $L_{\odot}$.

6.5   Discussion

The HR diagram with the two components of HD113449, together with three set of evolutionary tracks is shown in Figure 6.8. As one can see, the two stars are almost on the main sequence. The three set of models give almost the same mass for the primary star, which also
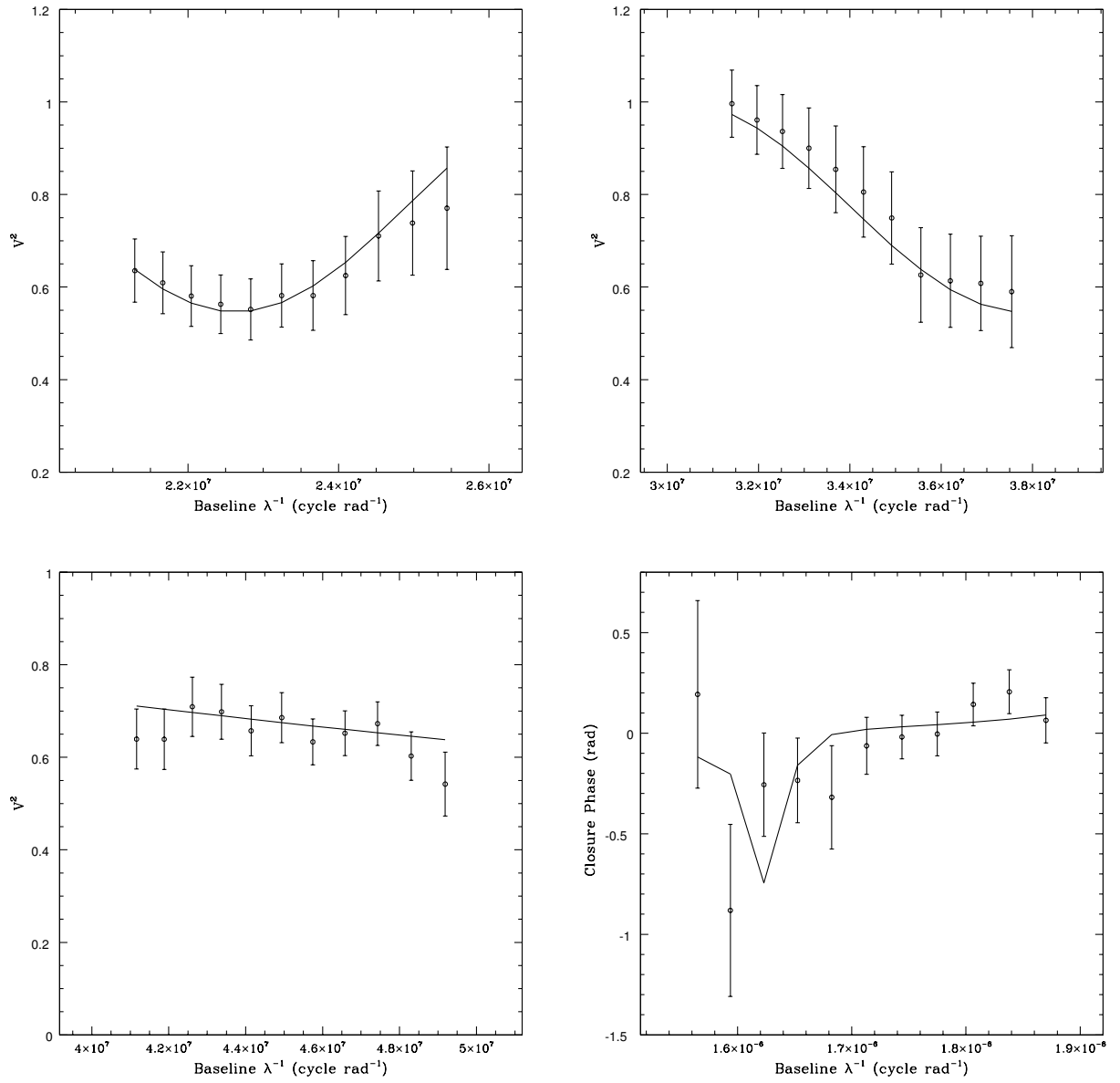
Figure 6.4: *The squared visibilities for the three different baselines and the closure phase of HD113449 in the H band. Starting from the top, shown on the left are as dots the observed squared visibilities for the baseline UT2-UT3, on the right the one for the baseline UT3-UT4. In the lower panel, shown on the left are the squared visibilities for the baseline UT2-UT4, and on the right the closure phase. The lines are the models calculated for the parameters given in Table 6.5.*
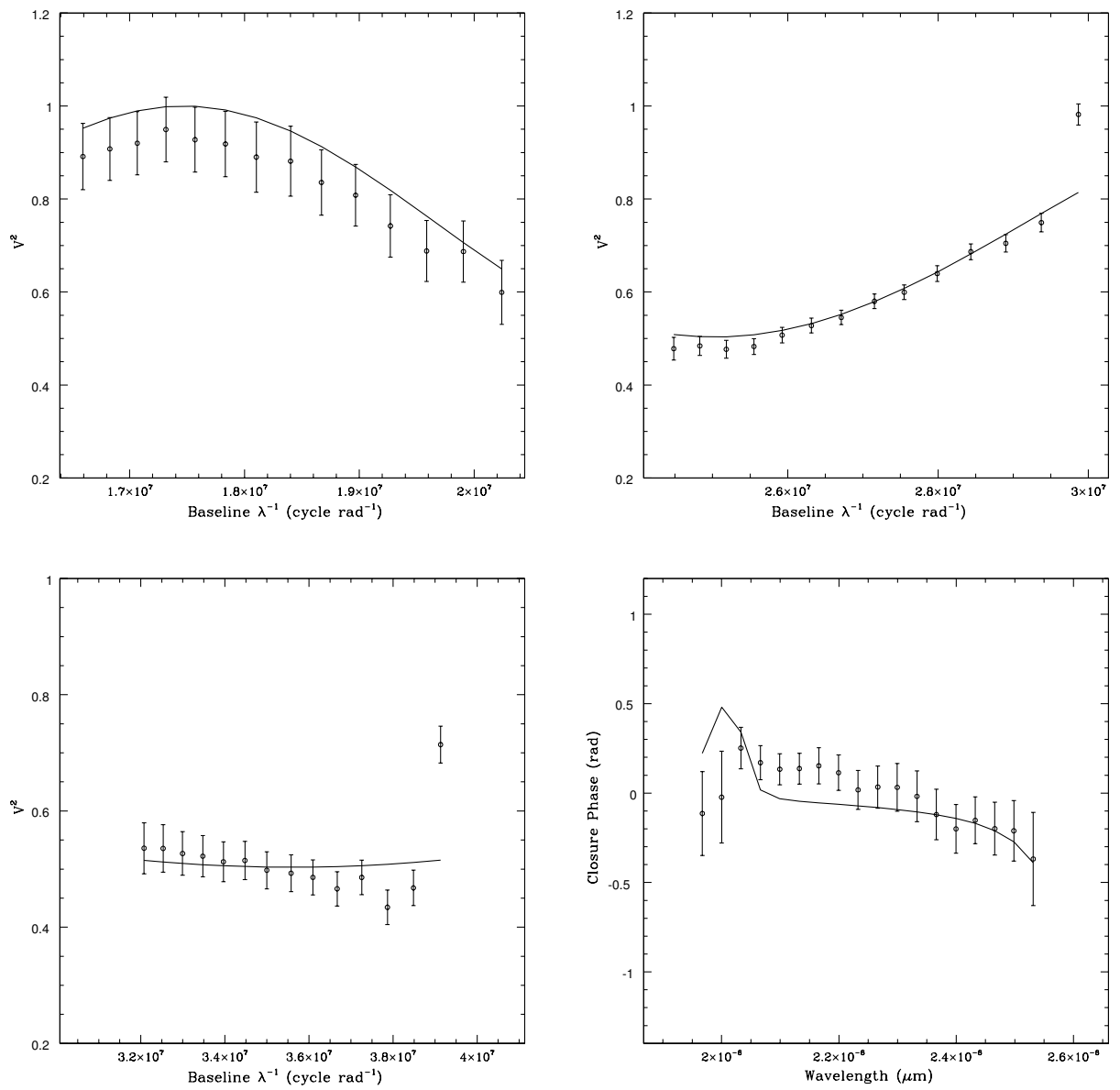
Figure 6.5: *Same as in Figure 6.4, but for the K band.*
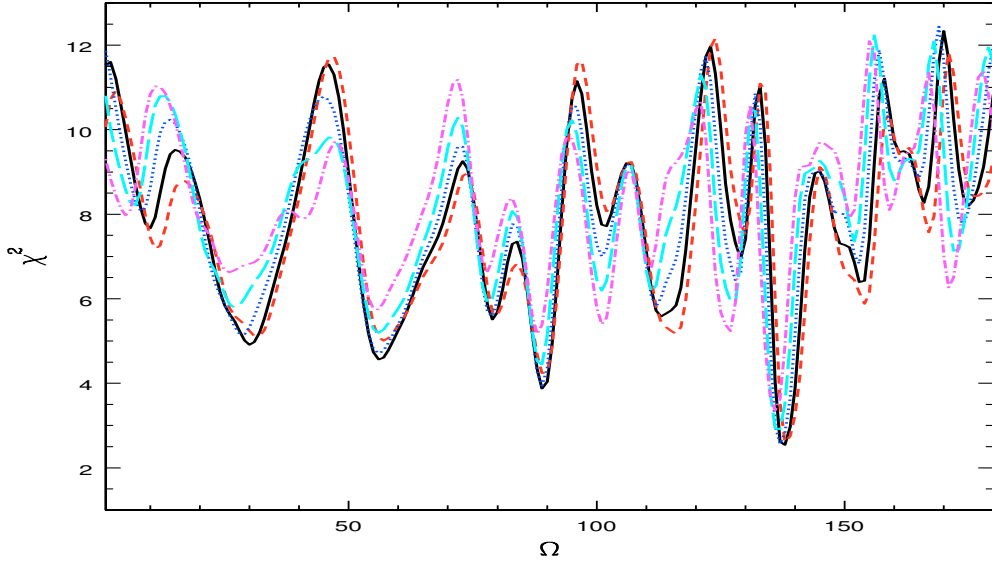
Figure 6.6: *Trend of the χ^2 with Ω for models with different inclinations. The thick black line is calculated for a model with an inclination of 57°, the other lines for 55, 56, 58 and 60°. The minimum at $\Omega = 138°$ is a true minimum, not a local one.*
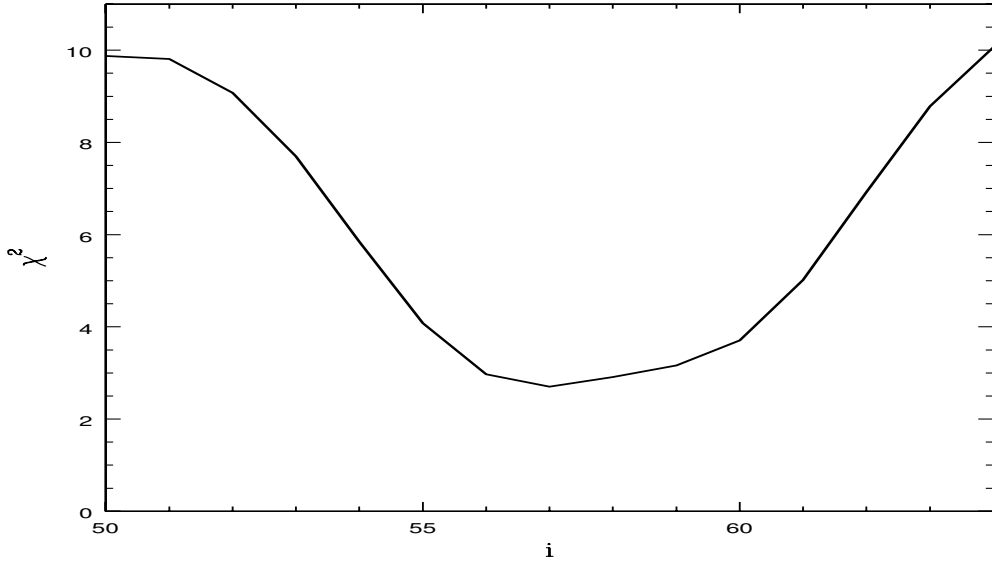
Figure 6.7: *Same as Figure 6.6, but for the inclination. The χ^2 has a minimum at 57°.*

agree with the observations. The mass of the secondary predicted by the models of Siess and Palla and Stahler, does not agree very well with the observation, as the average difference is 2.5 σ_{dyn}. The Baraffe tracks turn out to be the best with a difference $< 1.2 \, \sigma_{dyn}$. The results of the mass determination from the tracks, together with the differences with respect to the dynamical values are summarized in Table 6.6.

According to the Baraffe and Siess models the components of HD113449 are coeval, with
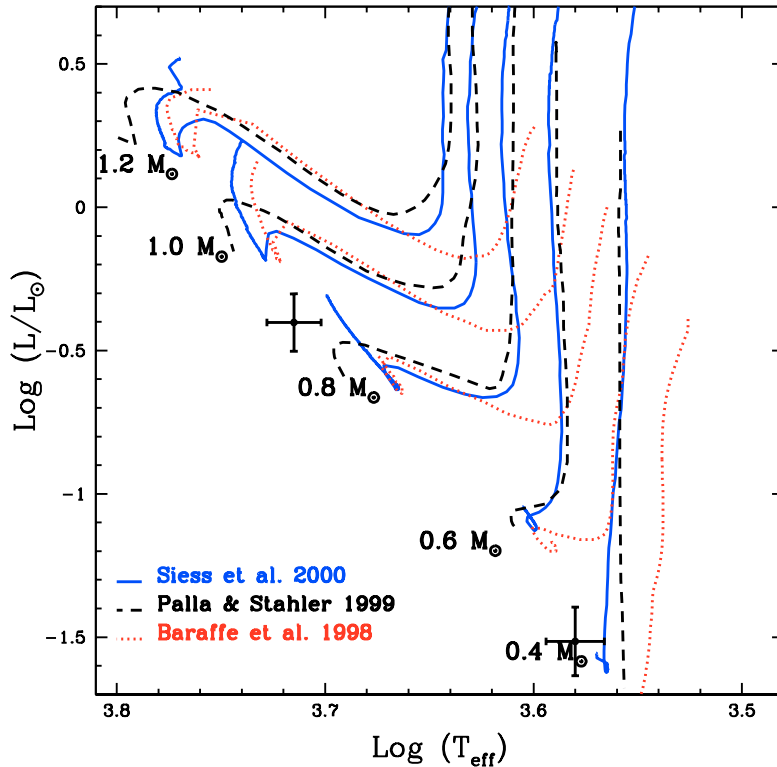
Figure 6.8: *HR diagram for the two components of HD113449. The tracks shown are for star of solar metallicity (Palla & Stahler 1999; Siess et al. 2000; Baraffe et al. 1998).*

an age of 100 Myrs and 150-200 Myrs, respectively. The tracks published by Palla give different age for the two components, with the primary of 100 Myrs and the secondary of 150 Myrs.

Adding together these results and the ones coming from the mass ratio analysis, a first statement can be made in the sense that the Baraffe models fit the observations best. The Baraffe tracks fit almost to 1 σ both the dynamical masses of the HD113449 components and the mass ratios of the two young SB2 systems RXJ 1559.2-3814 and GSC 06213-00306. The other tracks do not reproduce the observations equaly well. The age of HD113449 derived from the Baraffe and Siess tracks are in agreement with the age (152 ± 16Myr) determined using gyrochronology by Barnes (2007). The Palla tracks give different ages for the two components, which is highly unlikely.

One of the main differences between the tracks used in my analysis concern the mixing length parameter chosen. The set of Baraffe tracks that I used was computed for l= 1 H_p, while Palla & Stahler use 1.5 H_p and Siess et al. 1.6 H_p. A lower value of the mixing length parameter predicts a less efficient energy transport by convection, giving rise to cooler photospheres of stars of the same masses and age, especially in the low mass regime.

My result thus is in agreement with the one presented in the work by Hillenbrand & White (2004), in which they tested the evolutionary tracks of PMS, using all the young stars for which dynamical mass determinations were carried out up to the year 2004. They state
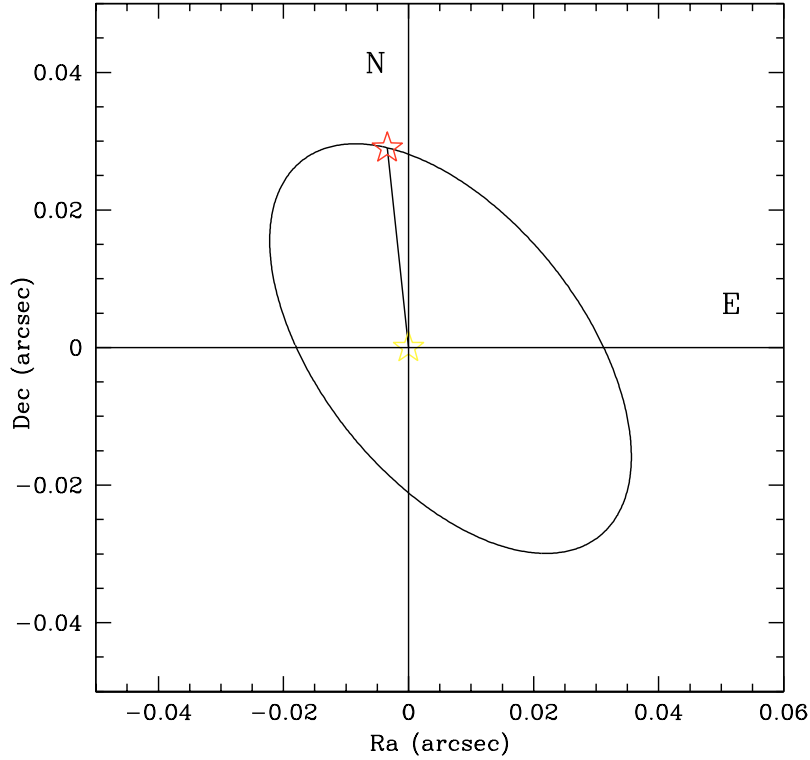
Figure 6.9: *The ellipse shows the relativ orbit of the HD113449 components calculated with the orbital parameters derived in this thesis (see Tables 6.5 and 5.1). The position of the stars in this figure is for the time when the AMBER observation was taken.*

Tracks	$A_t[M_\odot]$	$B_t[M_\odot]$	$(A_t\text{-}A_d)[M_\odot]$	$(B_t\text{-}B_d)[M_\odot]$	$(A_t\text{-}A_d)/\sigma_d$	$(B_t\text{-}B_d)/\sigma_d$
Siess	0.85-0.90	0.40-0.45	0.09	0.13	1.03	2.60
Palla	0.80-0.85	0.40-0.45	0.14	0.13	1.61	2.60
Baraffe	0.90-0.95	0.50	0.04	0.06	0.40	1.11

Table 6.6: *Masses of the HD113449 A and B components derived from the evolutionary tracks (columns 2 and 3) and compared to the dynamical masses (4, 5, 6 and 7). A_t and B_t are the masses derived from the tracks of the primary and secondary, respectively. A_d and B_d are the dynamical masses of the primary and secondary, respectively. σ_d is the error on the dynamical mass.*

in their work that the Baraffe tracks computed with l= 1 H_p in the mass range 0.5-1 $M_\odot$ are more consistent with the dynamical masses.

Chapter 7

Testing the evolutionary tracks of giant stars. I: Introduction

As explained in this chapter, by combining stellar oscillations and measurements of the diameters of giant stars obtained interferometrically, the mass of the stars can be determined. The combination of interferometry and observations of the stellar oscillations allows one to test the evolutionary tracks of post-main sequence stars. Interferometry thus opens new possibilities in this branch of research.

7.1 Application of optical interferometry to stellar physics of evolved stars

Since the masses of post-main sequence star are usually only derived from evolutionary tracks, it is necessary to test them. Depending on the author, the physical parameters derived by the evolutionary tracks can different substantially (see Figure 7.1). The problems arise also because stars spanning a wide range of masses all converge to the same region in the HR diagram. If the true masses for a number of giant stars are known, it is possible to calibrate the evolutionary tracks empirically. This is very important especially for the theory of planet formation. Only if one knows the mass of the host star it is possible to derive the mass of the planet. It is also expected, that the mass of the host star is an important parameter for planet formation. The mass of the host star certainly influences the properties of a planetary system that can be formed. Radial velocity surveys demonstrate that the frequency of Jupiter-mass around M-type stars is much lower than that of the more massive solar-like stars (Endl et al. 2006; Johnson et al. 2007). The question naturally thus arises whether stars more massive than the sun have a correspondingly higher frequency of massive planets. While theoretical studies tend to support this (Wuchterl et al. 2007; Kornet et al. 2007) the question can only be answered observationally. For RV-surveys of stars more massive than the sun, giant stars are preferred over main sequence stars, because the latter have high effective temperatures (i.e few spectral lines) and large rotation rates (i.e broad and shallow spectral lines). Both factors reduce the accuracy of the RV precision ($\approx$ 100-1000 m/s) for A-F type main sequence stars. Cool giant stars of similar mass are, instead, slowly rotating and have a sufficiently large number of absorption lines for excellent RV precision. The main sequence progenitor stars of
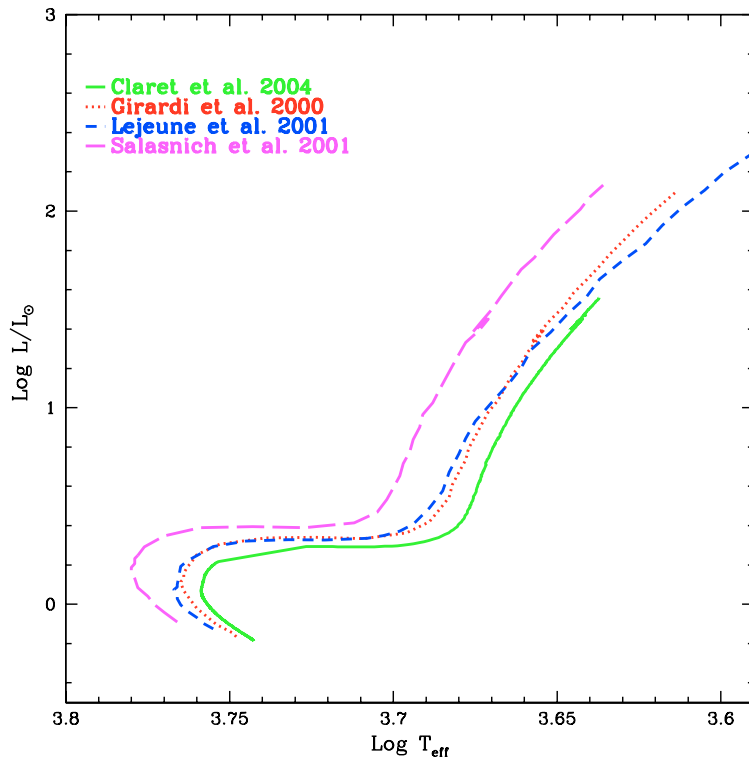
Figure 7.1: *Evolutionary tracks for stars of 1 $M_\odot$ and Z~0.02. The differences between the theoretical model from four different groups are shown here.*

giant stars are A-G type star with masses in the range between 1–3 $M_\odot$. Up to now about 30 giant stars with estimated stellar masses in the range of 1–3 $M_\odot$ have been found to host giant planets (see Planet Encyclopaedia: www.exoplanet.eu). Usually the masses of single giant stars, are determined using evolutionary tracks. Mass estimates in this way however depend critically on the parameters and assumptions that are hidden in the tracks, like the mixing length parameter and its assumed constancy for all stars, and the helium content. As a result different tracks will give different masses, and, in the absence of good calibrating objects, no set of tracks can presently be claimed to provide the best results. Fortunately, these theoretical evolutionary tracks can be tested and refined. Stellar isochrones yield a number of stellar parameters which can be determined directly, including mass, radius, and luminosity. Many bright giant stars have distances determined by Hipparcos and thus well-determined luminosities. Giant stars also have large angular diameters which can be measured directly via optical interferometry.

The interferometric observed diameters are compared directly to the output of the models, putting constraints on them. Although the measure of the diameters tells nothing about the mass, again the combination with spectroscopy allows the determination of this parameter. The frequency spacing of the p-mode oscillations (pressure is the restoring force) depends on the mean density of the star. For high order p-mode oscillations (of the kind expected for giant stars) the modes are evenly spaced with a frequency spacing of $\Delta\nu = (M^{0.5}/R^{1.5})$

135 μHz, where M and R are the stellar mass and radius in solar units (Kjeldsen & Bedding 1995). The maximum oscillation frequencies also is related to some physical parameters by the equation: $\nu_{max} = [M/R^2(T/5777K)^{0.5}]$ 3.05 mHz (Kjeldsen & Bedding 1995). By determining the radius and the oscillations frequencies the mass is then derived. In principle, one can derive the mass and radius from a knowledge of $\Delta\nu$ and ν_{max}, but this is still not as accurate as using additional information on the stellar radius. Furthermore, while it is relatively easy to determine ν_{max}, an accurate determination of $\Delta\nu$ requires considerable observational time with radial velocity measurements (photometric amplitudes are too low to be detected by ground-based facilities).

Unlike for main sequence stars, giant stars of similar effective temperatures have a wide range of radii (10–60 $R_\odot$) and a 20% error in the radius results in a 60% error of the mass (and for planet formation theory it is important to know if the star has a mass of 1 $M_\odot$ or 1.6 $M_\odot$). Thus asteroseismology alone, via the spacing of p-modes, does not give us the mass of a star with the accuracy that is needed (see Kjeldsen & Bedding 1995). However, by combining the interferometric radius with stellar oscillation, it is possible determine masses of giant star with an accuracy of few percent. A recent application of this method was made to β Hyi (North et al. 2007) and to β Gem (Hatzes & Zechmeister 2007). The latter is a planet hosting K0III star (Hatzes et al. 2006). The stellar oscillation spectrum gives a frequency spacing that combined with the interferometric radius (Nordgren et al. 2001) results in a stellar mass of $M = 1.91 \pm 0.09$ (Hatzes et al. 2012). This result is consistent with the Girardi et al. (2000) tracks which give $M = 1.95 \pm 0.3$ $M_\odot$. Once stellar isochrones have been refined and calibrated these can be used with some confidence to determine the stellar mass of all planet hosting giant stars.

From the diameter is also possible, estimating the bolometric luminosity, to determine the temperature through the Stefan-Boltzmann law, that is L$_{bol}$= 4 π R^2 σ T$_{eff}^4$, where L is the bolometric luminosity of the star, R is the radius, σ is the Stefan-Boltzmann constant and T$_{eff}$ the effective temperature. In this way it is possible to test the evolutionary tracks of evolved stars comparing simultaneously the observed effective temperature, the radius and the mass with the theory.

In here I measured the diameters of a sample of 30 giants stars, using the VLTI and the CHARA array. For one star HD170693 also the mass is measured with a new method based on the combination of the interferometric determined diameter with the detected frequency of the maximum amplitude RV oscillations.

7.2   Post main sequence evolutionary tracks

The large part of the discussion that I made about the PMS evolutionary tracks, is also valid for models of more evolved stars. A small difference in the input physics used by separate groups, can result in tracks of different luminosities and temperatures for the same mass value. The problems here are even worse for the complexity of the physical process involved in the different evolutionary status. Here I consider just the early post main sequence evolution of low mass stars, what is called the red giant branch (RGB) phase of a star. I discuss here the evolution of a star up to beginning of the so called asymptotic giant branch (AGB) phase, connected with the onset of Helium burning in the core through the He flash. The main

critical point of the these models are connected in modelling the convection, the values of the opacity, the mass loss rate (that for star at this stage is not negligible), the EOS and the nuclear reaction rate. The discussions about EOS, convection and opacity are the same as for PMS stars (see Chapter 4.2) given that the temperature involved are more or less the same. Usually also convective overshooting is taken into account, that is the phenomena in which convective cells overshoot into convective stable regions. This effects the heat transfer rate and the interior temperature of the star. The overshooting is parametrised by Λ_c which describes its extent across the border of the convective zone, expressed in units of pressure scale height. There are some problems of formalism regarding this parameter that is described in different ways depending on the author. For example the value Λ_c=0.5 given in Bressan et al. (1981) correspond to 0.25 pressure scale height in the work of Meynet et al. (1994). The lack of a standard formalism in the definition of Λ_c, has been a recurrent source of misunderstanding in the literature.

An important role in the computation of the models is also played by the treatment of mass loss and nuclear reaction rates. When a star moves up from the main-sequence to the giant branch, the mass loss increases dramatically. The difference between the mass loss rate per year between the two evolutionary stages, is of the order of 10^{10}. Hence, this parameter is of fundamental importance in the development of the models. The problem is that at the moment there is not an universal value adopted in the different theories.

Hereafter are shortly described the three different set of evolutionary tracks for RGB stars that I used in this thesis.

7.2.1 Girardi et al. tracks

The set of tracks, published in Girardi et al. (2000), includes stars with initial masses that go from 0.15 to 7 $M_\odot$. The models are presented for six different initial chemical compositions. In this thesis I consider only the one with solar metallicity (that means Z=0.019 and Y=0.273). The radiative opacities, for low temperature stars (i.e. T $< 10^4$ K), are from Alexander & Ferguson (1994). The energy transport in the outer convection zone is described according to the MLT with the parameter l that is calibrated by means of the solar model. For the overshooting the authors considered three different values: a) Λ_c=0 for stellar masses M $\leq$ 1 $M_\odot$; b) Λ_c=M/$M_\odot$ - 1.0 for stars in the range 1.0 $<$ M $<$ 1.5 $M_\odot$; c) Λ_c=0.5 for M $>$ 1.5 $M_\odot$. The equations of state used are two depending on the temperature. For temperature higher than 10^7 K they used the EOS for a fully-ionized gas described in Kippenhahn et al. (1965). For lower temperature (i.e. $< 10^7$ K) they adopted the EOS from Mihalas et al. (1990). They use reaction rates from Caughlan & Fowler (1988). Mass loss by stellar wind during the RGB of low-mass stars is considered using the empirical formulation by Reimers (1975), but with mass-loss rates multiplied by a parameter equal to 0.4.

7.2.2 Claret et al. tracks

The second set of tracks that I use is from Claret (2004). The track cover the mass range between 0.8 and 125 $M_\odot$ for stars of solar metallicity (Z=0.02 and X=0.70). For radiative opacities they adopted the calculations by Iglesias & Rogers (1996) completed with Alexander & Ferguson (1994) results for lower temperatures. The mixing length parameter used is l=1.68

H_p. For the overshooting they adopt a parameter of 0.20 H_p. Other mixing processes are not considered, like semi-convection or that due to rotation. For what concern nuclear reaction they developed a nuclear network and used nuclear reaction rated from Caughlan & Fowler (1988). The mass loss rates has been considered using the formalism of Nieuwenhuijzen & de Jager (1990) for all models expect that for stars smaller than 4 $M_\odot$. In the latter case, they used the work by Reimers (1977). The adopted EOS for cooler models was the so called CEFF (Christensen-Dalsgaard & Daeppen 1992), which physically is based on ionization processes modelled by the Saha equation together with a Columb pressure correction. For hotter ones partial ionisation was taken into account for the same element as in CEFF.

7.2.3   Salasnich et al. tracks

The Salasnich et al. (2000) models are for masses from 0.15 to 20 $M_\odot$ and three different initial chemical compositions. The input physics is the same as in Girardi et al. (2000), apart from differences in the opacities and the rates of energy loss by plasma neutrinos. The opacity used in this models are complete and consistent (Salaris et al. 1997), which means that the opacity were generated for the same pattern of abundances adopted in the stellar models, both at low and high temperature.

Chapter 8

Testing the evolutionary tracks of giant stars. II: Methods and data reduction

In this chapter I present the interferometric observations of two samples of giant stars, one in the Southern and the other in the Northern Hemisphere. The first sample was observed with the VLTI using AMBER, and consists of 5 giant stars, of which one is known to host a planet. The second sample is composed by 25 giant stars of which 6 host a planet, observed with the CHARA interferometer.

8.1 Observations and data reduction

It is of fundamental importance, for the understanding of the stellar physics evolution, to determine the masses of giant stars. In practise, giant stars are observed spectroscopically to determine their physical parameters like surface gravities ($\log g$), effective temperature and iron abundances ([Fe/H]), which are then combined with the model atmosphere and evolutionary tracks to determine mass. Unfortunately, mass estimates derived from the evolutionary tracks depend critically on several parameters and assumptions that are hidden in the tracks, such as the mixing length parameter and its assumed constancy for all stars, and the helium content. As a result different tracks give different masses.

Nevertheless it is possible to measure the masses of giant stars, without using the evolutionary or the stellar atmospheric models. This is done by combining interferometric stellar diameter measurements with observations of oscillation frequencies. Depending on the accuracy of the diameter measurements, the masses can be measured to an accuracy of $\sim 2\%$ (Teixeira et al. 2009) to $\sim 15\%$ (Hatzes & Zechmeister 2007). Because collecting data on oscillation frequencies is time-consuming, the first step in this direction is the determination of the giant stars' diameters.

In order to demonstrate that the method really works, the oscillation frequencies of one star are determined and combined with the interferometric observations. The mass of this star is thus determined.
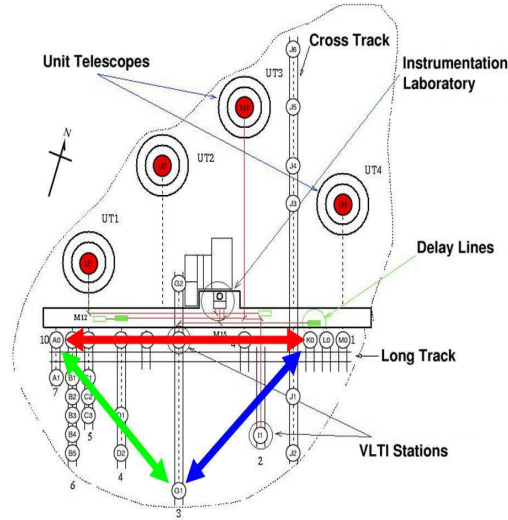
Figure 8.1: *ATs configurations used for observing the five giant stars (Southern Hemisphere program). The arrows indicate the baselines used. For the observations the ATs were placed at the positions A0, G0 and K1.*

Telescopes	Baseline (m)	Position Angle (degree)
G1-K0	90.500	26.006
A0-G1	90.522	116.005
A0-K0	128.003	71.013

Table 8.1: *Baselines used for the AMBER observations of the five giants. The position angles are measured respect to the North direction clock-wise.*

8.1.1   The Southern sample

Interferometric observations were performed on a sample of 5 giant stars in southern hemisphere using AMBER (Cusano et al. 2011). These are listed in Table 9.1. One of these stars HD11977, is known to host a planet (Setiawan et al. 2005). All these targets are bright enough to be observed with the ATs using also the fringe tracker FINITO. AMBER was used in the low resolution mode using the telescope configuration A0-K0-G1. The lengths and the orientations of the baselines are summarised in Table 8.1. The telescope configuration chosen was triangular as shown in Figure 8.1. Thanks to the different orientations of the baselines it was possible to discover that one of the giant stars is a binary. The data were taken in service

Telescopes	Baseline (m)	Position Angle (degree)
E2-W2	156.262	243.260
W1-S2	177.450	317.161
S1-E1	330.705	22.293

Table 8.2: *Baselines used for the CHARA observations of the 25 giants. The first column gives the telescope identification in the CHARA array (ten Brummelaar et al. 2005). The position angles are measured clock-wise towards North.*

mode in 6 night between October 2008 and January 2009. The total observing time was 20 hours. The data acquisition sequence was different respect to the HD113449 observation. In order to achieve an optimal calibration of the visibility, two calibrators were observed for each of the five giant stars, one shortly before and the other after the science target. The observations, both of the calibrator and the scientific target, consist of 5 exposures of 1000 frames each. The single DIT for each exposure was of 0.050 s, twice as long as used for the observations of HD113449, because the fringe tracker FINITO was used. In total for the 5 exposures of each star, 0.5 hours of observing time were needed. This means in order to obtain the full sequence calibrator-star-calibrator, 1.5 hours of observing time was required. For the calibration, stars were chosen with a distance $\leq 5^{\circ}$ from the science target, which also have a brightness which is within 0.5 mag of the science target in the K band. The two calibrators for each giant star were chosen from the CHARM2 catalogue (Richichi et al. 2005). A total of 10 calibrators was used for all the observations. In the LR mode AMBER gives spectral dispersed visibilities in the H and K bands. In total 27 visibility points were measured in LR, of which 12 are in the H band and 17 in K band. This gives the possibility to derive the diameters at different wavelength, allowing us to study possible variations of the diameters with wavelength. The AMBER data reduction was done in the same way as discussed in the section 5.3.2 (see also section 3.4). The software-package *amdlib* was used in order to derive the squared visibilities for each spectral channel in the H and K band. The same selection of the frame performed for HD113449 and consisting in the selection of the 20% of the best frame, was performed in order to obtain averaged visibilities of each exposure. The visibilities of the scientific targets were calibrated deriving the tf of the instrument (see section 3.4) by using the calibrators and taking the values of the angular diameters from the CHARM2 catalogue. Thanks to the use of the fringe tracker FINITO and to the adoption of the observation sequence calibrator-star-calibrator, visibilities with an accuracy up to 1% were measured.

8.1.2   The Northern sample

In collaboration with Baines et al. (2009), I performed interferometric observations, using the CHARA array, of a sample of 25 stars in the northern sky. The giant stars observed are listed in Table 9.3. Six of these, HD703106, HD170693, HD139357, HD32518, HD136726 and HD167042 are known to host a planet (Döllinger 2008). Three additional stars show long-period variations in their radial velocity measurements (HD106574, HD200205 and HD157681, Döllinger 2008). All the targets are bright enough to be easily observable with the CHARA interferometer.

Interferometric observations were obtained using the CHARA Array, together with the "CHARA Classic" beam combiner in the K'-band at 2.15 μm. The configurations of the baselines used are summarised in Table 8.2. The light in visible wavelengths (470-800 nm) was used for tracking and tip/tilt corrections. The observing procedure and the data reduction process employed here are described in detail in ten Brummelaar et al. (2005). I now shortly describe the main steps.

In contrast to AMBER where fringes are recorded simultaneously on the detector, for CHARA the fringes are recorded by rapidly changing the path-difference in time and then

recording the output-signal. The frequency with which the path-difference in changed is 150 Hz. One data set consists of 200 scans of the fringes. Because of the way CHARA works it is very important that the light intensity coming from each telescope is monitored. This is done periodically, inserting a shutter into the output of one telescope so that only the output of the other telescope is measured. A full data-set thus consists of the fringe scans and the measurements of the flux coming from each telescope. Taking a full data-set requires about 5 minutes. The fringes are recorded by simply fitting a sine-wave to the signal recorded for each scan of the path-difference. In the case of these measurements, scans containing low-quality data are removed. The good-quality data are instead averaged.

The conversion from the visibilities measured of the science target to calibrated visibilities is done as in the standard practise, by dividing the first by the tf of the instrument (CHARA+beam combiner). This procedure is the same as for the VLTI (see section 3.4). For all the giant stars of the sample, our team observed alternatively the calibrators and the target stars, to make the observation conditions for both as equal as possible. Reliable calibrators were chosen to be single stars and nearly unresolved on the baseline used, to reduce the impact of systematic errors on the target diameter calculation.

8.2   Diameter and T$_{\text{eff}}$ determinations

8.2.1   The Southern sample

The angular diameters are derived by fitting the visibilities, measured with AMBER, to the model of a uniform stellar disk (UD, see section 2.3.1.1). I use UD models for the stars in this sample, because the limb-darkened diameter can only be determined if visibility measurements are available for baselines larger than the first null of the visibility which is not the case for the VLTI observations. The fit of the UD models is performed for each of the spectral channels in the H and K band. In total I derived the angular diameters corresponding to 12 different wavelengths from 1.56 to 1.87 μm, with a bin-size of 0.03 μm, and to 17 wavelengths from 1.97 to 2.50 μm with the same bin-size. As an example the fits for the UD model at the wavelength 1.83 and 2.36 μm for the giant star HD27256 are shown in Figure 8.2.

The diameters are then calculated by averaging all values derived in the H and K bands. The results are presented in the Section 9.1. Once the diameters are determined interferometrically, the effective temperatures T$_{\text{eff}}$ are calculated using the relation:

$$F_{\text{bol}} = \frac{1}{4}\theta_{\text{LD}}^2 \sigma T_{\text{eff}}^4 \tag{8.1}$$

where F_{bol} is the bolometric flux and σ is the Stefan-Bolzmann constant. The stars' V and K magnitudes are de-reddened using the extinction curve described in Cardelli et al. (1989). The intrinsic (V-K) colour is calculated and the bolometric corrections are determined using Alonso et al. (1999). F_{Bol} is determined by applying the BC for each star and the T$_{\text{eff}}$ is calculated (see Paragraph 9.1). To determine the temperatures I used the value of the angular diameters averaged over all spectral channels.

The average error on the fit to the model for every single spectral channels, is less than 1% for all the stars, but HD12438. Since the quality of the data is the same as for the other
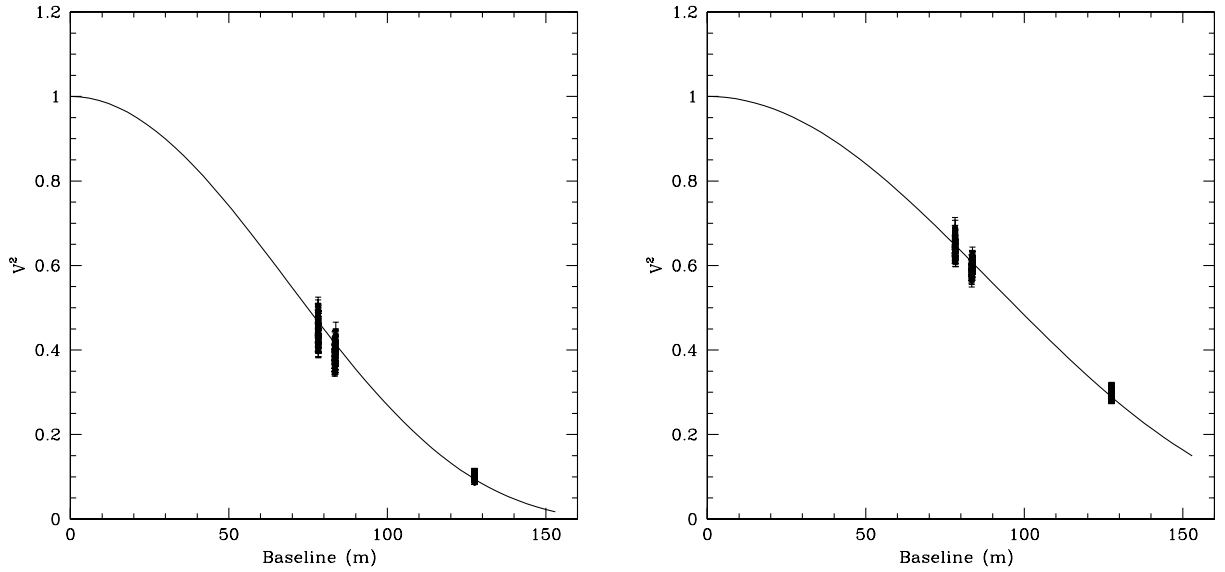
Figure 8.2: *Fit to the AMBER observed visibilities of HD27256 for 1.83 µm (right) and for 2.36 µm (left). The solid lines represent the UD models with the best fitting angular diameters to the corresponding wavelength.*

stars, the large error for the diameter of HD12438 is surprising. A reasonable explanation is that HD12438 is a binary. This idea is further supported by the fact that the visibilities for the G1-K0 baseline are significantly different from those of the A0-G1 baseline, although the two baselines have almost the same length, but different orientations. Different visibilities for the same baseline length, but different position angles, certainly is strong evidence that this object is a binary.

I developed at this point a software to fit the observed visibilities to a model of a pair of resolved stars, to confirm this hypothesis. HD12438 was observed 4 times in the ESO semester P82 (October 2008 - March 2009). More precisely this giant star was observed once on the 6th of October, two times on the 7th of October and once on the 20th December 2008. This software calculates the angular separation between the components of the binary, the position angle, the flux ratio and the angular diameters of the two components. The modelled squared visibilities are given by the equation:

$$V^2 = \frac{J_1(\theta_1) + J_2(\theta_2)f^2 + 2J_1(\theta_1)J_2(\theta_2)f\cos(2\pi\frac{\mathbf{B}\cdot\rho}{\lambda})}{(1+f)^2} \tag{8.2}$$

where f is the flux ratio, J_1 and J_2 are the Bessel functions corresponding to the single binary components with angular diameters θ_1 and θ_2, $\mathbf{B}$ is the baseline vector and ρ is the separation vector.

In contrast to the model of a single stars, the binary model fits the data extremely well. I thus conclude that HD12438 is in fact a binary. The parameters of this binary are reported in section 9.3.
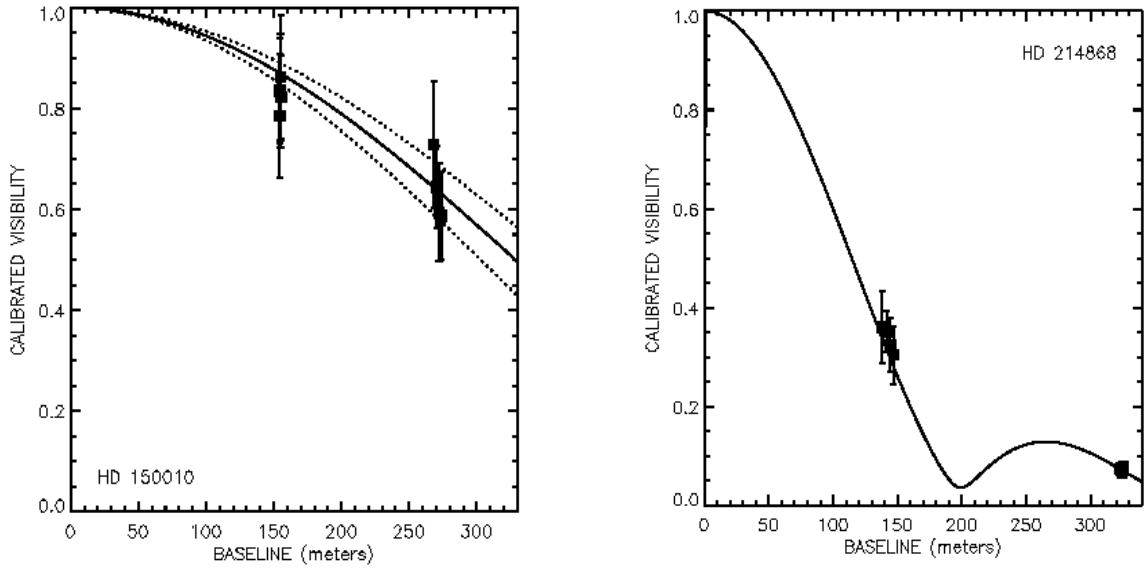
Figure 8.3: *Limb-darkening disk diameter for HD150010 (left) and HD214868 (right). The solid line represents the theoretical visibility curve for a star with the best fit θ_{LD}, the dashed lines are the 1 σ error limits of the diameter fit, the solid symbols are the calibrated visibilities with the errors.*

8.2.2   The Northern sample

Once calibrated visibilities are derived for all 25 stars, I calculated in the first step the diameter of all the stars using an uniform disk model. Because the CHARA-array has baselines up to 330m, I obtained for many stars also visibility measurements beyond the first null of the Bessel function. For these stars it is thus possible to derive the limb-darkening. I did this by using the model from Hanbury Brown et al. (1974):

$$V = \left(\frac{1-\mu_\lambda}{2} + \frac{\mu_\lambda}{3}\right)^{-1} \left[(1-\mu_\lambda)\frac{J_1(\frac{\pi B\theta}{\lambda})}{\frac{\pi B\theta}{\lambda}} + \mu_\lambda\left(\frac{\pi}{2}\right)^{1/2} + \frac{J_{3/2}(\frac{\pi B\theta}{\lambda})}{\left(\frac{\pi B\theta}{\lambda}\right)^{3/2}}\right] \tag{8.3}$$

The limb-darkening coefficients for all the stars were taken from Claret et al. (1995) after using the T$_{\text{eff}}$ and log g values of the stars. The resulting limb-darkened angular diameters are given in Section 9.2. Figure 8.3 shows as an example the fit of a limb-darkened model to the observed visibilities of HD214868 and HD150010.

The average difference between the uniform disk and the limb-darkened diameters are of the order of a few percent, and the angular diameters are not much affected by the choice of μ_λ. All but four stars have θ_{LD} errors of 2% or less, three of the four stars have errors of only 3%, and the one star has a 5% error. By combining the interferometric measured star's angular diameter with the Hipparcos distance (van Leeuwen 2007), it allows one to determine the star's linear radius. The errors are calculated by deriving the diameter at χ^2+1 on both sides of the minimum χ^2 and determining the difference between the χ^2 diameter and χ^2+1 diameter.

The temperatures and luminosities are calculated as explained in Section 8.2.1.

8.3 K giant oscillations

Combining the interferometrically-measured diameter with the mean density of a star determined from the analysis of the oscillation frequencies, it allows one to derive the mass of a giant star. Since the determination of the oscillation frequencies requires a large amount of observing time, this analysis is carried out just for one star to demonstrate how the method works. The giant star chosen is HD170693. In order to detect the oscillations of giant stars an accuracy in the RV determination of few m/s is required. Such precision can only be reached by using echelle spectrograph combined with a large CCD, so that large S/N spectra with both high spectral resolution and broad wavelength coverage are obtained. The important factor which defines the ultimate RV precision is the accuracy of the wavelength calibration. Different techniques are used to obtain precise RV-measurements. In my case I used the iodine absorption cell technique (Butler et al. 1996; Valenti et al. 1995). The idea of this technique is to acquire a wavelength calibration spectrum at the same time and with the same light path as the stellar spectrum. Precise RVs are measured in Tautenburg Observatory using this technique. The echelle spectrograph used to acquire spectra at high resolution is coupled to the 2 m telescope (Alfrend-Jensch-Teleskop). The iodine cell contains low pressure (~ 0.01 atm) molecular iodine (I_2) at a working temperature of 80°C. The cell is placed right in front of the slit so that the stellar light has to pass through it before entering the spectrograph. The spectral region where iodine lines are present ranges from ~ 5000 to ~ 6300 Å; this part of the spectrum is almost useless for any other purpose than RV measurements. The TLS echelle spectrograph that has a resolution of R=67.000 combined with the iodine cell is able to give RV measurements with an error of few m/s.

At the TLS I collected 304 high resolution spectra of HD170693, spread over three months of observations, using the iodine cell technique. A total of over 25 hours of observations were made on this star. HD170693 is a K giant star hosting a planet (Döllinger et al. 2009). This star is very bright with V=4.8 mag and is circumpolar at the Tautenburg latitude (TLS-Longitude 11°42'40.2"Est, Latitude 50°58'48.4"Nord; HD170693 coord. (J2000) 18h25m59.14s +65°33'48.530"). The average signal to noise ratio of the spectra with 5 minutes exposure was of S/N∼50. Standard procedure under IRAF were used to reduce the spectra (bias subtraction, flat-field correction and wavelength calibration). To measure RVs I used the software package RADIAL which extracts RV information from a stellar spectrum with superimposed iodine absorption lines. The RVs measured by this program are relative to one template spectrum of the star under investigation acquired without iodine cell and with high S/N. Complete details on the working principles of this program are given in Cochran et al. (1997) and Hatzes et al. (2000).

A period analysis was performed using the program Period04 (Lenz & Breger 2005). This program extract individual frequencies from the multiperiodic content of a time series, using different tools. Period04 performs a sine waves fit using the dominant period found by the Fourier analysis. This is subtracted to the data and additional periods are found in the residuals by further Fourier analysis. The final fit is computed as a sum of sinus waves with all the significant frequencies. For HD170693 the results of this analysis are presented in Section 9.4. In Figure 8.4 is shown the periodogram relative to all the data, obtained with Period04. In this Figure is visible the frequency of the maximum amplitude pulsation found
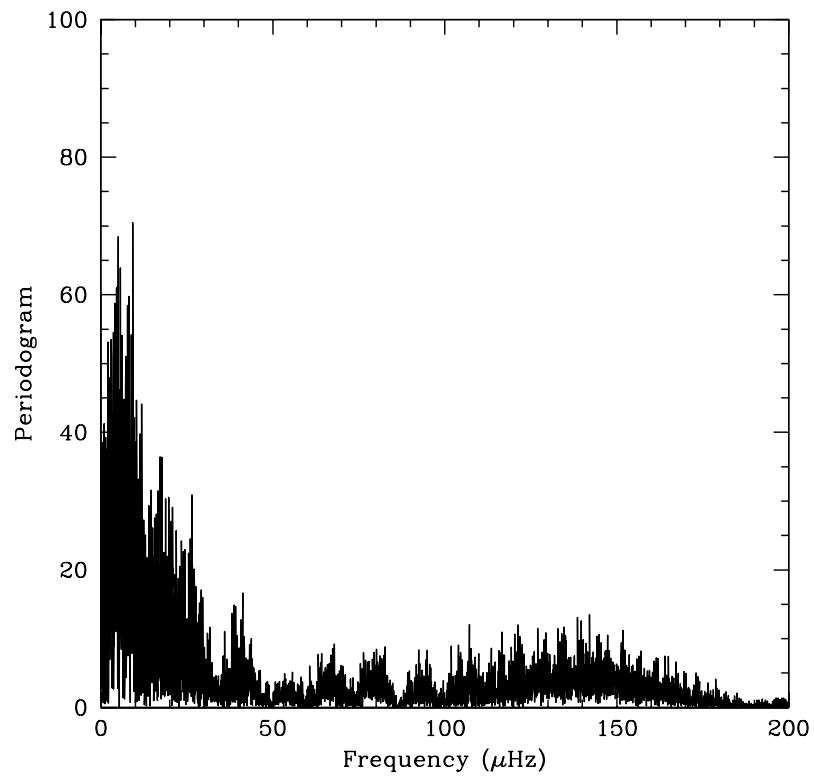
Figure 8.4: *Power spectrum of the HD170693 RVs. A power excess around 8.75µHz is observed.*

for HD170693.

Chapter 9

Testing of the evolutionary tracks of giant stars. III: Results and discussion

In this chapter I present the result of the interferometric observations of the 30 giant stars. The interferometrically-measured angular diameters are compared to the one derived by three set of evolutionary tracks for post-main sequence stars, and the results are discussed. The mass of the giant star HD170693 derived here is also compared to the models.

9.1   Angular diameters

The angular diameter for 30 giants were measured interferometrically and the results are presented in the Table 9.1 and Table 9.3, respectively. Five giant stars were observed with AMBER at VLTI and 25 giant stars were observed with CHARA. For the AMBER sample I computed the averaged diameters in the H and K band, using the values derived in the spectral range 1.6-1.8 μm for the H band and 2.1-2.4 μm for the K band. The stars in the AMBER sample do not show significant variations between the measured angular diameters in the two different bands. Figure 9.1 shows the angular diameters vs. the wavelength in the H and K bands, for four of the five giant stars (HD12438 is not shown, because is a binary).

The temperatures and the luminosities for each star are derived as explained in Section 8.2.1, and are listed in Table 9.1 and Table 9.3.

9.2   Comparison with evolutionary tracks

In order to test the tracks, I use the T_{eff} and the luminosities of the stars to derive the radii from the tracks (Salasnich et al. 2000; Claret 2004; Girardi et al. 2000) which I then compare to the interferometrically derived radii.

As a first step the masses are derived by comparing the position of the giant stars in the HR diagram with respect to the evolutionary tracks. The values of the masses are then combined with the log g values in determining the theoretical diameters. For each star these are given in Table 9.2 and Table 9.4, together with the differences to the measured diameters.

id	V (mag)	K (mag)	Spec. Type	π	θ_{H} (mas)	θ_{K} (mas)	$R_{linear}(R_\odot)$	L $(L_\odot)$	T_{eff}
HD11977	4.70	2.590 ± 0.240	G8.5 III	14.91 ± 0.16	1.579 ± 0.013	1.573 ± 0.015	11.37 ± 0.12	64.5 ± 2.3	4855 ± 84
HD12438	5.35	3.218 ± 0.298	G5 III	11.08 ± 0.29	1.100 ± 0.050	1.150 ± 0.050	10.68 ± 0.28	58.5 ± 6.1	5005 ± 150
HD23319	4.60	2.639 ± 0.274	K2.5 III	17.70 ± 0.22	1.962 ± 0.009	1.929 ± 0.019	11.82 ± 0.15	51.4 ± 5.5	4498 ± 126
HD27256	3.34	1.439 ± 0.312	G8 II-III	20.18 ± 0.10	2.563 ± 0.010	2.559 ± 0.002	13.64 ± 0.07	103.0 ± 5.9	4981 ± 78
HD36848	5.46	2.804 ± 0.268	K2 III	18.93 ± 0.23	1.369 ± 0.017	1.369 ± 0.025	7.77 ± 0.09	17.8 ± 1.0	4280 ± 86

Table 9.1: *Diameters measured with AMBER for the 5 giants. Note that for HD12438 is given the angular diameter obtained by fitting the model of a resolved binary as explained in the text. The V magnitude and the spectral types are from SIMBAD. The K magnitude are from 2MASS. The parallaxes are from van Leeuwen (2007).*

id	θ_{Sal} (mas)	($\theta_{\mathrm{UD,observed}}$ - θ_{Sal}) (mas)	θ_{Gir} (mas)	($\theta_{\mathrm{UD,observed}}$ - θ_{Gir}) (mas)	θ_{Cla} (mas)	($\theta_{\mathrm{UD,observed}}$ - θ_{Cla}) (mas)
HD11977	1.603 ± 0.044	-0.029 ± 0.055	1.543 ± 0.085	0.031 ± 0.091	1.627 ± 0.045	-0.053 ± 0.041
HD12438	1.081 ± 0.040	-0.031 ± 0.045	1.033 ± 0.073	0.017 ± 0.076	1.129 ± 0.055	-0.079 ± 0.059
HD23319	1.966 ± 0.043	-0.031 ± 0.053	2.045 ± 0.136	-0.110 ± 0.139	1.989 ± 0.058	-0.054 ± 0.066
HD27256	2.697 ± 0.042	-0.091 ± 0.048	2.810 ± 0.100	-0.204 ± 0.103	2.762 ± 0.035	-0.156 ± 0.042
HD36848	1.247 ± 0.045	0.103 ± 0.057	1.446 ± 0.056	-0.096 ± 0.066	1.155 ± 0.056	0.195 ± 0.066

Table 9.2: *Diameters from the evolutionary tracks. The comparison was done using the averaged angular diameter between the H an K bands.*

Table 9.3: *Interferometric diameters and effective temperatures of the Northern K giants. θ_{UD} and θ_{LD} represent respectively the uniform disk and limb-darkened diameters measured with the CHARA array. L and T_{eff} are the luminosities and temperatures derived as explained in the text. The K magnitude with the a apex are from 2MASS (Skrutskie et al. 2006), with the b from the Two-Micron Sky Survey (Neugebauer & Leighton 1969). The V magnitude are from Mermilliod (1991) and the spectral types are from SIMBAD Astronomical Database. The parallaxes are from van Leeuwen (2007).*

id	V (mag)	K (mag)	Spec. Type	π (mas)	θ_{UD} (mas)	θ_{LD} (mas)	R_{linear} ($R_\odot$)	L ($L_\odot$)	T_{eff}
HD32518	6.41	3.91 ± 0.04^a	K1 III	8.29 ± 0.58	0.828 ± 0.022	0.851 ± 0.022	11.04 ± 0.77	46.0 ± 2.7	4524 ± 98
HD60294	5.92	3.55 ± 0.22^a	K2 III	12.24 ± 0.39	1.014 ± 0.010	1.044 ± 0.010	9.17 ± 0.29	32.5 ± 1.6	4552 ± 63
HD73108	4.60	1.92 ± 0.07^b	K1 III	12.74 ± 0.26	2.161 ± 0.019	2.225 ± 0.020	18.79 ± 0.38	111.1 ± 7.9	4324 ± 80
HD102328	5.29	2.55 ± 0.06^b	K3 III	15.13 ± 0.30	1.546 ± 0.006	1.606 ± 0.006	11.42 ± 0.23	42.7 ± 3.2	4367 ± 82
HD103605	5.84	3.10 ± 0.30^a	K1 III	10.54 ± 0.37	1.066 ± 0.009	1.098 ± 0.010	11.20 ± 0.41	52.8 ± 3.9	4647 ± 91
HD106574	5.71	2.94 ± 0.08^b	K2 III	7.00 ± 0.28	1.458 ± 0.027	1.498 ± 0.028	23.02 ± 0.92	134.7 ± 10	4099 ± 88
HD113049	6.00	3.66 ± 0.31^a	K0 III	6.02 ± 0.37	0.945 ± 0.021	0.971 ± 0.022	17.35 ± 1.07	119.5 ± 5.9	4581 ± 85
HD118904	5.51	2.69 ± 0.07^b	K2 III	7.93 ± 0.24	1.842 ± 0.031	1.871 ± 0.031	25.38 ± 0.88	135.3 ± 11.5	3908 ± 91
HD136726	5.01	1.92 ± 0.05^b	K4 III	8.19 ± 0.19	2.264 ± 0.020	2.293 ± 0.020	30.12 ± 0.70	229.2 ± 23.3	4093 ± 106
HD137443	5.79	2.74 ± 0.06^b	K4 III	8.86 ± 0.22	1.638 ± 0.030	1.690 ± 0.031	20.51 ± 0.62	96.0 ± 9.5	3989 ± 106
HD138265	5.88	2.38 ± 0.04^b	K5 III	5.11 ± 0.31	1.998 ± 0.037	2.062 ± 0.038	43.40 ± 2.75	338.5 ± 47.5	3758 ± 139
HD139357	5.97	3.41 ± 0.32^a	K4 III	8.47 ± 0.30	1.040 ± 0.012	1.073 ± 0.013	13.63 ± 0.51	72.8 ± 4.0	4567 ± 72
HD150010	6.28	3.18 ± 0.38^a	K2 III	6.95 ± 0.43	0.995 ± 0.028	1.024 ± 0.029	15.84 ± 1.08	98.7 ± 10.0	4570 ± 136
HD152812	6.00	2.83 ± 0.09^b	K2 III	4.97 ± 0.45	1.393 ± 0.003	1.440 ± 0.004	31.16 ± 2.82	260.3 ± 25.6	4153 ± 113
HD157681	5.67	2.19 ± 0.05^b	K5 III	5.23 ± 0.27	1.600 ± 0.009	1.664 ± 0.010	34.22 ± 1.78	384.9 ± 54.0	4371 ± 156
HD160290	5.36	2.67 ± 0.07^b	K1 III	9.23 ± 0.12	1.467 ± 0.010	1.515 ± 0.010	17.65 ± 0.42	113.9 ± 8.0	4487 ± 81
HD167042	5.98	3.44 ± 0.24^a	K1 III	19.91 ± 0.26	0.898 ± 0.017	0.922 ± 0.018	4.98 ± 0.07	11.7 ± 0.6	4782 ± 81
HD170693	4.83	1.95 ± 0.05^b	K1.5 III	10.36 ± 0.20	1.981 ± 0.041	2.041 ± 0.043	21.19 ± 0.60	144.7 ± 11.4	4349 ± 98
HD175823	6.22	3.57 ± 0.32^a	K5 III	5.63 ± 0.28	0.958 ± 0.022	0.988 ± 0.023	18.88 ± 1.04	132.2 ± 9.3	4505 ± 99
HD176408	5.66	3.00 ± 0.27^a	K1 III	11.81 ± 0.27	1.092 ± 0.022	1.125 ± 0.023	10.24 ± 0.23	48.3 ± 3.4	4735 ± 97
HD186815	6.28	4.32 ± 0.25^a	K2 III	12.86 ± 0.39	0.713 ± 0.020	0.731 ± 0.020	6.11 ± 0.25	18.0 ± 0.5	4809 ± 76
HD192781	5.79	2.33 ± 0.07^b	K5 III	5.62 ± 0.23	1.787 ± 0.002	1.859 ± 0.003	35.57 ± 1.46	394.6 ± 33.5	4313 ± 94
HD195820	6.18	3.90 ± 0.22^a	K0 III	8.68 ± 0.29	0.840 ± 0.040	0.863 ± 0.041	10.69 ± 0.62	50.3 ± 2.3	4700 ± 125
HD200205	5.51	2.25 ± 0.06^b	K4 III	5.30 ± 0.24	1.963 ± 0.043	2.032 ± 0.045	41.23 ± 2.08	519.3 ± 36.4	4291 ± 92
HD214868	4.48	1.41 ± 0.07^b	K2 III	9.08 ± 0.26	2.721 ± 0.020	2.731 ± 0.024	29.98 ± 0.84	283.6 ± 27.9	4327 ± 109

Table 9.4: *Diameters derived from the evolutionary tracks.* θ_{Sal}, θ_{Gir} *and* θ_{Cla} *are respectively the diameters estimated from the evolutionary tracks of Salasnich et al. (2000), Girardi et al. (2000) and Claret (2004). The differences between these last and the observed diameters (UD) are also reported.*

| id	θ_{Sal} (mas)	($\theta_{\mathrm{UD,observed}}$ - θ_{Sal}) (mas)	θ_{Gir} (mas)	($\theta_{\mathrm{UD,observed}}$ - θ_{Gir}) (mas)	θ_{Cla} (mas)	($\theta_{\mathrm{UD,observed}}$ - θ_{Cla}) (mas)
HD32518	0.810 ± 0.115	0.018 ± 0.117	0.809 ± 0.110	0.019 ± 0.112	0.826 ± 0.076	0.002 ± 0.079
HD60294	1.024 ± 0.054	-0.010 ± 0.055	1.084 ± 0.091	-0.070 ± 0.092	1.013 ± 0.053	0.001 ± 0.054
HD73108	2.263 ± 0.234	-0.102 ± 0.237	2.303 ± 0.172	-0.142 ± 0.173	2.562 ± 0.093	-0.401 ± 0.094
HD102328	1.603 ± 0.071	-0.066 ± 0.043	1.590 ± 0.122	-0.044 ± 0.122	1.612 ± 0.043	-0.223 ± 0.083
HD103605	1.084 ± 0.083	-0.018 ± 0.083	1.028 ± 0.070	0.038 ± 0.071	1.138 ± 0.089	-0.085 ± 0.085
HD106574	1.513 ± 0.091	-0.055 ± 0.094	1.575 ± 0.167	-0.117 ± 0.170	1.453 ± 0.088	0.005 ± 0.092
HD113049	0.991 ± 0.105	-0.046 ± 0.107	1.013 ± 0.151	-0.068 ± 0.152	1.020 ± 0.108	-0.075 ± 0.11
HD118904	1.728 ± 0.052	0.114 ± 0.061	1.988 ± 0.130	-0.146 ± 0.134	1.782 ± 0.086	0.060 ± 00.091
HD136726	2.303 ± 0.164	-0.039 ± 0.165	2.413 ± 0.236	-0.149 ± 0.237	2.329 ± 0.185	-0.065 ± 0.190
HD137443	1.654 ± 0.073	-0.016 ± 0.079	1.616 ± 0.120	0.022 ± 0.124	1.593 ± 0.069	0.045 ± 0.075
HD138265	2.086 ± 0.251	-0.088 ± 0.254	2.449 ± 0.510	-0.451 ± 0.511	1.978 ± 0.160	0.020 ± 00.164
HD139357	1.110 ± 0.064	-0.070 ± 0.065	0.997 ± 0.100	0.043 ± 0.100	1.118 ± 0.081	-0.078 ± 0.082
HD150010	1.001 ± 0.112	-0.006 ± 0.115	0.850 ± 0.125	0.145 ± 0.128	1.112 ± 0.079	-0.117 ± 0.084
HD152812	1.416 ± 0.180	-0.023 ± 0.180	1.415 ± 0.287	-0.022 ± 0.287	1.539 ± 0.181	-0.146 ± 0.181
HD157681	1.686 ± 0.145	-0.086 ± 0.145	1.336 ± 0.099	0.264 ± 0.099	1.593 ± 0.083	0.007 ± 0.083
HD160290	1.527 ± 0.110	-0.060 ± 0.110	1.432 ± 0.182	0.035 ± 0.182	1.530 ± 0.107	-0.063 ± 0.107
HD167042	0.935 ± 0.092	-0.037 ± 0.094	0.885 ± 0.060	0.013 ± 0.062	0.968 ± 0.040	-0.070 ± 00.043
HD170693	2.051 ± 0.172	-0.070 ± 0.177	1.987 ± 0.137	-0.006 ± 0.143	2.157 ± 0.117	-0.176 ± 0.124
HD175823	0.976 ± 0.049	-0.018 ± 0.054	0.964 ± 0.121	-0.006 ± 0.123	1.028 ± 0.094	-0.070 ± 00.097
HD176408	1.141 ± 0.083	-0.049 ± 0.086	1.097 ± 0.087	-0.005 ± 0.090	1.177 ± 0.037	-0.085 ± 0.043
HD186815	0.681 ± 0.043	0.032 ± 0.047	0.757 ± 0.068	-0.044 ± 0.071	0.782 ± 0.037	-0.069 ± 0.042
HD192781	1.921 ± 0.123	-0.117 ± 0.130	1.312 ± 0.234	0.475 ± 0.234	1.885 ± 0.082	-0.097 ± 0.079
HD195820	0.886 ± 0.070	-0.046 ± 0.081	0.840 ± 0.056	0.000 ± 0.069	0.861 ± 0.088	-0.021 ± 0.097
HD200205	$2.0860.129$	-0.123 ± 0.136	1.579 ± 0.188	0.384 ± 0.193	2.055 ± 0.169	-0.092 ± 0.174
HD214868	2.782 ± 0.122	-0.061 ± 0.124	2.461 ± 0.230	0.260 ± 0.231	2.845 ± 0.074	-0.124 ± 0.077
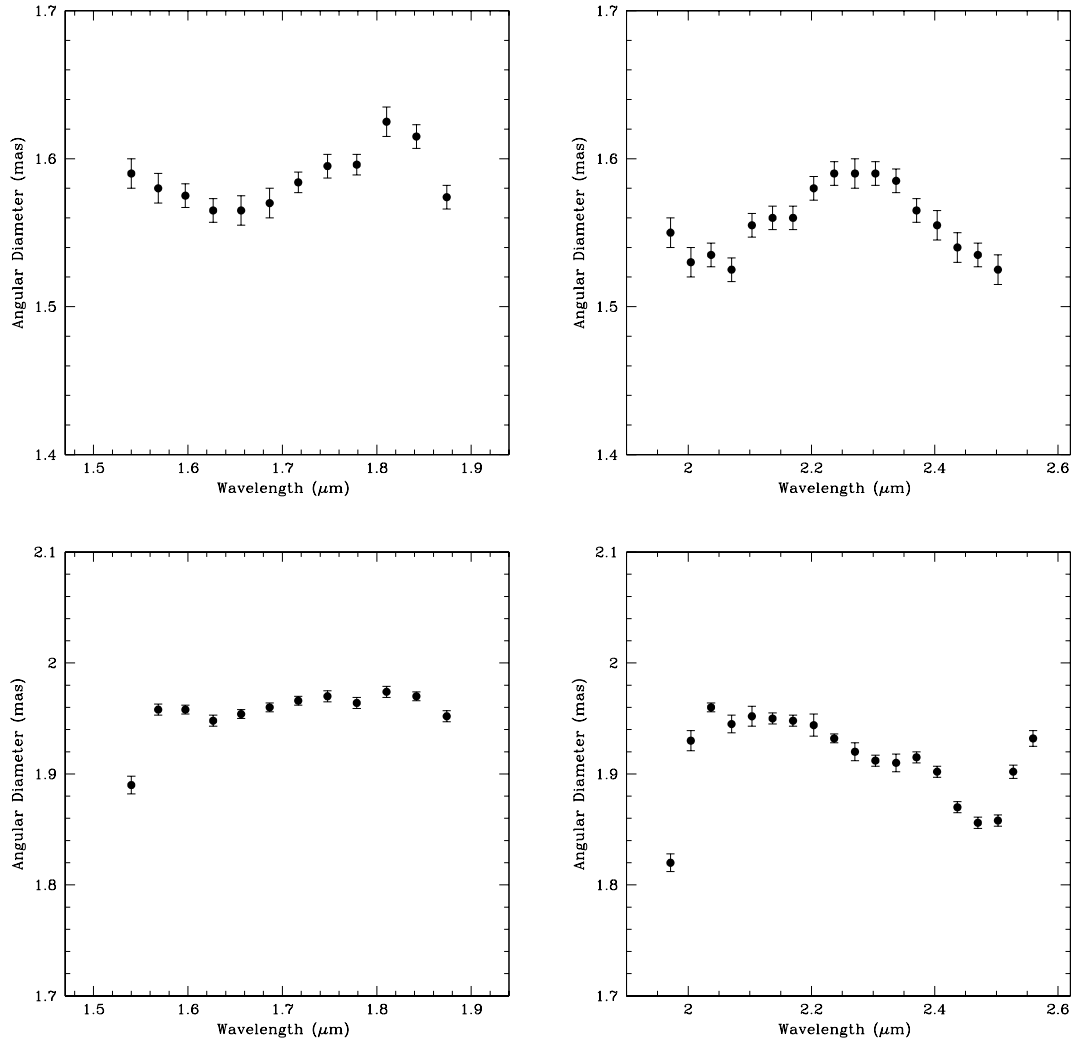
Figure 9.1: *The interferometrically-measured angular diameter vs. wavelength, for HD11977 (top panel)and HD23319 (low panel). Shown on the left is the H band and on the right the K band.*

Figure 9.3 shows the interferometrically-observed diameters vs. the theoretical ones. These plots clearly show the advantage of measuring angular diameters interferometrically, as the errors are significantly smaller than the ones derived from the models in all cases. The agreement between the tracks and the measured diameters is in general good. A careful inspection shows that the tracks published by Salasnich et al. (2000) reproduce the observed diameters best.

9.3   HD12438

The detailed analysis of the interferometric data taken with AMBER shows that this star is a binary (see Section 8.2.1). By fitting the observed visibilities of this star taken at four different epochs to the model of a binary star, I was able to estimate the position angle (p.a.) and the separation between the components: $\rho = 12.0 \pm 4$ mas and p.a.$=120 \pm 20^{\circ}$.
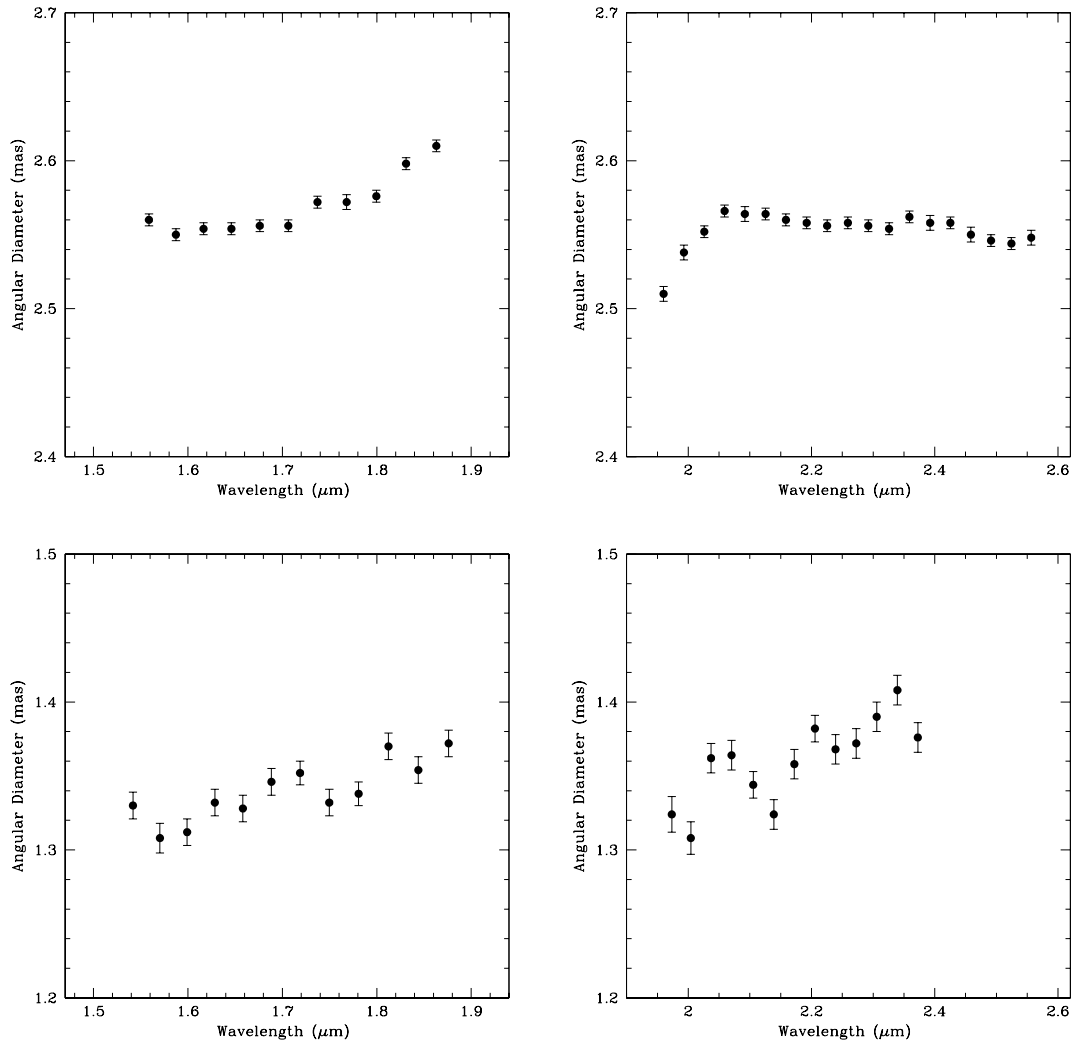
Figure 9.2: *The interferometrically-measured angular diameter vs. wavelength, of HD27256 (top panel) and HD36848 (low panel). On the left is shown the H band on the right the K band.*

The p.a. changes only by a very tiny amount for observations separated by 2.5 months (6 October - 20 December 2008), indicating a very long orbital period. The p.a. is on average $120 \pm 20°$. The primary star is resolved with the baselines used. The angular diameters of the primary and secondary are of 1.00 ± 0.10 and ≤ 0.30 mas, respectively. The flux ratio ratio is ~ 0.028, both in the H and K band. The closure phases (Figure 9.4) also indicate that the object is not centro-symmetric. Four of the five targets have closure phase equal to zero for each wavelength, while HD12438 has a closure phase that is changing with wavelength indicating that the object is not a single star. The binarity of HD12438 is further supported by RV-measurements taken by Setiawan et al. (2004) and Döllinger (private communication). Although these authors did not recognise that the star is a binary, they found a trend in the RV-data which also indicates that the object is a binary. Setiawan observed the object for 5 years with HARPS, Döllinger for 2.8 years with FEROS. The two sets of data combined cover a period of almost 8 years. After the correction for the different zero point of the two
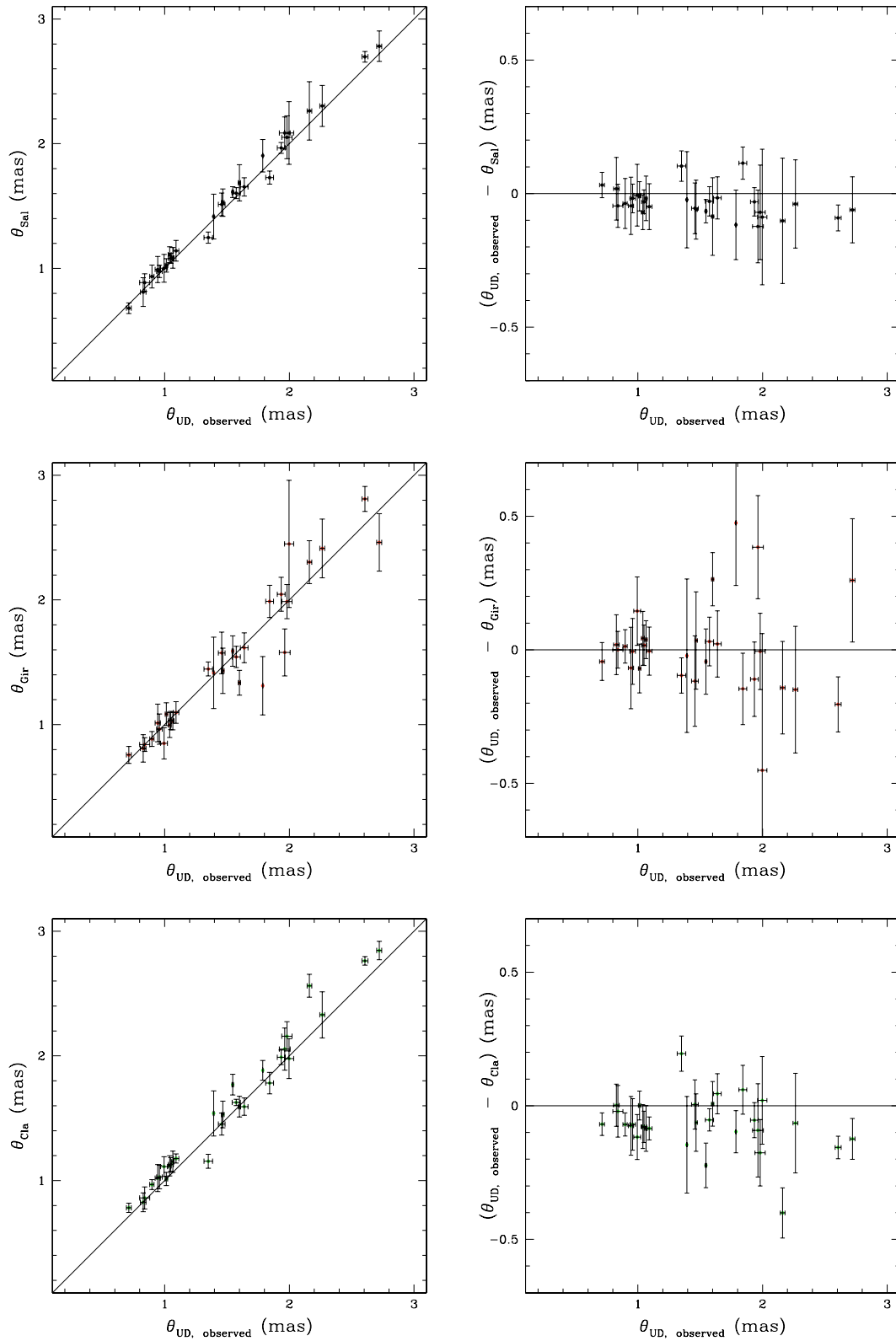
Figure 9.3: *Comparison between the diameters estimated from the tracks and the interferometrically-measured ones. Starting from the top panel are shown the diameters estimated from the Salasnich et al. (2000), Girardi et al. (2000) and Claret (2004) tracks. The diagonal solid line indicates a 1:1 ratio for the diameters. Note the significantly larger error bars associated with the diameters determined from the tracks.*
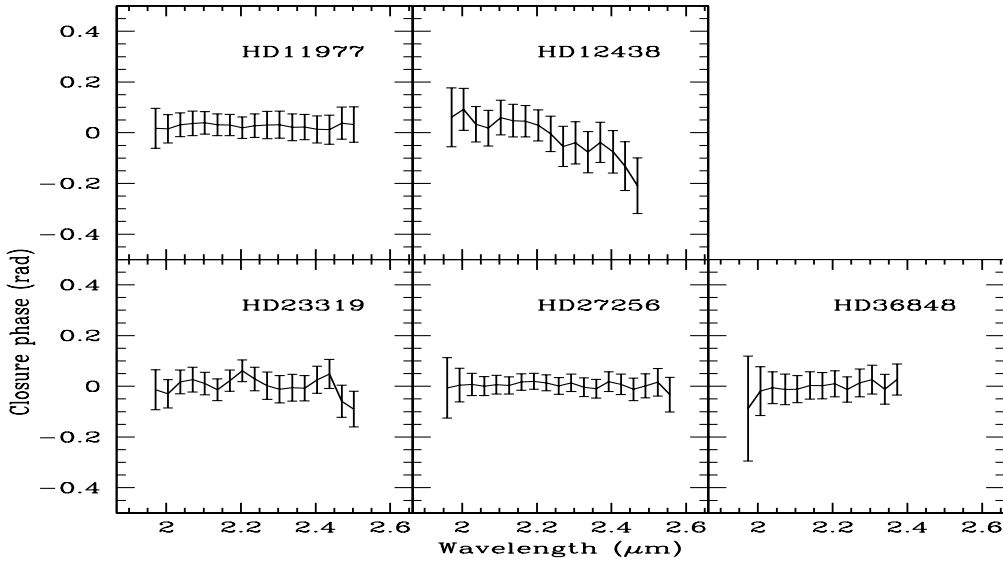
Figure 9.4: *Closure phase in the K band for the 5 giant stars observed with AMBER. In the case of HD12438, the closure phase is not zero and depends on wavelengths, indicating that the object is a binary. The other giant stars have zero closure phase as expected.*

Mode	Frequency (μHz)	Amplitude (m s^{-1})
f_1	8.75 ± 0.13	22.31 ± 1.06
f_2	4.79 ± 0.15	22.09 ± 1.15
f_3	23.96 ± 0.28	14.96 ± 1.31
f_4	29.62 ± 0.43	10.29 ± 1.49

Table 9.5: Oscillation frequencies of HD170693.

instruments (de Medeiros et al. 2009), I found that the binary must have a period longer than 9 years. A detailed discussion of the spectroscopic orbital parameters is far from the purpose of this work, where the RV data were used only to confirm the binarity of HD12438. I only estimate a Msini ~ 16 $M_{\rm jup}$ for the secondary star from the RV curve. Using the mass estimation $M_1{=}1.02 \pm 0.19$ M$_\odot$ for the primary component taken from da Silva et al. (2006), and the H and K band flux ratios, together with the mass-magnitude relation given by Kroupa & Tout (1997), the mass of the secondary is expected to be M$_2 \sim 0.5$ M$_\odot$. Comparing the latter with mass estimated by the RV curve, I deduce that the binary is highly inclined (i < 9º) toward the line of sight. This explains also the small amplitude of the RV-variations observed.

9.4   HD170693

The pulsation frequencies of HD170693, found in the asterosismological analysis, are reported in Table 9.5. Figure 9.5 shows part of the fit to the data. By combining the interferometrically-measured radius with the frequencies of maximum amplitude oscillation
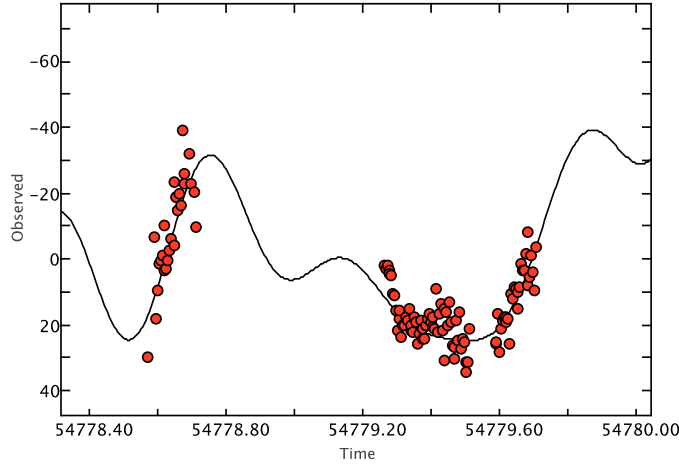
Figure 9.5: *The red points are the observed RVs (m s^{-1}) of HD170693 relative to one template spectra. The continuum line is result of the sum of four sinus waves each with a frequency listed in Table 9.5. The data set plotted is relative to 2 consecutive nights of observation in November 2008.*

the mass is derived using the equation (Kjeldsen & Bedding 1995):

$$\mathrm{M/M_\odot} = \nu_{\mathrm{max}}(\mathrm{R/R_\odot})^2\sqrt{T_{\mathrm{eff}}/5777\ \mathrm{K}}\ 3.05^{-1}\mathrm{mHz} \tag{9.1}$$

where M is the mass of the star in solar units, ν_{max} is the frequency of the maximum amplitude oscillation, T_{eff} is the temperature of the star and 3.05 mHz is the frequency of the maximum amplitude oscillation of the sun.

The values of the inferometric radius and T_{eff} of HD170693 are given in the Table 9.3. Using f$_1$=8.75 $\pm$ 0.01μHz as maximum frequency I obtained a value for the mass of $\mathrm{M}_{\nu_{max}} = 1.12 \pm 0.09\ \mathrm{M_\odot}$.

In order to derive the primary frequency splitting $\Delta\nu_0$, I applied the comb-response method (Kjeldsen et al. 1995). $\Delta\nu_0$ is defined as the separation between two consecutive modes with the same l, which differ by one radial order. Using this definition the strongest picks in the power spectrum of a star showing solar-like oscillations are separated by interval of $\frac{1}{2}$ $\Delta\nu_0$. Given ν_{max}, the comb-response function (Kjeldsen et al. 1995) is given by the product:

$$\mathrm{CR}(\Delta\nu) = \mathrm{PS}(\nu_{\mathrm{max}} - \frac{1}{2}\Delta\nu)\mathrm{PS}(\nu_{\mathrm{max}} + \frac{1}{2}\Delta\nu)\mathrm{PS}(\nu_{\mathrm{max}} - \Delta\nu)\mathrm{PS}(\nu_{\mathrm{max}} + \Delta\nu) \tag{9.2}$$

$$\times[\mathrm{PS}(\nu_{\mathrm{max}} - \frac{3}{2}\Delta\nu)\mathrm{PS}(\nu_{\mathrm{max}} + \frac{3}{2}\Delta\nu)\mathrm{PS}(\nu_{\mathrm{max}} - 2\Delta\nu)\mathrm{PS}(\nu_{\mathrm{max}} + 2\Delta\nu)]^{0.5}$$

where CR is the comb-response function and PS is the power spectrum. A peak in this function for a particular value allows one to find $\Delta\nu_0$. I implemented the comb function with a software. The frequency splitting of HD170693 which I found in the analysis is $\Delta\nu_0$= 1.28 $\pm$ 0.10 μHz. Figure 9.6 shows the comb response function vs. the large separation expressed in μHz. The maximum is observed for $\Delta\nu_0 \sim 1.28\ \mu$Hz. Hekker et al. (2009) found that there is a relation between the maximum amplitude of oscillations and the primary
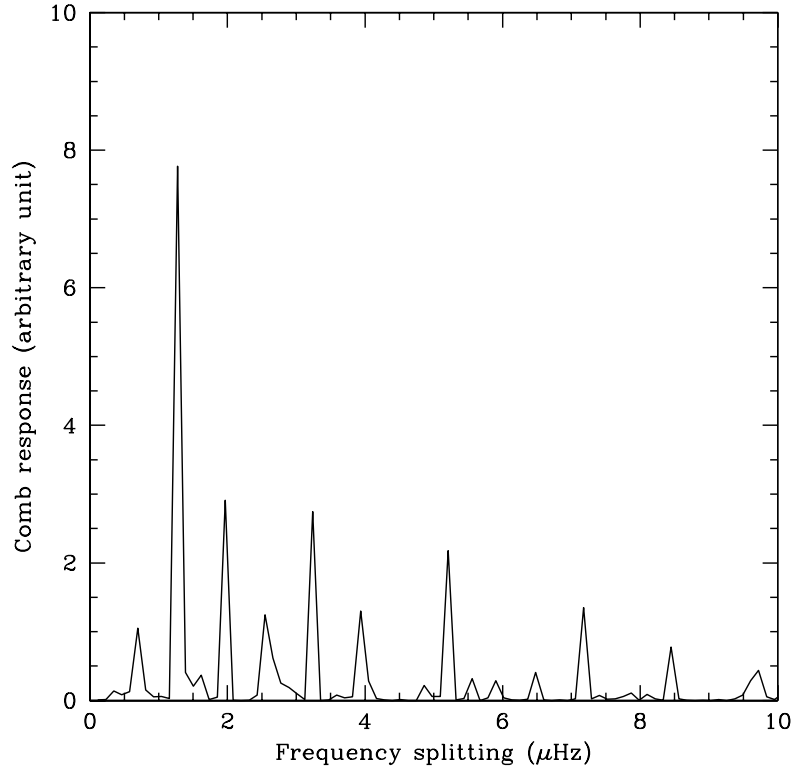
Figure 9.6: *The comb response function obtained for the central frequency 8.75 μHz. The peak is at*
$\Delta\nu \sim 1.28\mu Hz$. *The error of the $\Delta\nu$ is the FWHM of the peak.*

frequency separation. This relation is $\Delta\nu_0$= 134.9 $(\nu_{\max}/3050)^{0.784}$ μHz. Using the last
equation and the value for the maximum frequency reported in Table 9.5 I obtained $\Delta\nu_0 = 1.37 \pm 0.04$ μHz. This value is consistent within the errors with the one found in the comb-
response analysis. The primary frequency splitting $\Delta\nu_0$ is directly proportional to the mean
density of the star. Scaled to the solar value it becomes (Kjeldsen & Bedding 1995):

$$M/M_\odot = \Delta\nu_0^2 (R/R_\odot)^3 134.9^{-2} \mu Hz \qquad (9.3)$$

Using this equation, and the interfometrically-measured radius I derive a value of the
mass of $M_{\Delta\nu_{0comb}}$=0.86 ± 0.21 $M_\odot$ and $M_{\Delta\nu_{0hekk}}$=0.98 ± 0.08 $M_\odot$ for the frequency splitting
found with the comb-function and the one found analytically, respectively. Performing a
weighted average of the three mass values derived using the oscillations ($M_{\nu_{max}}$, $M_{\Delta\nu_{0comb}}$
and $M_{\Delta\nu_{0hekk}}$), the resultant mass is $M_{average}$=1.01 ± 0.14 $M_\odot$.

In order to compare the true mass of HD170693 with the models, I derive the mass from
the evolutionary tracks using the observed temperature and luminosity of HD170693 given
in Table 9.3. From the Salasnich, Girardi and Claret tracks, using metallicity as close as
possible to [Fe/H]=-0.54 (Soubiran et al. 2008), I obtain masses of $M_{Sal} = 1.00 \pm 0.10 M_\odot$,
$M_{Gir} = 0.98 \pm 0.05 M_\odot$ and $M_{Cla} = 1.00 \pm 0.11$ $M_\odot$, respectively. Figure 9.7 shows the position
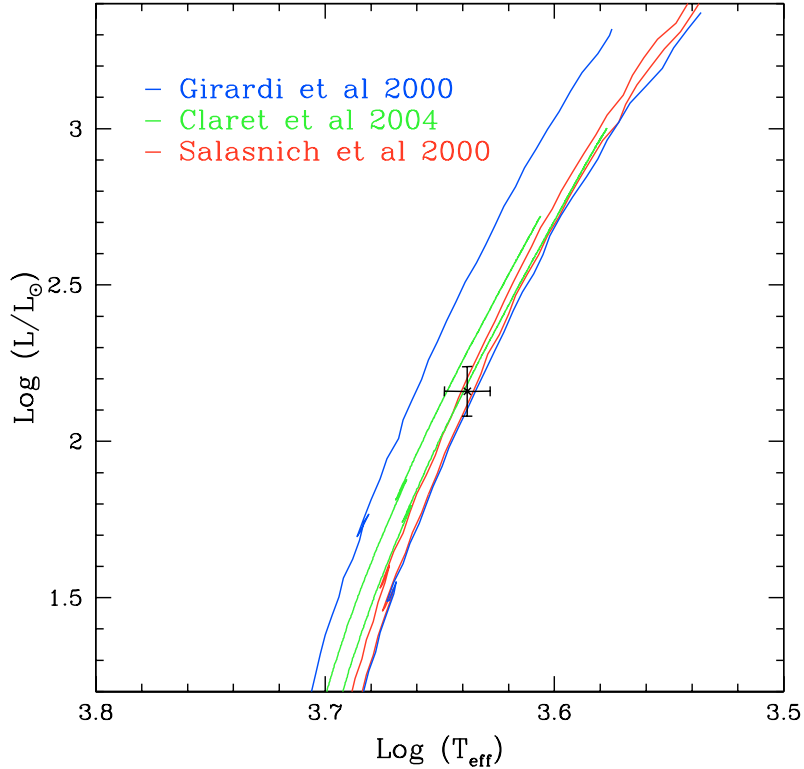of HD170693 in the HR diagram, together with the evolutionary tracks used in this work.

Figure 9.7: *HR diagram for HD170693. The blue lines are the evolutionary tracks calculated by Girardi et al. (2000) for Z=0.004 and masses of 1.10 and 1.00 M$_\odot$. The green lines are the Claret (2004) tracks for 1.12 and 1.00 M$_\odot$ and Z=0.004. The red lines are the Salasnich et al. (2000) tracks for 1.10 and 1.00 M$_\odot$ and Z=0.008. The mass of the tracks decrease from left to right.*

9.5   Discussion on the result obtained for giant stars

Figures 9.1 and 9.2 show the radii vs. wavelength determined for the HD11977, HD23319, HD27256 and HD36848. Deviations from a constant radius are observed mostly at the borders of the H and K bands. These deviations are certainly due to absorption lines of molecules like the H_2O and CO_2 in the atmosphere of the earth. The situation is different for HD36848, the coolest star of the southern sample. The variations of the diameter of this star are larger than for the others stars and they do not coincide with the telluric absorption band. This effect can be best explained considering that interferometry measures the diameter of the $\tau=1$[1] surface, and the atmosphere of cool stars are so tenuous and extended that they become opaque at a substantial larger radius in absorption bands of molecules that in the continuum. Thus for this star the measured angular diameter depends on the wavelength of observation.

   The comparison of the interferometrically-observed diameters with the evolutionary tracks shows that the difference is on average smaller than 1 σ (see Figure 9.3). Thus the agreement is excellent. I just remark that the differences are larger for stars of lower temperature, than for stars of higher temperature. This indicates that the available models have some difficulties

---

[1]The absorption and/or scattering of radiation by a medium is measured by optical depth τ. Intensity falls by a factor of e (2.718...) when $\tau = 1$.
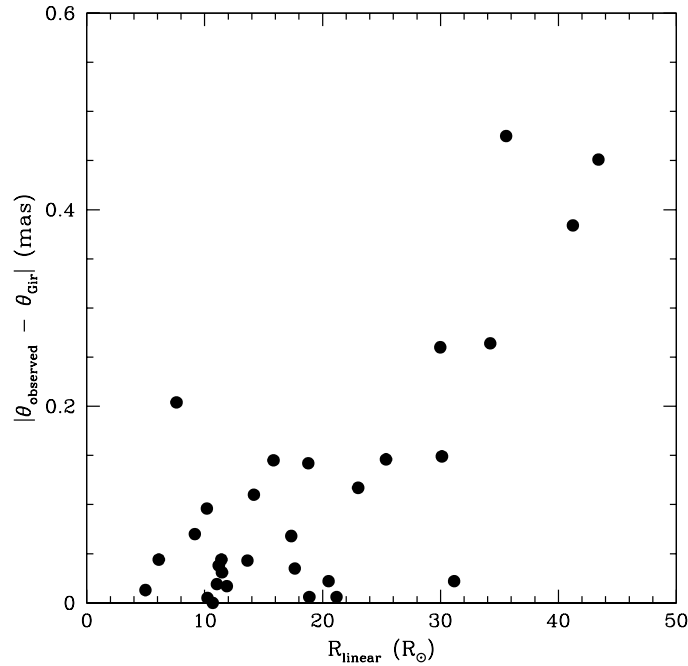
Figure 9.8: *Trend of the ($\theta_{\rm UD,observed}$ - $\theta_{\rm Gir}$) absolute value with the linea radii. The difference between the model and the observation enhances for bigger radii.*

in describing the opacity of some molecules like the TiO molecule, which are present in the outer layer of the cooler atmosphere. As an example Figure 9.8 shows the trend of the difference between models and observation with the measured linear radii for the Girardi tracks. The agreement between theory and observations is better for giant star of smaller physical radii.

Among the three set of evolutionary tracks for post-main sequence stars that I used in this thesis, the Salasnich tracks are the ones that fit the observations best. A possible explanation is that Salasnich et al. (2000) use up to date opacities, whereas the others do not. For example, Salasnich et al. (2000) adopt the Itoh et al. (1983) conductive opacities instead of the older ones by Hubbard & Lampe (1969) used by Girardi et al. (2000). Different numerical technique are also used by Salasnich et al. (2000) to interpolate within the grids of opacity tables.

In order to demonstrate how to derive the masses of giant stars by combining interferometric data and observations of stellar oscillations, I derived the mass of HD170693. The limitation is currently that the observations of the oscillations are very time consuming. If more data will be added, the accuracy in the determination of the mass would improve. The results obtained nevertheless show that masses can be derived with very high accuracy to test the tracks. In the case of HD170693 I find an agreement between the measured mass and the one derived by the models.

Chapter 10

Conclusions

This thesis illustrates the results of the application of optical interferometry to the study of pre-main sequence and giant stars at high angular resolution. In particular, it has been proved that interferometry is a powerful tool to determine fundamental physical parameters of stars independently of physical models.

The determination of stellar masses in young binary systems obtained combining optical interferometry and spectroscopy can be used to test the theoretical models of young stars. One of the outcome of these models are the so-called PMS evolutionary tracks, which delineate in the HR diagram the evolution of a star with a fixed mass from the early phase of a proto-star up to the main sequence. The tracks are largely used by the scientific community to estimate the masses of PMS stars in the star-forming regions. These tracks, at a given mass value, differ from author to author. This is because the input physics used by each author is different, as for instance the treatment of convection, opacity, and boundary conditions. Using different tracks the estimated mass of a star can differ from one set of tracks to another one up to 50-60%. It is therefore crucial to test them measuring a large number of young stellar masses. This is possible if spectroscopic observations of binary systems are combined with optical interferometry in order to derive the mass of the single components. In this thesis:

- A sample of 13 PMS spectroscopic binaries suitable for interferometric observations was collected by Guenther et al. (2007) and me. For all these objects, I determined the spectroscopic orbits and in two cases I was able to determine the mass ratio and compare it with the one derived from the evolutionary tracks by three different authors.

- I also discovered a young binary system, namely HD113449, in the course of exo-planet hunting with HARPS at ESO. I determined the spectroscopic orbit of this SB1 system and through high-resolution infrared spectroscopy performed with CRIRES at ESO I was able to detect the secondary component. Measuring the relative velocity at the time of the CRIRES at ESO observation, I was able to determine the mass ratio of the two stars in the binary system. With AMBER at VLTI I measured the relative position of the two stars during one night of observation and, modelling it, I derived the missing parameter of the orbit, reaching in the end the determination of the masses of the two components. Comparing the mass values, with the ones estimated by means of the evolutionary tracks, and also considering the result obtained from the mass ratios

analysis, I concluded that the Baraffe tracks for l=1 H_p are the ones that fit better with the observations presented in this thesis. This result is in agreement with Hillenbrand & White (2004) which found that the Baraffe tracks are the ones that best fit the masses of the young stars in the range 0.5-1.0 $M_\odot$.

In the future, more observations will be needed and the next generation interferometric instruments (such as PRIMA at VLTI) will be able to observe all the binary systems that I collected, allowing the determination of more than 20 masses of young stars.

The same problem is connected with the evolutionary tracks of post main-sequence stars. First, they depend on the authors, and what is more important is their position in the HR diagram, because they converge to the same region of it. The masses of giant stars estimated from the tracks are indeed affected by large uncertainty. The knowledge of the mass of giant stars with high accuracy is of crucial importance in the exo-planet theory because, since the discovery of the first planet with RV technique, more than 30 planets have been discovered around giant stars and more will be found by the ongoing surveys. An error in the determination of the mass of the hosting star reflects in a wrong determination of the upper limit value of the planet mass. For this reason, it is important to provide several model independent mass estimations to test the theories. In this thesis:

- I observed 30 giant stars with two interferometers, the CHARA array and the VLTI. I determined the interferometric angular diameters of these stars comparing them with the one from three sets of evolutionary tracks. Among these, the Salasnich et al. (2000) tracks resulted to be the ones that better predict the measured diameters.

- One of the stars analysed, namely HD12438, resulted to be an unknown binary system, demonstrating the power of interferometry also in detecting unseen close binaries. This discovery was confirmed by RVs present in the literature that show a regular variation in a very long period (P > 9.5 years).

- For one of the 30 giants, namely HD170693, I performed also time series observations with the high resolution Tautenburg spectrograph at the 2m-Alfred-Jensch-Telescope. Measuring accurate RVs, I performed a frequency analysis and I found the frequency of maximum oscillation and the primary frequency splitting. Combining this results with the interferometrically-measured diameter, I obtained an estimation of the stellar mass, which resulted to be in good agreement to what expected by the evolutionary tracks.

In the near future, time series observations of all the giant stars in the sample will allow the determination of 29 giant star masses without any dependence from the physical models, allowing a test of the evolutionary tracks. Seven of these are hosting a planet and the mass determined with the interferometry-asteroseismology technique will allow us to improve also the upper limits of the exo-planet masses.

Bibliography

Alexander, D. R. and Ferguson, J. W. 1994, Astroph. J., 437, 879

Alonso, A., Arribas, S., and Martínez-Roger, C. 1999, Astron. & Astroph. Suppl., 140, 261

Anderson, J. A. 1920, Astroph. J., 51, 263

Armstrong, J. T. 1994, in Society of Photo-Optical Instrumentation Engineers (SPIE) Conference Series, Vol. 2200, Society of Photo-Optical Instrumentation Engineers (SPIE) Conference Series, ed. J. B. Breckinridge, 62–70

Baines, E. K., Döllinger, M. P., Cusano, F., Guenther, E. W., and Hatzes, A. P. et al. 2009, Interferometric and Spectroscopic Observations of Twenty-five K Giant Stars, sumbitted to Astroph. J.

Baldwin, J. E., Beckett, M. G., Boysen, R. C., Burns, D., Buscher, D. F., Cox, G. C., Haniff, C. A., Mackay, C. D., Nightingale, N. S., Rogers, J., Scheuer, P. A. G., Scott, T. R., Tuthill, P. G., Warner, P. J., Wilson, D. M. A., and Wilson, R. W. 1996, Astron. & Astroph., 306, L13+

Baldwin, J. E., Boysen, R. C., Cox, G. C., Haniff, C. A., Rogers, J., Warner, P. J., Wilson, D. M., and Mackay, C. D. 1994, in Society of Photo-Optical Instrumentation Engineers (SPIE) Conference Series, Vol. 2200, Society of Photo-Optical Instrumentation Engineers (SPIE) Conference Series, ed. J. B. Breckinridge, 112–117

Baldwin, J. E., Haniff, C. A., Mackay, C. D., and Warner, P. J. 1986, Nature, 320, 595

Baraffe, I., Chabrier, G., Allard, F., and Hauschildt, P. H. 1998, Astron. & Astroph., 337, 403

Barnes, S. A. 2007, Astroph. J., 669, 1167

Boden, A. F., Sargent, A. I., Akeson, R. L., Carpenter, J. M., Torres, G., Latham, D. W., Soderblom, D. R., Nelan, E., Franz, O. G., and Wasserman, L. H. 2005, Astroph. J., 635, 442

Böhm-Vitense, E. 1958, Zeitschrift fur Astrophysik, 46, 108

Bressan, A. G., Chiosi, C., and Bertelli, G. 1981, Astron. & Astroph., 102, 25

Brown, R. H. and Twiss, R. Q. 1957, Royal Society of London Proceedings Series A, 242, 300

Butler, R. P., Marcy, G. W., Williams, E., McCarthy, C., Dosanjh, P., and Vogt, S. S. 1996, Publ. Astron. Soc. Pacific, 108, 500

Cardelli, J. A., Clayton, G. C., and Mathis, J. S. 1989, Astroph. J., 345, 245

Casey, B. W., Mathieu, R. D., Vaz, L. P. R., Andersen, J., and Suntzeff, N. B. 1998, Astron. J., 115, 1617

Caughlan, G. R. and Fowler, W. A. 1988, Atomic Data and Nuclear Data Tables, 40, 283

Christensen-Dalsgaard, J. and Daeppen, W. 1992, Astron. & Astroph. Rev., 4, 267

Claret, A. 2004, Astron. & Astroph., 424, 919

Claret, A., Diaz-Cordoves, J., and Gimenez, A. 1995, Astron. & Astroph. Suppl., 114, 247

Cochran, W. D., Hatzes, A. P., Butler, R. P., and Marcy, G. W. 1997, Astroph. J., 483, 457

Connes, P., Shaklan, S., and Roddier, F. 1987, in Interferometric Imaging in Astronomy, ed. J. W. Goad, 165–+

Cornwell, T. J. 1989, Science, 245, 263

Coude Du Foresto, V., Ridgway, S., and Mariotti, J.-M. 1997, Astron. & Astroph. Suppl., 121, 379

Covino, E., Frasca, A., Alcalá, J. M., Paladino, R., and Sterzik, M. F. 2004, Astron. & Astroph., 427, 637

Cusano, F., Paladini, C., Richichi, A., Guenther, E. W., Aringer, B., Biazzo, K., Pasquini, L., and Hatzes, A. P. 2011, Astron. & Astroph., submitted

da Silva, L., Girardi, L., Pasquini, L., Setiawan, J., von der Lühe, O., de Medeiros, J. R., Hatzes, A., Döllinger, M. P., and Weiss, A. 2006, Astron. & Astroph., 458, 609

Davis, J. and Tango, W. J. 1985, Proceedings of the Astronomical Society of Australia, 6, 38

de Medeiros, J. R., Setiawan, J., Hatzes, A. P., Pasquini, L., Girardi, L., Udry, S., Döllinger, M. P., and da Silva, L. 2009, Astron. & Astroph., 504, 617

di Benedetto, G. P. and Rabbia, Y. 1987, Astron. & Astroph., 188, 114

Döllinger, M. P. 2008, Ph.D., LMU Münich

Döllinger, M. P., Hatzes, A. P., Pasquini, L., Guenther, E. W., Hartmann, M., and Girardi, L. 2009, Astron. & Astroph., 499, 935

Dyck, H. M., Benson, J. A., and Ridgway, S. T. 1993, Publ. Astron. Soc. Pacific, 105, 610

Endl, M., Cochran, W. D., Kürster, M., Paulson, D. B., Wittenmyer, R. A., MacQueen, P. J., and Tull, R. G. 2006, Astroph. J., 649, 436

Esposito, M., Covino, E., Alcalá, J. M., Guenther, E. W., and Schisano, E. 2007, Mon. Not. R. Astron. Soc., 376, 1805

Frasca, A., Alcalá, J. M., Covino, E., Catalano, S., Marilli, E., and Paladino, R. 2003, Astron. & Astroph., 405, 149

Gaidos, E. J. and Gonzalez, G. 2002, New Astronomy, 7, 211

Gaidos, E. J., Henry, G. W., and Henry, S. M. 2000, Astron. J., 120, 1006

Girardi, L., Bressan, A., Bertelli, G., and Chiosi, C. 2000, Astron. & Astroph. Suppl., 141, 371

Gray, R. O., Corbally, C. J., Garrison, R. F., McFadden, M. T., and Robinson, P. E. 2003, Astron. J., 126, 2048

Guenther, E. W., Covino, E., Alcalá, J. M., Esposito, M., and Mundt, R. 2005, Astron. & Astroph., 433, 629

Guenther, E. W., Esposito, M., Mundt, R., Covino, E., Alcalá, J. M., Cusano, F., and Stecklum, B. 2007, Astron. & Astroph., 467, 1147

Haguenauer, P., Abuter, R., Alonso, J., Argomedo, J., Bauvir, B., Blanchard, G., Bonnet, H., Brillant, S., Cantzler, M., Derie, F., Delplancke, F., Di Lieto, N., Dupuy, C., Durand, Y., Gitton, P., Gilli, B., Glindemann, A., Guniat, S., Guisard, S., Haddad, N., Hudepohl, G., Hummel, C., Jesuran, N., Kaufer, A., Koehler, B., Le Bouquin, J.-B., Lév"que, S., Lidman, C., Mardones, P., Ménardi, S., Morel, S., Percheron, I., Petr-Gotzens, M., Phan Duc, T., Puech, F., Ramirez, A., Rantakyrö, F., Richichi, A., Rivinius, T., Sahlmann, J., Sandrock, S., Schöller, M., Schuhler, N., Somboli, F., Stefl, S., Tapia, M., Van Belle, G., Wallander, A., Wehner, S., and Wittkowski, M. 2008, in Presented at the Society of Photo-Optical Instrumentation Engineers (SPIE) Conference, Vol. 7013, Society of Photo-Optical Instrumentation Engineers (SPIE) Conference Series

Hanbury Brown, R., Davis, J., Lake, R. J. W., and Thompson, R. J. 1974, Mon. Not. R. Astron. Soc., 167, 475

Hanisch, R. J., Farris, A., Greisen, E. W., Pence, W. D., Schlesinger, B. M., Teuben, P. J., Thompson, R. W., and Warnock, III, A. 2001, Astron. & Astroph., 376, 359

Hatzes, A. P., Cochran, W. D., Endl, M., Guenther, E. W., Saar, S. H., Walker, G. A. H., Yang, S., Hartmann, M., Esposito, M., Paulson, D. B., and Döllinger, M. P. 2006, Astron. & Astroph., 457, 335

Hatzes, A. P., Cochran, W. D., McArthur, B., Baliunas, S. L., Walker, G. A. H., Campbell, B., Irwin, A. W., Yang, S., Kürster, M., Endl, M., Els, S., Butler, R. P., and Marcy, G. W. 2000, Astroph. J., 544, L145

Hatzes, A. P. and Zechmeister, M. 2007, Astroph. J., 670, L37

Hatzes, A. P., Zechmeister, M., Matthews, J., Kuschnig, R., Walker, G. A. H., Döllinger, M., Guenther, D. B., Moffat, A. F. J., Rucinski, S. M., Sasselov, D., and Weiss, W. W. 2012, Astron. & Astroph., 543, A98

Hauschildt, P. H., Allard, F., and Baron, E. 1999, Astroph. J., 512, 377

Hayashi, C. 1961, Publ. Astron. Soc. Japan, 13, 450

Hekker, S., Kallinger, T., Baudin, F., De Ridder, J., Barban, C., Carrier, F., Hatzes, A. P., Weiss, W. W., and Baglin, A. 2009, ArXiv e-prints

Hillenbrand, L. A. and White, R. J. 2004, Astroph. J., 604, 741

Hubbard, W. B. and Lampe, M. 1969, Astroph. J. Suppl., 18, 297

Iglesias, C. A. and Rogers, F. J. 1996, Astroph. J., 464, 943

Itoh, N., Mitake, S., Iyetomi, H., and Ichimaru, S. 1983, Astroph. J., 273, 774

Jennison, R. C. 1958, Mon. Not. R. Astron. Soc., 118, 276

Johnson, J. A., Butler, R. P., Marcy, G. W., Fischer, D. A., Vogt, S. S., Wright, J. T., and Peek, K. M. G. 2007, Astroph. J., 670, 833

Kervella, P. 2007, Astron. & Astroph., 464, 1045

Kervella, P., Coude du Foresto, V., Glindemann, A., and Hofmann, R. 2000, in Presented at the Society of Photo-Optical Instrumentation Engineers (SPIE) Conference, Vol. 4006, Society of Photo-Optical Instrumentation Engineers (SPIE) Conference Series, ed. P. Léna & A. Quirrenbach, 31–42

Kervella, P. and Domiciano de Souza, A. 2006, Astron. & Astroph., 453, 1059

Kippenhahn, R., Thomas, H. C., and Weigert, A. 1965, Zeitschrift fur Astrophysik, 61, 241

Kjeldsen, H. and Bedding, T. R. 1995, Astron. & Astroph., 293, 87

Kjeldsen, H., Bedding, T. R., Viskum, M., and Frandsen, S. 1995, Astron. J., 109, 1313

Koechlin, L., Bonneau, D., and Vakili, F. 1979, Astron. & Astroph., 80, L13+

Koechlin, L. and Rabbia, Y. 1985, Astron. & Astroph., 153, 91

Kornet, K., Wolf, S., and Różyczka, M. 2007, Planetary and Space Science, 55, 536

Kraus, S., Weigelt, G., Balega, Y. Y., Docobo, J. A., Hofmann, K.-H., Preibisch, T., Schertl, D., Tamazian, V. S., Driebe, T., Ohnaka, K., Petrov, R., Schöller, M., and Smith, M. 2009, Astron. & Astroph., 497, 195

Kroupa, P. and Tout, C. A. 1997, Mon. Not. R. Astron. Soc., 287, 402

Kurucz, R. L. 1991, in NATO ASIC Proc. 341: Stellar Atmospheres - Beyond Classical Models, 441–+

Labeyrie, A. 1970, Astron. & Astroph., 6, 85

Labeyrie, A. 1975, Astroph. J., 196, L71

Laskar, T., Soderblom, D. R., Valenti, J. A., and Stauffer, J. R. 2009, Astroph. J., 698, 660

Le Bouquin, J.-B., Abuter, R., Bauvir, B., Bonnet, H., Haguenauer, P., di Lieto, N., Menardi, S., Morel, S., Rantakyrö, F., Schoeller, M., Wallander, A., and Wehner, S. 2008, in Presented at the Society of Photo-Optical Instrumentation Engineers (SPIE) Conference, Vol. 7013, Society of Photo-Optical Instrumentation Engineers (SPIE) Conference Series

Le Bouquin, J.-B., Lacour, S., Renard, S., Thiébaut, E., Merand, A., and Verhoelst, T. 2009, Astron. & Astroph., 496, L1

Lenz, P. and Breger, M. 2005, Communications in Asteroseismology, 146, 53

López-Santiago, J., Montes, D., Crespo-Chacón, I., and Fernández-Figueroa, M. J. 2006, Astroph. J., 643, 1160

Lovis, C., Mayor, M., Bouchy, F., Pepe, F., Queloz, D., Santos, N. C., Udry, S., Benz, W., Bertaux, J.-L., Mordasini, C., and Sivan, J.-P. 2005, Astron. & Astroph., 437, 1121

Mathieu, R. D. 1994, Annu. Rev. Astro. Astroph., 32, 465

Mege, P., Malbet, F., and Chelli, A. 2003, in Society of Photo-Optical Instrumentation Engineers (SPIE) Conference Series, Vol. 4838, Society of Photo-Optical Instrumentation Engineers (SPIE) Conference Series, ed. W. A. Traub, 329–337

Mermilliod, J. C. 1991, Catalogue of Homogeneous Means in the UBV System, Institut dAstronomie, Universite de Lausanne

Meynet, G., Maeder, A., Schaller, G., Schaerer, D., and Charbonnel, C. 1994, Astron. & Astroph. Suppl., 103, 97

Michelson, A. A. 1891a, Publ. Astron. Soc. Pacific, 3, 274

Michelson, A. A. 1891b, Publ. Astron. Soc. Pacific, 3, 217

Michelson, A. A. and Pease, F. G. 1921, Astroph. J., 53, 249

Mihalas, D., Hummer, D. G., Mihalas, B. W., and Daeppen, W. 1990, Astroph. J., 350, 300

Murdoch, K. A., Hearnshaw, J. B., and Clark, M. 1993, Astroph. J., 413, 349

Neugebauer, G. and Leighton, R. B. 1969, Two-micron sky survey. A preliminary catalogue, ed. R. B. Neugebauer, G. & Leighton

Nieuwenhuijzen, H. and de Jager, C. 1990, Astron. & Astroph., 231, 134

Nordgren, T. E., Sudol, J. J., and Mozurkewich, D. 2001, Astron. J., 122, 2707

North, J. R., Davis, J., Bedding, T. R., Ireland, M. J., Jacob, A. P., O'Byrne, J., Owens, S. M., Robertson, J. G., Tango, W. J., and Tuthill, P. G. 2007, Mon. Not. R. Astron. Soc., 380, L80

Palla, F. and Stahler, S. W. 1999, Astroph. J., 525, 772

Pauls, T. A., Young, J. S., Cotton, W. D., and Monnier, J. D. 2005, Publ. Astron. Soc. Pacific, 117, 1255

Pease, F. G. 1931, Ergebnisse der Exakten Naturwissenschaften, 10, 84

Petrov, R. G., Malbet, F., Weigelt, G., Antonelli, P., Beckmann, U., Bresson, Y., Chelli, A., Dugué, M., Duvert, G., Gennari, S., Glück, L., Kern, P., Lagarde, S., Le Coarer, E., Lisi, F., Millour, F., Perraut, K., Puget, P., Rantakyrö, F., Robbe-Dubois, S., Roussel, A., Salinari, P., Tatulli, E., Zins, G., Accardo, M., Acke, B., Agabi, K., Altariba, E., Arezki, B., Aristidi, E., Baffa, C., Behrend, J., Blöcker, T., Bonhomme, S., Busoni, S., Cassaing, F., Clausse, J.-M., Colin, J., Connot, C., Delboulbé, A., Domiciano de Souza, A., Driebe, T., Feautrier, P., Ferruzzi, D., Forveille, T., Fossat, E., Foy, R., Fraix-Burnet, D., Gallardo, A., Giani, E., Gil, C., Glentzlin, A., Heiden, M., Heininger, M., Hernandez Utrera, O., Hofmann, K.-H., Kamm, D., Kiekebusch, M., Kraus, S., Le Contel, D., Le Contel, J.-M., Lesourd, T., Lopez, B., Lopez, M., Magnard, Y., Marconi, A., Mars, G., Martinot-Lagarde, G., Mathias, P., Mège, P., Monin, J.-L., Mouillet, D., Mourard, D., Nussbaum, E., Ohnaka, K., Pacheco, J., Perrier, C., Rabbia, Y., Rebattu, S., Reynaud, F., Richichi, A., Robini, A., Sacchettini, M., Schertl, D., Schöller, M., Solscheid, W., Spang, A., Stee, P., Stefanini, P., Tallon, M., Tallon-Bosc, I., Tasso, D., Testi, L., Vakili, F., von der Lühe, O., Valtier, J.-C., Vannier, M., and Ventura, N. 2007, Astron. & Astroph., 464, 1

Pickles, A. J. 1998, Publ. Astron. Soc. Pacific, 110, 863

Plez, B. 1992, Astron. & Astroph. Suppl., 94, 527

Pols, O. R., Tout, C. A., Eggleton, P. P., and Han, Z. 1995, Mon. Not. R. Astron. Soc., 274, 964

Preibisch, T. and Zinnecker, H. 1999, Astron. J., 117, 2381

Reimers, D. 1975, Memoires of the Societe Royale des Sciences de Liege, 8, 369

Reimers, D. 1977, Astron. & Astroph., 57, 395

Reipurth, B., Lindgren, H., Mayor, M., Mermilliod, J.-C., and Cramer, N. 2002, Astron. J., 124, 2813

Richichi, A., Percheron, I., and Khristoforova, M. 2005, Astron. & Astroph., 431, 773

Salaris, M., degl'Innocenti, S., and Weiss, A. 1997, Astroph. J., 479, 665

Salasnich, B., Girardi, L., Weiss, A., and Chiosi, C. 2000, Astron. & Astroph., 361, 1023

Saumon, D., Chabrier, G., and van Horn, H. M. 1995, Astroph. J. Suppl., 99, 713

Schmidt-Kaler, Th. 1982, The Physical Parameters of the Star, ed. B. Springer

Schwarzschild, K. 1896, Astronomische Nachrichten, 139, 353

Setiawan, J., Pasquini, L., da Silva, L., Hatzes, A. P., von der Lühe, O., Girardi, L., de Medeiros, J. R., and Guenther, E. 2004, Astron. & Astroph., 421, 241

Setiawan, J., Rodmann, J., da Silva, L., Hatzes, A. P., Pasquini, L., von der Lühe, O., de Medeiros, J. R., Döllinger, M. P., and Girardi, L. 2005, Astron. & Astroph., 437, L31

Shao, M. and Colavita, M. M. 1992, Astron. & Astroph., 262, 353

Shao, M., Colavita, M. M., Hines, B. E., Staelin, D. H., and Hutter, D. J. 1988, Astron. & Astroph., 193, 357

Shao, M. and Staelin, D. H. 1977, Journal of the Optical Society of America (1917-1983), 67, 81

Shao, M. and Staelin, D. H. 1980, Ap. Opt., 19, 1519

Siess, L., Dufour, E., and Forestini, M. 2000, Astron. & Astroph., 358, 593

Simon, M. and Prato, L. 2004, Astroph. J., 613, L69

Skrutskie, M. F., Cutri, R. M., Stiening, R., Weinberg, M. D., Schneider, S., Carpenter, J. M., Beichman, C., Capps, R., Chester, T., Elias, J., Huchra, J., Liebert, J., Lonsdale, C., Monet, D. G., Price, S., Seitzer, P., Jarrett, T., Kirkpatrick, J. D., Gizis, J. E., Howard, E., Evans, T., Fowler, J., Fullmer, L., Hurt, R., Light, R., Kopan, E. L., Marsh, K. A., McCallon, H. L., Tam, R., Van Dyk, S., and Wheelock, S. 2006, Astron. J., 131, 1163

Song, I., Bessell, M. S., and Zuckerman, B. 2002, Astron. & Astroph., 385, 862

Soubiran, C., Bienaymé, O., Mishenina, T. V., and Kovtyukh, V. V. 2008, Astron. & Astroph., 480, 91

Stassun, K. G., Mathieu, R. D., Cargile, P. A., Aarnio, A. N., Stempels, E., and Geller, A. 2008, Nature, 453, 1079

Stassun, K. G., Mathieu, R. D., Vaz, L. P. R., Stroud, N., and Vrba, F. J. 2004, Astroph. J. Suppl., 151, 357

Stephan, M. 1874, Comptes Rendus Hebdomadaires des Sèances de lAcademie des Sciences, 78, 1008

Tango, W. J. and Twiss, R. Q. 1980, in Progress in optics. Volume 17. (A81-13109 03-74) Amsterdam, North-Holland Publishing Co., 1980, p. 239-277. Research supported by the Australian Research Grants Committee., ed. E. Wolf, Vol. 17, 239–277

Tatulli, E., Mège, P., and Chelli, A. 2004, Astron. & Astroph., 418, 1179

Teixeira, T. C., Kjeldsen, H., Bedding, T. R., Bouchy, F., Christensen-Dalsgaard, J., Cunha, M. S., Dall, T., Frandsen, S., Karoff, C., Monteiro, M. J. P. F. G., and Pijpers, F. P. 2009, Astron. & Astroph., 494, 237

ten Brummelaar, T. A., McAlister, H. A., Ridgway, S. T., Bagnuolo, Jr., W. G., Turner, N. H., Sturmann, L., Sturmann, J., Berger, D. H., Ogden, C. E., Cadman, R., Hartkopf, W. I., Hopper, C. H., and Shure, M. A. 2005, Astroph. J., 628, 453

Torres, G., Guenther, E. W., Marschall, L. A., Neuhäuser, R., Latham, D. W., and Stefanik, R. P. 2003, Astron. J., 125, 825

Valenti, J. A., Butler, R. P., and Marcy, G. W. 1995, Publ. Astron. Soc. Pacific, 107, 966

van Leeuwen, F. 2007, Astron. & Astroph., 474, 653

Wichmann, R., Krautter, J., Covino, E., Alcala, J. M., Neuhaeuser, R., and Schmitt, J. H. M. M. 1997, Astron. & Astroph., 320, 185

Wuchterl, G., Broeg, C., Krause, S., Pecnik, B., and Schoenke, J. 2007, ArXiv Astrophysics e-prints

Zernike, F. 1938, Physika, 5, 785

Zuckerman, B., Song, I., and Bessell, M. S. 2004, Astroph. J., 613, L65

Acknowledgements

First of all, I would like to express all my gratitude to Dr. Eike Guenther, the supervisor of my Ph.D. work. He helped me and teached me a lot during the period of the thesis. We discussed together most of the issues that I met during my work and his suggestions were always important. I thank him also for the german translation in this thesis. Thanks to him I also solved most of the logistic questions at the begining of my staying in Germany.

Many thanks also to Massimiliano Esposito known as the "professore" who introduced me in the Tautenburg's comunity. He aswered to most of my scientific and non-scientific questions, teaching me a lot. I learned from him also how to cook a wonderful pasta with beans (Past e fasull).

I would like to thank also some of mine scientific collaborators: thanks to A. Richichi and E. Baines for the collaboration concerning the measure of the diameters of giant stars; thanks to D. Gandolfi for the collaboration regarding the spectral classification of HD113449; thanks to A. Hatzes and M. Hartman for the suggestions concerning the reduction and analysis of the Tautenburg echelle spectra; thanks to K. Biazzo for the discussions concerning the spectral synthesis analysis. I would like also to thank the teachers of the interferometry schools in Porto and Keszthely that I attended. During these schools I learned most of the maters concerning the reduction and the analysis of interferometric data.

Thanks also to the Italian comunity in Tautenburg (Alessio, Andrea, Davide, Massimiliano, Patrizia and Rebecca) for the pleasant days that we spent together.

Ehrenwörtliche Erklärung

Ich erkläre hiermit ehrenwörtlich, dass ich die vorliegende Arbeit selbständig, ohne unzulässige Hilfe Dritter und ohne Benutzung anderer als der angegebenen Hilfsmittel und Literatur angefertigt habe. Die aus anderen Quellen direkt oder indirekt übernommenen Daten und Konzepte sind unter Angabe der Quelle gekennzeichnet.

Bei der Auswahl und Auswertung folgenden Materials haben mir die nachstehend aufgeführten Personen in der jeweils beschriebenen Weise unentgeldlich geholfen:

1. Dr. Eike Guenther half bei der Datenreduktion, versorgte allgemeinen Informationen über Sternentstehung und übersetzte manche Texten von English auf Deutsch

2. Dr. D. Gandolfi half bei der Klassifizierung des Sterns HD113449

3. Dr. A. Richmond und Dr. E. Baines halfen bei der Analyse der interferometrische Daten von Riesensterne.

Weitere Personen waren an der inhaltlich-materiellen Erstellung der vorliegenden Arbeit nicht beteiligt. Insbesondere habe ich hierfür nicht die entgeltliche Hilfe von Vermittlungs bzw. Beratungsdiensten (Promotionsberater oder andere Personen) in Anspruch genommen. Niemand hat von mir unmittelbar oder mittelbar geldwerte Leistungen für Arbeiten erhalten, die in Zusammenhang mit dem Inhalt der vorgelegten Dissertation stehen.

Die Arbeit wurde bisher weder im In- noch im Ausland in gleicher oder ähnlicher Form einer anderen Prüfungsbehörde vorgelegt.

Die geltende Promotionsordnung der Physikalisch-Astronomischen Fakultät ist mir bekannt.

Ich versichere ehrenwörtlich, dass ich nach bestem Wissen die reine Wahrheit gesagt und nichts verschwiegen habe.

Jena, den 09. Juni 2011   Felice Cusano

Lebenslauf

Zur Person:

Name: Cusano
Vorname: Felice
Geburtsdatum: 17.07.1979
Geburtsort: Neapel (Italien)

Werdegang:

Apr. 2011 - bis Heute	Wissenschaftliche Mitarbeiter am INAF-OABo Bologna (Italien)
Nov. 2009 - Apr. 2011	Wissenschaftliche Mitarbeiter am INAF-OACn Neapel (Italien)
	Betreuer: Dr. Vincenzo Ripepi
	Wissenschaftliche Arbeit
seit Okt. 2006:	Doktorand an der Thüringer Landessternwarte Tautenburg
	Betreuer: Dr. Eike Guenther
	Titel: Interferometry as a tool to calibrate evolutionary tracks
Jun. 2006 - Sep. 2006	Wissenschaftliche Mitarbeiter am INAF-OACn Neapel (Italien)
	Betreuer: Dr. Vincenzo Ripepi
	Wissenschaftliche Arbeit
Okt. 1998 - Mai. 2006	Physikalisches-Studium an der Universität Federico II Neapel (Italien)
	und Diplomarbeit am Osservatorio Astronomico di Capodimonte
	Betreuer: Prof. Massimo Capaccioli
	Titel: Fotometria e spettroscopia dell'ammasso aperto giovane Dolidze 25
	Abschluß: Dott. Magistrale in Fisica
Sep. 1993 - Jul. 1998	Liceo Scientifico "P. Calamandrei"- Neapel (Italien)
	Abschluß: Maturitá Scientifica (Hochschulzugangsberechtigung)

Jena, den 01. Juni 2011   Felice Cusano

Publications on International Refereed Journals

1. **Cusano F.**, Paladini C., Richichi A., Guenther E. W., Aringer B., Biazzo K., Pasquini L., and Hatzes A. P. *High precision AMBER/VLTI observations of 5 giant stars* , 2011 re-submitted to A&A;

2. Ripepi V., **Cusano F.**, Di Criscienzo M., Catanzaro G., Palla F., Marconi M., Ventura P., Neiner C., Catala C. and Bernabei S., *CoRoT 102699796, the first metal-poor Herbig Ae pulsator: a hybrid δ Sct-γ Dor variable?* , 2011 in press in MNRAS, 2011arXiv1106.0418R;

3. **Cusano F.**, Ripepi V., Alcalá J. M., Gandolfi D., Marconi M., Degl'Innocenti S., Palla F., Guenther E. W., Bernabei S., Covino E., Neiner C., Puga E. and Hony S.*Pre-main-sequence stars in the star-forming complex Sh 2-284*, 2011, MNRAS, 410, 227;

4. Baines Ellyn K., Döllinger Michaela P., **Cusano Felice**, Guenther Eike W., Hatzes Artie P., McAlister Harold A., ten Brummelaar Theo A., Turner Nils H., Sturmann Judit, Sturmann Laszlo, Goldfinger P. J., Farrington Christopher D. and Ridgway Stephen T. *Angular Diameters and Effective Temperatures of 25 K Giant Stars from the CHARA Array*, 2010, ApJ, 710, 1365;

5. Guenther E. W., Hartmann M., Esposito M., Hatzes A. P., **Cusano F.** and Gandolfi D. *A substellar component orbiting the F-star 30 Arietis B*, 2009, A&A, 507, 1659;

6. Puga E., Hony S., Neiner C., Lenorzer A., Hubert A.-M., Waters L. B. F. M., **Cusano F.** and Ripepi V. *Spitzer/IRAC view of Sh 2-284. Searching for evidence of triggered star formation in an isolated region in the outer Milky Way*, 2009, A&A, 503, 107;

7. Guenther E. W., Esposito M., Mundt R., Covino E., Alcalá J. M., **Cusano F.** and Stecklum, B. *Pre-main sequence spectroscopic binaries suitable for VLTI observations*, 2007, A&A, 467, 1147.

Publications on Refereed Conference Proceedings

1. Ripepi V., Leccia S., Baglin A., Ruoppo A., Bernabei S., Zwintz K., **Cusano F.**, Gandolfi D., Guenther E. W., Alencar S., Marconi M., Monteiro M.J.P.F.G., Palla F., Alcalá J.M., Boehm T., Catala C., Chavero C., Corradi W.S., Degl'Innocenti S., de la Reza R. , Deluil M., Favata F., Fernandez M., Gregorio-Hetem J., Lepine J.D.R., Pinheiro F.J.G., Prada Moroni P. G., Quast G., Torres C.A.O. and Weiss W. *CoRoT observations of variable stars in the young open cluster Dolidze 25*, 2011 in press Astron. Nachr.;

2. Ripepi V., Leccia S., Baglin A., Ruoppo A., Bernabei S., Zwintz K., **Cusano F.**, Gandolfi D., Guenter E. W., Alencar S., Marconi M., Monteiro M. J. P. F. G., Palla F., Alcalá J. M., Boehm T., Catala C., Chavero C., Corradi W. S., Degl'Innocenti S., de La Reza R., Deluil M., Favata F., Fernandez M., Gregorio-Hetem J., Lepine J. D. R., Pinheiro F. J. G., Prada Moroni P. G., Quast G., Torres C. A. O. and Weiss W. *CoRoT observations of the young open cluster Dolidze 25*, 2010, Ap&SS, 328, 119.

Publications on non-refereed Conference Proceedings

1. **Cusano F.**, Ripepi V., Marconi M. and Gandolfi D. *TT1 time-series observations of the star forming region Sh 2-284*, 2011, MmSAI in press;

2. Ripepi, V., Cortecchia, F., **Cusano, F.**, Dall'Ora, M., Leccia, S., Mancini, D. et al. *Scientific results after the first year of operation with Toppo di Castelgrande telescope (TT1)*, 2011, MmSAI in press;

3. **Cusano F.**, Guenther E. W., Esposito M., Gandolfi D. *VLTI/AMBER observation of HD113449*, 2010, RMxAC, 38, 34

4. Baines Ellyn K., McAlister H. A., ten Brummelaar T. A., Sturmann J., Sturmann L., Turner N. H., Goldfinger P. J., Farrington C. D., Ridgway S. T., Doellinger M. P., **Cusano F.**, Guenther E. W. and Hatzes A. P. *Angular Diameters and Effective Temperatures for Eleven Exoplanet Host Stars and Twenty-five K Giant Stars from the CHARA Array*, 2010, AAS, 21541606

5. **Cusano F.**, Guenther E. W., Esposito M., Mundt M., Covino E. and Alcalá J. M. *Testing evolutionary tracks of Pre-Main Sequence stars: the case of HD113449* 2009, AIPC, 1094, 788

6. Ripepi V., Marconi M., Palla F., Bernabei S., Ruoppo A., **Cusano F.** and Alcalá J. M. *Recent results on Pre-main sequence delta Scuti stars*, 2006, MmSAI, 77, 317

Catalogues and GCN Circulars

1. Puga E., Hony S., Neiner C., Lenorzer A., Hubert A.-M., Waters L. B. F. M., **Cusano F.**, Ripepi, V. *Spitzer/IRAC view of Sh2-284*, 2009yCat, 35030107

2. Guenther E. W., Hartmann M., Esposito M., Hatzes A. P., **Cusano F.** and Gandolfi D. *Radial velocity measurements of 30 Ari B*, 2009yCat, 35071659

3. Kann D. A., **Cusano F.** and Ludwig F. *GRB 090817 - TLS observations* 2009, GCN, 9842, 1

Posters and Talks

I presented the following talks:

1. March 2010, at Workshop "The origin and the fate of the Sun", Garching (Germany), title: "Interferometric observations of young and evolved stars"

2. September 2009, Seminar at the Thüringer Landessternwarte Tautenburg, Tauteburg (Germany), title: "Interferometry as a tool to calibrate evolutionary tracks"

3. March 2007, at AMBER scienfic workshop, Grenoble (France), title: "Pre-main sequence spectroscopic binaries suitable for VLTI observations"

4. April 2006, at Workshop di astronomia e astrofisica per studenti, Napoli (Italy), title:" Caratterizzazione delle stelle di pre-sequenza principale nel campo dell'ammasso aperto giovane e povero di metalli Dolidze 25"

I presented the following posters:

1. May 2011, at "The fundamental cosmic distance scale: state of the art and the Gaia perspective", Napoli (Italy), title: "Stellar Archeaology in the M31 halo: variable stars and stellar populations in the And IX dwarf spheroidal galaxies"

2. May 2010, at 54º Congresso nazionale Sait, Napoli (Italy), title: "TT1 time-series observations of the star forming region Sh 2-284"

3. March 2009, at "The Interferometric View on Hot Stars", Viña del Mar (Chile), title: "VLTI/AMBER observation of HD113449"

4. July 2008, at 15th Cambridge Workshop: "Cool Stars, stellar system and the sun", St Andrews (Scotland), title: "Testing Pre-Main Sequence evolutionary tracks: the case of HD113449"